

**SIMULATION OF CATALYTIC COMBUSTION OF AUTOMOTIVE EXHAUST
GAS IN MONOLITHIC REACTOR**

CHAI KIM YONG

**A project report submitted in partial fulfilment of the
requirements for the award of Bachelor of Engineering
(Hons.) Chemical Engineering**

**Lee Kong Chian Faculty of Engineering and Science
Universiti Tunku Abdul Rahman**

April 2015

DECLARATION

I hereby declare that this project report is based on my original work except for citations and quotations which have been duly acknowledged. I also declare that it has not been previously and concurrently submitted for any other degree or award at UTAR or other institutions.

Signature : _____

Name : _____

ID No. : _____

Date : _____

APPROVAL FOR SUBMISSION

I certify that this project report entitled “**SIMULATION OF CATALYTIC COMBUSTION OF AUTOMOTIVE EXHAUST GAS IN MONOLITHIC REACTOR**” was prepared by **CHAI KIM YONG** has met the required standard for submission in partial fulfilment of the requirements for the award of Bachelor of Engineering (Hons.) Chemical Engineering at Universiti Tunku Abdul Rahman.

Approved by,

Signature : _____

Supervisor : _____

Date : _____

The copyright of this report belongs to the author under the terms of the copyright Act 1987 as qualified by Intellectual Property Policy of Universiti Tunku Abdul Rahman. Due acknowledgement shall always be made of the use of any material contained in, or derived from, this report.

© 2015, Chai Kim Yong. All right reserved.

Specially dedicated to
my beloved family members, friends and supervisor

ACKNOWLEDGEMENTS

I would like to thank everyone who had contributed to the successful completion of this project. I would like to express my gratitude to my research supervisor, Dr. Yap Yeow Hong for his invaluable advice, guidance and his enormous patience throughout the development of the research.

In addition, I would also like to express my gratitude to my loving parent and friends who had helped and given me encouragement throughout the preparation of this report.

SIMULATION OF CATALYTIC COMBUSTION OF AUTOMOTIVE EXHAUST GAS IN MONOLITHIC REACTOR

ABSTRACT

Catalytic converters in the form of monolithic reactor are widely used to control the exhaust emission from motor vehicles. Many research and developments on catalytic converter are increasingly rely on computer models to help save resources and shorten the product development time. Despite the advantages of using computer models, it has limitation in modelling the ignition-extinction phenomena, which is an increasingly popular approach to study the performance of catalytic converter. In this project, a computer model has been developed to simulate the CO ignition-extinction phenomena for a 5mm thin slice Pt/ γ -Al₂O₃ diesel oxidation catalyst (catalytic converter for diesel-powered vehicles). The transient 1D-gas phase, 1D-solid phase single channel model considers the mass and energy transport as well as the change of the adsorbed species on the catalyst surface. Compressed oxygen reaction mechanism developed by Salomons *et al* (2007) was used as the kinetic model. The model was able to simulate the ignition-extinction hysteresis and confirmed that CO covered surface at low temperature and oxygen covered surface at high temperature is the reason for the ignition and extinction phenomena. In addition, the effect of length of the reactor and inlet CO concentration on the ignition-extinction has also been studied. It was also found that the pre-exponential factors for the adsorption of CO and oxygen and the pre-exponential factors for the surface reaction between CO and adsorbed oxygen have significant impact on the ignition-extinction hysteresis. These are the parameters that should be optimized to achieve a better fit between simulation and experimental result.

TABLE OF CONTENTS

DECLARATION	ii
APPROVAL FOR SUBMISSION	iii
ACKNOWLEDGEMENTS	vi
ABSTRACT	vii
TABLE OF CONTENTS	viii
LIST OF TABLES	xi
LIST OF FIGURES	xiii
LIST OF APPENDICES	xvii
LIST OF SYMBOLS / ABBREVIATIONS	xviii

CHAPTER

1	INTRODUCTION	1
	1.1 Background	1
	1.1.1 Environmental Regulation on Vehicles' Emission	3
	1.2 Problem Statement	4
	1.3 Aims and Objectives	5
	1.4 Scope of Study	6
2	LITERATURE REVIEW	7
	2.1 Diesel Exhaust Emission Control System	7
	2.2 Diesel Oxidation Catalyst	10
	2.2.1 Substrate	11
	2.2.2 Washcoat	11
	2.2.3 Catalyst	12
	2.3 Heterogeneous Catalysis in Catalytic Converter	12

2.4	Ignition-Extinction Hysteresis	14
2.4.1	Effects of change in inlet CO concentration to ignition-extinction hysteresis	17
2.4.2	Effects of change in rate of temperature ramp up to ignition-extinction hysteresis	19
2.4.3	Other factors that affect the ignition-extinction hysteresis	20
2.4.4	Theoretical explanation for ignition-extinction hysteresis	20
2.5	Modelling ignition-extinction hysteresis	24
2.5.1	Nibbelke <i>et al</i> (1998)	26
2.5.2	Chatterjee <i>et al</i> (2001)	27
2.5.3	Salomons <i>et al</i> (2007)	28
2.6	Modelling	29
2.6.1	Steady-state and Transient Modelling	29
2.6.2	Single channel and multi-channel models	30
2.6.3	1D and 2D Modelling	30
2.7	Python Programming	31
3	METHODOLOGY	33
3.1	Introduction	33
3.2	Single Channel Monolith Model	34
3.2.1	Mass Transport Model	36
3.2.2	Energy Transport Model	40
3.2.3	Model Parameters, Operating Conditions and Chemical Properties	43
3.3	Kinetic Model	49
3.3.1	Mechanistic Model of CO Oxidation	49
3.3.2	Global Kinetic Model of Propane Oxidation	56
3.4	Numerical Methods	56
3.5	Algorithms for Programming	57
3.5.1	Flow Chart	66

4	RESULT AND DISCUSSION	76
4.1	Ignition-Extinction Curve	76
4.2	Study on the Effect of Change of the Length of Channel	83
4.3	Study on the Effect of Change of the CO Concentration in Inlet Gas of Channel	84
4.4	Study on the Effect of Ramping Up and Ramping Down of the CO Concentration in Inlet Gas of Channel	87
4.5	Study on the Effect of Square Pulse of the CO Concentration in Inlet Gas of Channel	89
4.6	Mechanistic Model Tuning	90
5	CONCLUSION AND RECOMMENDATION	95
5.1	Conclusion	95
5.2	Recommendations	96

LIST OF TABLES

TABLE	TITLE	PAGE
1.1	European emission standard on CO, NO _x and particulates (Burch, 2004, EUROPA)	3
3.1	Partial differential equations describing the mass transfer of CO, CO ₂ and propane in the 1D gas phase	38
3.2	Partial differential equations describing the mass transfer of CO, CO ₂ and propane in the 1D solid phase	39
3.3	Partial differential equations describing the energy transfer of CO, CO ₂ and propane in the 1D gas phase	41
3.4	Partial differential equations describing the energy transfer of CO, CO ₂ and propane in the 1D solid phase	42
3.5	Monolith channel physical properties	43
3.6	Operating conditions	43
3.7	Physical properties for the reacting species	43
3.8	Properties of Gas Phase	45
3.9	Properties of Solid Phase	46
3.10	Heat Transfer Coefficient Related Equations	47
3.11	Mass Transfer Coefficient Related Equations	48
3.12	Reaction rate equations	50
3.13	Reaction Rate Equation Parameters	54
3.14	Equations for Rate of Change of Fractional Coverage of Adsorbed Species and Vacant Site	55
3.15	Equations for Rate of Release of Chemical Species into Solid Phase	55

TABLE	TITLE	PAGE
3.16	Reaction Rate Equation	56
3.17	Reaction Rate Equation Parameters	56
4.1	Ignition Point and Extinction Point for Different CO Concentration	CO 85

LIST OF FIGURES

FIGURE	TITLE	PAGE
2.1	Modern Diesel Exhaust Gas System (adapted from Mercedes BLUETEC, 2007)	8
2.2	Overview of a catalytic converter that shows the substrate, washcoat and metal catalyst nanoparticles (adapted from Rao <i>et al.</i> , 2009)	10
2.3	Steps of heterogeneous solid-gas catalytic reaction (adapted from Froment and Bischoff, 1990)	13
2.4	Two possible mechanisms of heterogeneous solid-gas catalytic reaction Langmuir-Henshelwood (LH) mechanism (left) and Eley-Rideal (ER) mechanism (right) (adapted from Thomas and Thomas, 1999).	13
2.5	New European Drive Cycle (NEDC) represents the typical usage of a car in Europe. It shows the speed of vehicles in a drive cycle	15
2.6	Typical temperature profile for the temperature ramp up and ramp down experiments (adapted from Ye, 2011)	16
2.7	A typical ignition-extinction hysteresis curve (adapted from Yap, 2011)	16
2.8	Experimental ignition-extinction curves generated from different inlet CO concentrations. (adapted from Salomons, 2006)	18
2.9	Ignition-extinction hysteresis curves for different inlet CO concentration on a 5mm thin slice diesel oxidation catalyst (adapted from Ye <i>et al.</i> , 2011)	18
2.10	Transient ignition-extinction hysteresis curve for different ramp-up temperature (adapted from Ye <i>et al.</i> , 2011)	19

FIGURE	TITLE	PAGE
2.11	Chemisorbed species on a Pt (111) surface at low coverages (i) adsorption of CO, (ii) adsorption of O and (iii) adsorption of CO within O-2×2 unit structure. (adapted from Engel, 2000)	21
2.12	Illustration of CO and O adsorption on the surface during ignition and extinction (adapted from Yap, 2011)	23
3.1	Example of grids set up in Python	58
3.2	Example of monolith parameter declaration in Python	59
3.3	Example of initialization of variable in Python	59
3.4	Example of stages and inlet gas temperature profile setup in Python	60
3.5	Example of “parameter” function setup in Python	61
3.6	Example of mechanistic model setup in Python	61
3.7	Example of step size of time declaration in Python	62
3.8	Example of loop for stages setup in Python	62
3.9	Example of loop for numerical iteration setup in Python	63
3.10	Example of value display setup in Python	64
3.11	Example of data storing in Python	64
3.12	Example of graph plotting in Python	65
3.13	Flow chart	67
4.1	Inlet gas temperature versus time	77
4.2	Ignition and extinction hysteresis of CO oxidation in a single channel 0.005m monolith	78
4.3	Thin slice diesel oxidation catalyst ignition-extinction hysteresis curve for different inlet CO concentration (adapted from Ye et al, 2011)	78
4.4	Gas phase CO concentration at various position along 0.005m channel	80

FIGURE	TITLE	PAGE
4.5	Solid phase CO concentration at various position along 0.005m channel	80
4.6	Fractional coverage of CO on washcoat in 0.005m channel	81
4.7	Fractional coverage of O on washcoat in 0.005m channel	82
4.8	Fractional coverage of compressed oxygen OO on washcoat in 0.005m channel	82
4.9	Fractional coverage of vacant site on washcoat in 0.005m channel	83
4.10	Hysteresis Curves for Various Channel Length	84
4.11	Hysteresis diagram of CO oxidation in a single channel 0.005m monolith with different inlet CO concentration.	86
4.12	Simulation output from a continuous linear ramp of CO concentration at constant feed temperature of 394.0K, 407.0K, 417.0K and 450K in a single channel 0.005m monolith	88
4.13	Experimental CO output from a continuous linear ramp of CO concentration in feed at constant feed temperature of 394K and 407K. (adapted from Salomons, 2006)	88
4.14	Simulation output from a square pulse of CO concentration at constant feed temperature of 394.0K, 407.0K, 417.0 K and 450K in a single channel 0.005m monolith	89
4.15	Hysteresis diagram of CO oxidation in a single channel 0.005m monolith with Tuned Pre-exponential for Carbon Monoxide Desorption	91
4.16	Hysteresis diagram of CO oxidation in a single channel 0.005m monolith with Tuned Pre-exponential value for Oxygen Adsorption	92
4.17	Hysteresis diagram of CO oxidation in a single channel 0.005m monolith with Tuned Pre-exponential for Reaction between CO and O	92
4.18	Hysteresis diagram of CO oxidation in a single channel 0.005m monolith with Tuned Pre-exponential for Oxygen Compression	93

FIGURE	TITLE	PAGE
4.19	Hysteresis diagram of CO oxidation in a single channel 0.005m monolith with Tuned Pre-exponential for Reaction between CO and OO	93
4.20	Hysteresis diagram of CO oxidation in a single channel 0.005m monolith with Tuned Pre-exponential for Reverse Oxygen Compression	94

LIST OF APPENDICES

APPENDIX	TITLE	PAGE
A	Derivation of Monolith Mode	99
B	Python Programming Codes	115

LIST OF SYMBOLS / ABBREVIATIONS

$A_{C_3H_8}$	pre-exponential value of propane oxidation, mol/mol·s
$A_{C_3H_8i}$	pre-exponential value of inhibition factor for propane oxidation
A_{aB}	pre-exponential value of backward reaction a, mol/mol·s
A_c	cross-sectional area of channel, m ²
A_{cF}	pre-exponential value of forward reaction c, mol/mol·s
A_{dF}	pre-exponential value of forward reaction d, mol/mol·s
A_{eF}	pre-exponential value of forward reaction e, mol/mol·s
A_{fF}	pre-exponential value of forward reaction f, mol/mol·s
A_v	internal surface area to volume ratio of washcoat, m ²
$C_{p_{air}}$	specific heat capacity of gas phase, J/kg K
$C_{p_{wc}}$	specific heat capacity of solid phase, J/kg K
C_A	concentration of CO in gas phase, mol/m ³
C_{As}	concentration of CO in solid phase, mol/m ³
C_B	concentration of CO ₂ in gas phase, mol/m ³
C_{Bs}	concentration of CO ₂ in solid phase, mol/m ³
C_C	concentration of C ₃ H ₈ in gas phase, mol/m ³
C_{Cs}	concentration of C ₃ H ₈ in solid phase, mol/m ³
D_H	hydraulic diameter, m
D_{air}	thermal diffusivity of air, m ² /s
D_{bA}	Bulk diffusion coefficient of CO in gas phase, m ² /s
D_{bAs}	Bulk diffusion coefficient of CO in solid phase, m ² /s
D_{bB}	Bulk diffusion coefficient of CO ₂ in gas phase, m ² /s
D_{bBs}	Bulk diffusion coefficient of CO ₂ in solid phase, m ² /s
D_{bC}	Bulk diffusion coefficient of C ₃ H ₈ in gas phase, m ² /s
D_{bCs}	Bulk diffusion coefficient of C ₃ H ₈ in solid phase, m ² /s
D_{eA}	effective diffusivity of CO, m ² /s

D_{eB}	effective diffusivity of CO ₂ , m ² /s
D_{eC}	effective diffusivity of C ₃ H ₈ , m ² /s
D_g	thermal dispersion coefficient of gas phase, m ² /s
D_{iA}	dispersion coefficient of CO, m ² /s
D_{iB}	dispersion coefficient of CO ₂ , m ² /s
D_{iC}	dispersion coefficient of C ₃ H ₈ , m ² /s
D_{kA}	Knudsen diffusion coefficient of CO, m ² /s
D_{kB}	Knudsen diffusion coefficient of CO ₂ , m ² /s
D_{kC}	Knudsen diffusion coefficient of C ₃ H ₈ , m ² /s
D_s	thermal dispersion coefficient of solid phase, m ² /s
D_{vA}	dispersion coefficient of CO in pores, m ² /s
D_{vB}	dispersion coefficient of CO ₂ in pores, m ² /s
D_{vC}	dispersion coefficient of C ₃ H ₈ in pores, m ² /s
$E_{C_3H_8}$	activation energy of propane oxidation, kJ/mol
$E_{C_3H_8i}$	activation energy of inhibition factor for propane oxidation, kJ/K
E_{aB}	activation energy of backward reaction a, kJ/mol
E_{cF}	activation energy of forward reaction c, kJ/mol
E_{dF}	activation energy of forward reaction d, kJ/mol
E_{eF}	activation energy of forward reaction e, kJ/mol
E_{fF}	activation energy of forward reaction f, kJ/mol
f_{cCO}	fractional coverage of CO
f_{cO}	fractional coverage of O
f_{cOO}	fractional coverage of OO
f_{cV}	fractional coverage of vacant site
F_A	molar flow rate of CO, mol/s
F_B	molar flow rate of CO ₂ , mol/s
F_C	molar flow rate of C ₃ H ₈ , mol/s
G	constant
GZ	Graetz number
h	heat transfer coefficient, W/m ² ·K
H	mol of catalyst per internal surface area of washcoat, mol/m ²
H_g	specific enthalpy of gas phase, J/kg
$Hr_{C_3H_8}$	heat of reaction of C ₃ H ₈ , J/mol

Hr_{CO}	heat of reaction of CO, J/mol
k_{mA}	convective mass transfer coefficient of CO, m/s
k_{mB}	convective mass transfer coefficient of CO ₂ , m/s
k_{mC}	convective mass transfer coefficient of C ₃ H ₈ , m/s
k_s	thermal conductivity of solid phase, W/m·K
L	distance from inlet
L_{Pt}	active sites to washcoat ratio, m/g
\dot{m}	average mass flow of gas phase, kg/s
mol_A	moles of CO, mol
mol_B	moles of CO ₂ , mol
mol_C	moles of C ₃ H ₈ , mol
m_{wc}	mass of washcoat, kg
$M_{C_3H_8}$	molar mass of C ₃ H ₈
M_{CO}	molar mass of CO
M_{CO_2}	molar mass of CO ₂
M_{O_2}	molar mass of O ₂
M_{air}	molar mass of air
M_{flow}	inlet molar flow
n	total mol of molecule in solid phase, mol
Nu_H	Nusselt number for wall flux
Nu_T	Nusselt number for wall temperature
Nu	Nusselt number
por	porosity
P	pressure, Pa
Pr	Prandtl number
Q	volume flow rate, m ³ /s
r	channel radius, m
r_e	equivalent pore radius, m
R	universal gas constant, Pa m ³ /mol K
Re	Reynolds number
$R_{C_3H_8}$	desorption rate of C ₃ H ₈ per mol of catalyst, mol/mol m ³
$R_{C_3H_8i}$	inhibition factor for propane oxidation
R_{CO}	desorption rate of CO per mol of catalyst, mol/mol m ³

R_{CO_2}	desorption rate of CO ₂ per mol of catalyst, mol/mol m ³
R_{O_2}	desorption rate of O ₂ per mol of catalyst, mol/mol m ³
R_a	rate of reaction a, mol/mol·s
R_b	rate of reaction b, mol/mol·s
R_c	rate of reaction c, mol/mol·s
R_d	rate of reaction d, mol/mol·s
R_e	rate of reaction e, mol/mol·s
R_f	rate of reaction f, mol/mol·s
s	washcoat thickness, m
S_{CO}	stick coefficient of CO
S_{O_2}	stick coefficient of O ₂
T	tortuosity
T_g	gas phase temperature, K
T_s	solid phase temperature, K
v	molar average inlet velocity, m/s
$V_{C_3H_8}$	molecular volume of C ₃ H ₈ (l) at boiling point
V_{CO}	molecular volume of CO(l) at boiling point
V_{CO_2}	molecular volume of CO ₂ (l) at boiling point
V_{act}	actual volume in washcoat, m ³
V_{air}	molecular volume of air(l) at boiling point
W_p	wetted perimeter of washcoat, m
$W_p A_c$	wetted perimeter to cross-sectional area ratio of washcoat, m ⁻¹
Y_A	mol fraction of gas phase CO
Y_{As}	mol fraction of solid phase CO
Y_B	mol fraction of gas phase CO ₂
Y_{Bs}	mol fraction of solid phase CO ₂
Y_C	mol fraction of gas phase C ₃ H ₈
Y_{Cs}	mol fraction of solid phase C ₃ H ₈
z	position in monolith, m
z_l	reactor length, m
θ_{CO}	CO on catalyst surface
θ_O	O on catalyst surface

θ_{OO}	OO on catalyst surface
θ_V	vacant site of catalyst surface
ΔA_s	differential surface area washcoat, m ²
ΔV_{WC}	differential washcoat volume, m ³
ΔV	differential channel volume, m ³
Δt	time, s
Δz	differential channel length, m
ρ_{air}	density of gas phase, kg/m ³
ρ_{wc}	bulk density of washcoat, kg/m ³
μ	viscosity of air, Pa·s
1D	one dimensional
2D	two dimensional
3D	three dimensional
C ₃ H ₈	propane
CO	carbon monoxide
CO ₂	carbon dioxide
O	oxygen atom
O ₂	oxygen molecule
OO	compressed oxygen
US	United States of America

CHAPTER 1

INTRODUCTION

1.1 Background

Although electric cars has become more popular in today's market, fossil fuel powered vehicles remains the most dominant mode of road transportation. Typically, these vehicles have internal combustion engine that operates with controlled combustion of fossil fuel. However, complete combustion is rarely achieved in the internal combustion engines and as a result, incomplete combustion will generate carbon monoxide and unburned hydrocarbon. Although supply of excess oxygen can drive the reaction of hydrocarbon towards complete combustion, presence of excess oxygen can also promote formation of oxide of nitrogen at high temperature. Even with the most precise control on fuel to air ratio to optimize the combustion reaction, carbon monoxide and oxide of nitrogen will be present in the effluent of engine. (Masters and Ela, 2008)

Carbon monoxide is a poisonous gas. Report published by Chen (2011) in Science of the Total Environment showed that there is short-term associations of ambient carbon monoxide with daily mortality and morbidity from cardiovascular diseases and the findings is consistent for Asia, US and Europe. On the other hand, oxides of nitrogen causes formation of acid rain when dissolved in water vapour in the air. Both oxides of nitrogen and hydrocarbon can cause smog.

As adverse effects from air pollution is gaining more attention, new rules and regulation on controlling emission of harmful gases is introduced. In 1970, United State Congress enacted the first Clean Air Act that requires a 90 percent reduction in toxic emissions from new automobiles by 1975. This leads to the invention of catalytic converter in automobile to control the emission of pollutants gas such as carbon monoxide, nitrogen oxides, and unburned hydrocarbons.

Catalytic converter is commonly installed as a device in the exhaust system of an automobile to convert toxic exhaust gas into less harmful gas. Catalyst metals are introduced in catalytic converter to increase the rate of destruction of toxic gases such as carbon monoxide, nitrogen oxide and unburned fuel resulted from incomplete combustion of fuel.

In a typical catalytic converter for gasoline engines, oxides of nitrogen is first reduced by catalyst into nitrogen gas and oxygen. Reaction equations for the reduction of nitrogen monoxide and nitrogen dioxide is as shown below:



When the exhaust gas flow through the second stage of the converter, carbon monoxide is oxidized into carbon dioxide. At the same time, unburned hydrocarbon is oxidized into carbon dioxide and water vapour. The oxidation reactions occurred in catalytic converter is as shown below:



Only oxidation of ethane vapour is shown above, however, there are more variety of unburned hydrocarbons present in the effluent gas from internal engine. For simplicity purposes, oxidation of other unburned hydrocarbons is not shown here.

1.1.1 Environmental Regulation on Vehicles' Emission

Malaysia started addressing emissions from mobile source in 1977 when Malaysian Government enacted The Motor Vehicle Rules (Control of Smoke and Gas Emissions) as part of the Road Traffic Ordinance of 1958. Excessive black smoke emission from diesel vehicles is controlled under this Act. In 1996, Environmental Quality Regulations 1996 (Control of Emission from Diesel Engines) and Environmental Quality Regulations 1996 (Control of Emission from Petrol Engines) are introduced. Emission from both petrol and diesel vehicles is regulated under these two Acts.

Malaysia adopts the European emission standards for the regulation on light duty vehicle emissions. European emission standards is categorized into 6 stages which are Euro 1, Euro 2, Euro 3, Euro 4, Euro 5 and Euro 6. The European emission standard is shown in the table below.

Table 1.1: European emission standard on CO, NO_x and particulates (Burch, 2004, EUROPA)

Standards	Mass CO (g/km)	Mass HC + NO _x (g/km)	Mass NO _x (g/km)	Particulates (g/km)
Euro 2	1.00	0.70	N/A	0.08
Euro 3	0.64	0.56	0.50	0.05
Euro 4	0.50	0.30	0.25	0.025
Euro 5	0.50	0.23	0.18	0.005
Euro 6	0.50	0.17	0.08	0.005

In 1997, Malaysia has adopted Euro 1 emissions standards for new light-duty vehicles. Euro 2 and Euro 3 standards were subsequently adopted for gasoline powered vehicles in year 2000 and 2007 respectively. Currently, Euro 2 standards is applicable for diesel vehicles while gasoline vehicles are required to comply with Euro 4 standards.

As society becomes more developed, regulations on emission from vehicles will only become more and more stringent in the future. As a result, catalytic converter technology will become more crucial to control toxic gas emission and achieve the emission standard.

1.2 Problem Statement

Catalytic converters allow vehicles to achieve the emission standards. However, performance of catalytic converter depends on many parameters and thus, it is not easy to predict it when designing a new catalytic converter. For example, several studies (e.g. salomons, 2006) shown that conversion of toxic gas is high only when the catalytic converter is at high temperature. During cold start, catalytic converter is not effective. This lead to the asymmetric behaviour when catalytic converter is heated up and cooled down gradually during a drive cycle (Salomons, 2006; Yap, 2011).

To build a better catalytic converter, engineers can conduct test on a pilot-scale model of catalytic converter to predict the performance of the designed product. However, cost for research and development is typically high, and fabrication of catalytic converter with different parameters is tedious and time-consuming. On the other hand, computer simulation on catalytic converter offers a better alternative to understand and predict the catalyst behaviour. With an accurate simulation, engineers can have better understanding on the relationship between specific parameter and effectiveness of catalytic converter without the need of constructing a pilot-scale testing model or proto-type. As a result, the cost and time for development cycle can be reduced.

Despite the numerous advantages offered by simulation, to model the catalytic converter, many proprietary models could not capture some important details during the catalytic combustion. In the converter, for example, the ignition-extinction hysteresis and the change in surface species, although they play important roles in the determining the

performance of catalyst. It is uncommon to see models of catalytic converters that could accurately model the ignition-extinction hysteresis with the reaction mechanism that agree with the observation from surface science studies (Engel and Ertl, 1979).

1.3 Aims and Objectives

The aim of this project is to simulate the ignition-extinction hysteresis observed during the catalytic combustion of a diesel oxidation catalyst. A diesel oxidation catalyst is the name commonly used to describe the catalytic converter installed in diesel-powered vehicles.

The computer model built to simulate the ignition-extinction hysteresis is based on the experimental work carried out by Ye *et al* (2011) where diesel exhaust stream was passed through a 5mm thin slice cut from a commercial diesel oxidation catalyst. This project aims to achieve the following objectives:

- Construct mathematical models to represent the mass transfer and heat transfer for 1D-gas phase and 1D-solid phase single channel monolith model. The reaction mechanism postulated by Salomons *et al* (2007) will be used as the kinetic model to describe the CO oxidation on platinum surface
- Program the mathematical equations using Python and use the *odeint* solver in the NumPy package to solve the ordinary differential equations and partial differential equations that represent the single channel monolith model
- Kinetic parameters are tuned to simulate the ignition-extinction hysteresis as observed from the experimental work carried out by Ye *et al* (2011).
- To study the effect of the change of kinetic parameters on the catalytic behaviour of the diesel oxidation catalyst

1.4 Scope of Study

This report comprises of the following chapters:

Chapter 2: Literature Review

- Brief review of operation of catalytic converter and its structure.
- Review of research done on ignition-extinction hysteresis
- Review on CO oxidation models and postulated reaction mechanisms
- Introduction to simulation by using Python programming

Chapter 3: Methodology

- Formulation of mathematical models for single channel monolith
- Formulation of mathematical models for CO oxidation
- Method of solving mathematical models by using Python programming

Chapter 4: Results and Discussion

- Analysis and interpretation of results from transient response simulation of single channel monolith

Chapter 5: Conclusion and Recommendations

- Conclusion of the research
- Recommendations to improve the accuracy of the simulations.

CHAPTER 2

LITERATURE REVIEW

2.1 Diesel Exhaust Emission Control System

Apart from generating the heat required to perform mechanical work, the combustion of fuel in the internal combustion engines also produce exhaust gas. These exhaust contain components such as carbon monoxide (CO), unburned hydrocarbons and nitrogen oxides (NO_x) that are harmful to human health and environment. Because of this, the exhaust gases are usually treated before they can be safely emitted into the atmosphere. Depending on the overall design of the exhaust system, the key features of an emission control system for a diesel-powered vehicle is shown in Figure 2.1.

Typically, the exhaust gas generated from the combustion of fuel in diesel engine is collected at the exhaust manifold. In certain designs, the exhaust gas drives the turbine for the turbochargers to increase the engine power by forcing extra air into the combustion chamber.

The exhaust gas then passes through the diesel oxidation catalyst where CO and hydrocarbons are oxidized to form carbon dioxide (CO₂) and water vapour. Generally there are two types of catalytic converters, i.e.: (a) diesel oxidation catalyst; (b) three-way catalyst. The diesel oxidation catalysts only oxidize CO and unburned hydrocarbons and they are mainly found in diesel-powered vehicles. On the other hand, a three-way catalytic

converter found in gasoline-powered vehicles can control the emission of nitrogen oxides (NO_x) in addition to the oxidation of CO and hydrocarbons (Volkswagen, 2015).

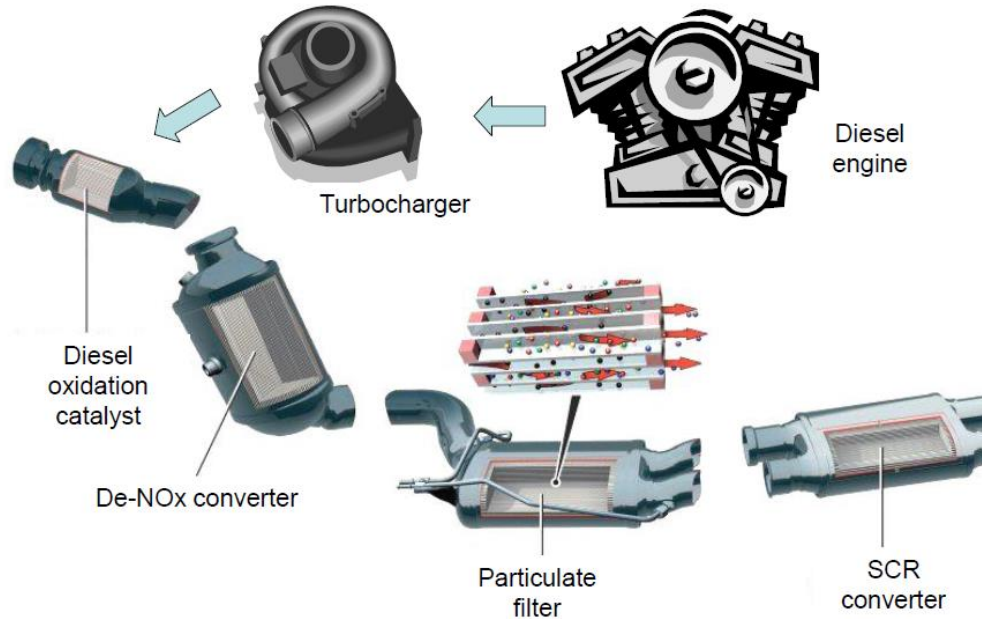


Figure 2.1: Modern Diesel Exhaust Gas System (adapted from Mercedes BLUETEC, 2007)

Due to the lean burn (oxygen rich) condition present in the diesel exhaust stream, the conversion of nitrogen oxides is generally not efficient in the diesel oxidation catalyst. Therefore, an additional de-NO_x converter (or NO_x adsorber) is usually installed after the diesel oxidation catalyst to bring down the level of NO_x. The de-NO_x converter features material made from zeolite that will trap and adsorb the NO and NO₂. When the capacity for NO_x adsorption is saturated, the NO_x compounds are purged *via* different proprietary technologies such as the injection of hydrocarbon fuel to form water and nitrogen (Parks II *et al*, 2012).

Compared to exhaust gas produced from gasoline engine, diesel exhaust stream tends to contain higher level of particulate matters (or soot). For this, diesel particulate filter (DPF) are commonly employed to reduce the level of particulate matters (United States Environmental Protection Agency, 2010). Typically, diesel soot is trapped in the

DPF, which has to be cleaned (regenerated) regularly to maintain the DPF efficiency. Regeneration can be done by combusting the soot with oxygen at above 550°C. However, the normal temperature of the exhaust gas is usually lower than this. Generally in practice, there are two ways to burn the diesel soot in a DPF: (a) by periodically injecting the fuel into exhaust gas which raise the temperature through oxidation of the fuel by platinum catalyst (Johnson Matthey, 2002); (b) oxidation of NO to NO₂ over a platinum catalyst. In fact, NO₂ is a much more powerful oxidising agent than oxygen and because of this, soot can be burned with NO₂ at temperature as low as 250°C. This concept is utilized in the Continuous Regenerating Trap (CRT) technology (Johnson Matthey, 2002).

NO_x control in catalytic converter (diesel oxidation catalyst) does not work effectively under high oxygen content which is common for diesel-powered vehicles. A relatively common approach to remove NO_x is to include selective catalytic reduction (SCR) (RTI International, 2003) after the diesel particulate filter (DPF). SCR works by injecting reducing agent, such as automotive-grade urea into the exhaust gas stream. Reactions take place on the surface of the SCR catalyst where NO_x is reduced by urea to form nitrogen, CO₂ and water.

Following the removal of NO_x from exhaust gas, the cleaned exhaust gas then passes through a silencer (also known as muffler) before it is emitted to the atmosphere.

2.2 Diesel Oxidation Catalyst

The focus of this project is the catalytic converter, specifically the diesel oxidation catalyst for the diesel exhaust emission control systems. Therefore, a more comprehensive review is provided below.

A typical catalytic converter consists of substrate, washcoat and catalyst nanoparticles embedded in washcoat as shown in Figure 2.2 below:

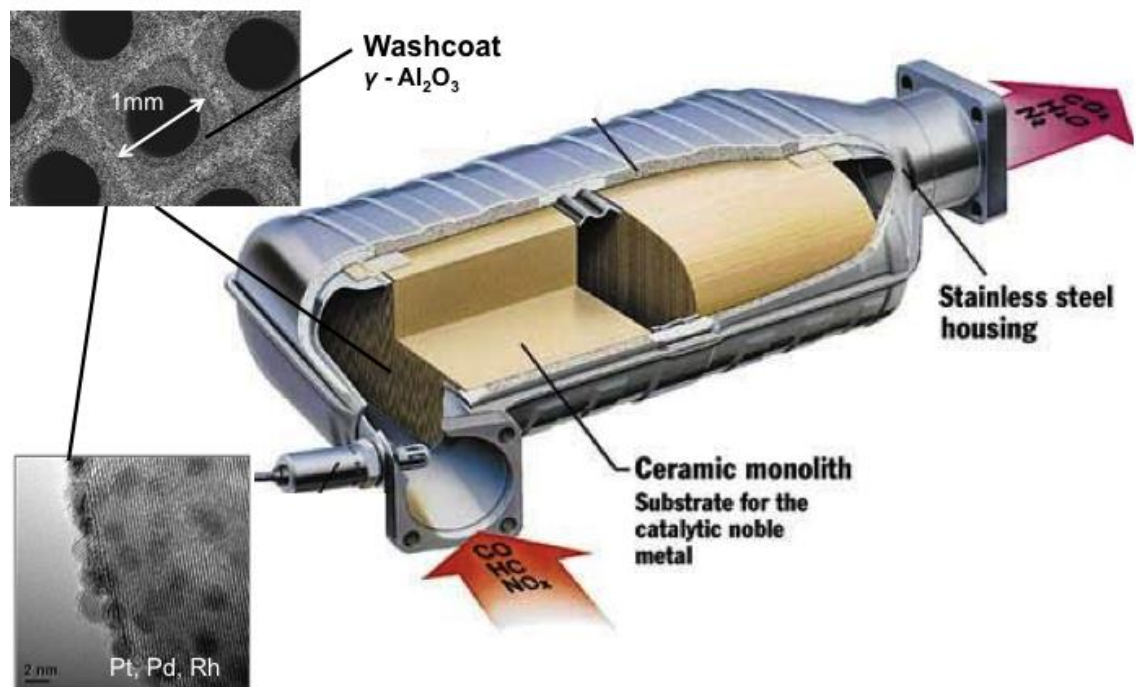


Figure 2.2: Overview of a catalytic converter that shows the substrate, washcoat and metal catalyst nanoparticles (adapted from Rao *et al.*, 2009)

2.2.1 Substrate

Substrate is the main support for the catalytic converter, which is represented as the ceramic monolith in Figure 2.2. Typically, substrate is made of refractory materials which has the ability to withstand high operating temperatures with low thermal expansion. As reported in Hayes and Kolaczkowski (1997), cordierite ($2\text{MgO}\cdot 2\text{Al}_2\text{O}_3\cdot 5\text{SiO}_2$) is mainly made from kaolin, talc and alumina. The macroporous structure of the cordierite support facilitates the anchoring of the washcoat layer (Nijhuis *et al*, 2001).

Multichannels monolith or honeycomb structures are commonly used substrate for catalytic converters. The unique design of multiple channels (about 1mm diameter) in monolith provide high surface-to-volume ratio which enhance the exposure of exhaust gas to the catalyst. The monolith structure also allows particles to pass through easily without clogging the channel and causing minimal pressure drop to the flow.

2.2.2 Washcoat

Washcoat is a layer of porous structure on the monolith channels that increases the surface area for the contacting between exhaust gas molecules and catalyst metals. Alumina (Al_2O_3) is the most common material as the washcoat layer in catalytic converter. With an increase in surface area, washcoat acts as a support for the metal nanoparticles.

As exhaust gas passes through the washcoat, gas molecules diffuse through the pores in washcoat and adsorbed on the surface of metal nanoparticles. It is at the surface of these metal nanoparticles that reactions take place to convert CO, hydrocarbons and NO_x to more benign materials such as carbon dioxide, water, and nitrogen.

2.2.3 Catalyst

Platinum, palladium and rhodium are three common precious metals that are used in catalytic converter. Platinum and palladium nanoparticles (typically 2 – 30 nm) are responsible for most of the oxidative reactions in catalytic converters such as oxidation of CO and unburned hydrocarbon. For exhaust systems incorporated with a continuous regeneration trap (CRT), platinum catalyst can also oxidize NO to NO₂ which is then used as an oxidising agent to remove particulate matter in diesel particulate filter (DPF). On the other hand, rhodium is better used for the reductive reaction that converts NO_x to nitrogen.

2.3 Heterogeneous Catalysis in Catalytic Converter

The reactions in catalytic converter are considered as heterogeneous as the gas phase reactants are catalysed by solid catalyst. Heterogeneous reaction can be represented as a series of individual elementary steps (Fogler, 1999):

Step 1: Mass transfer of the reactants from the bulk fluid to the external surface of the washcoat.

Step 2: Diffusion of the reactants to the catalyst from the pore mouth through the catalyst pores to the immediate vicinity of the internal catalytic surface.

Step 3: Adsorption of the reactant(s) onto the catalyst active sites (chemisorption).

Step 4: Reaction at the active sites (of platinum) and conversion of reactants to product(s).

Step 5: Desorption of product(s) from catalyst active sites.

Step 6: Diffusion of the products to the catalyst through the pore channel to the pore mouth

Step 7: Mass transfer of the products from the external surface to the bulk fluid.

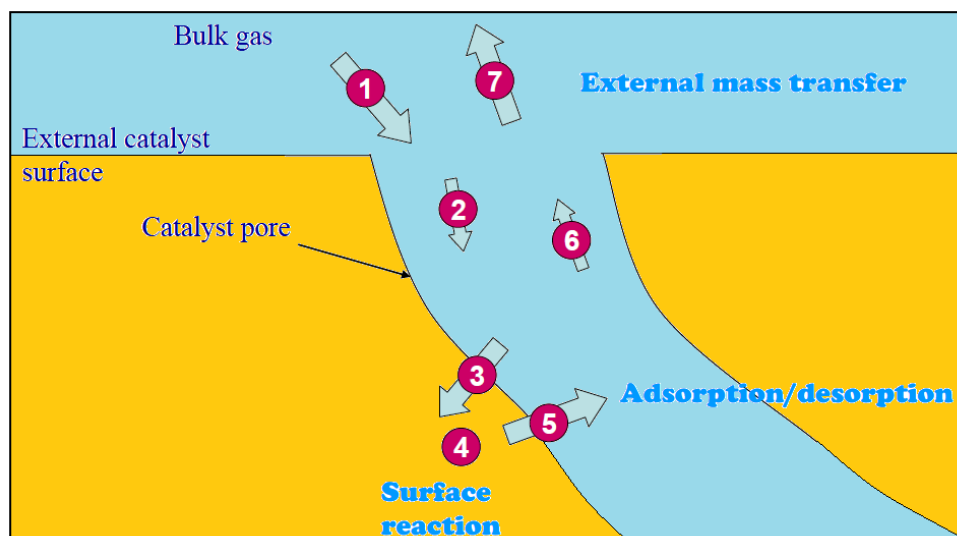


Figure 2.3: Steps of heterogeneous solid-gas catalytic reaction (adapted from Froment and Bischoff, 1990)

On the surface of the catalyst, catalysed transformation of gas-phase species A and B to product C can arise from two distinct mechanisms: (i) Langmuir-Hinshelwood (LH); and (ii) Eley-Rideal (ER). Both types of surface reactions is illustrated in Figure 2.4. In LH surface reaction mechanisms, both species A and B are attached to the catalyst surface followed by atomic reorganization; while in ER surface reaction mechanisms, either one of the gas-phase species is bound on the catalyst surface when the other species impinges upon it from gas phase.

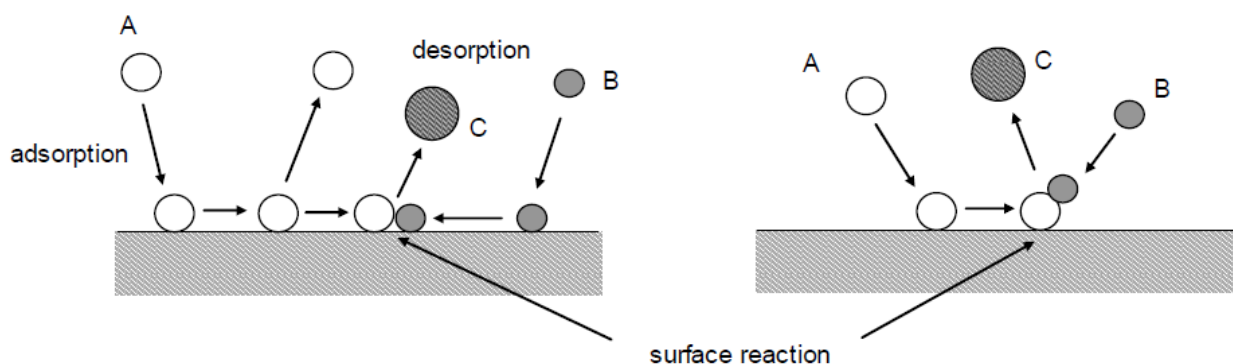


Figure 2.4: Two possible mechanisms of heterogeneous solid-gas catalytic reaction: Langmuir-Hinshelwood (LH) mechanism (left) and Eley-Rideal (ER) mechanism (right) (adapted from Thomas and Thomas, 1999).

2.4 Ignition-Extinction Hysteresis

There are many studies that can be performed when testing and benchmarking the performance of a catalytic converter. The most common one is the conversion of toxic compounds (e.g. CO, hydrocarbons) at a given temperature with the given amount of catalyst. For example, at a temperature of 200°C, the CO conversion of converter A is 30% and CO conversion of converter B is 40%, which indicates that converter B performs better.

Instead of comparing the conversion of the pollutants (e.g. CO) at a given temperature, the automotive industry favours the use of ignition point, which is defined as the inlet gas temperature when the conversion of a reactant (e.g. CO) is 50% (Salomons *et al.*, 2006) at steady state. The ignition point is used extensively to benchmark the performance of different catalytic converters. A lower ignition point for a catalytic converter means that the catalyst is able to convert 50% of the pollutants at a lower temperature (e.g. 180°C), which means the catalyst is more efficient than a catalytic converter that has a higher ignition point (e.g. 200°C).

However, this steady state ignition point does not reflect the highly transient nature of the reactions taking place in a catalytic converter. Frequently, a drive cycle in the urban area (see Figure 2.5) includes many accelerations and decelerations that come from frequent turnings and traffic light stops. As a result, the exhaust gas flow rate and temperature also vary considerably throughout the drive cycle.

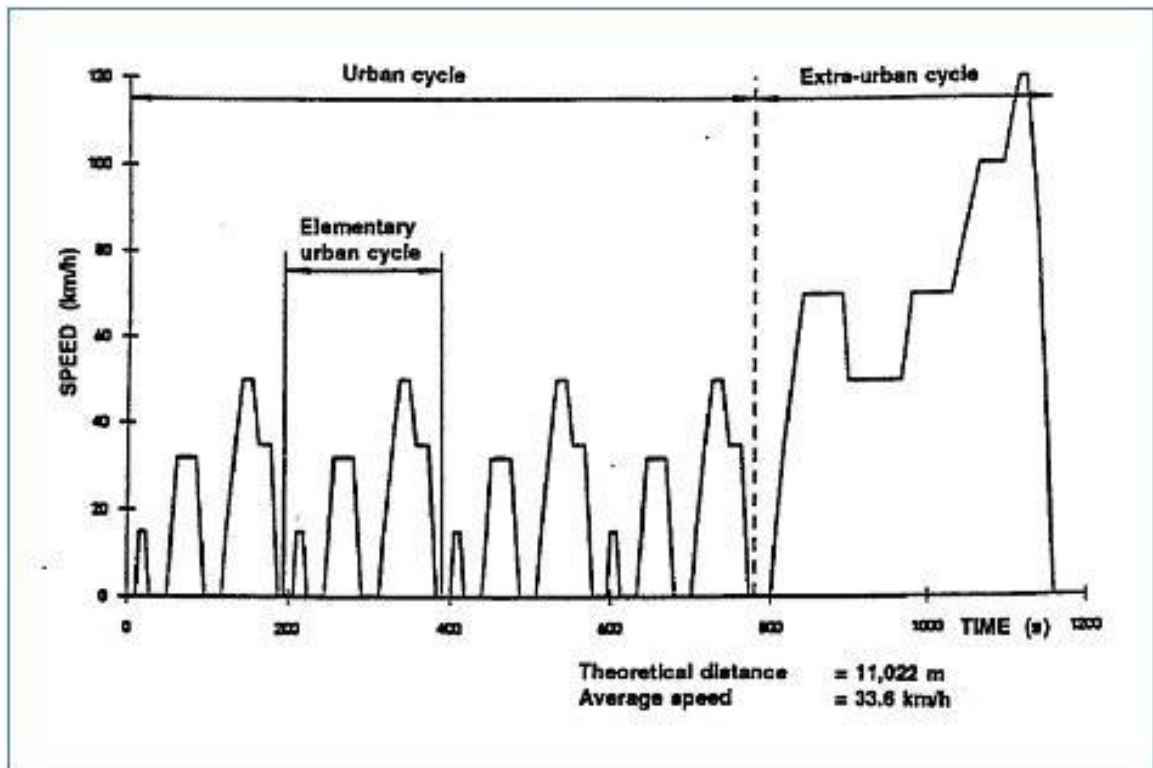


Figure 2.5: New European Drive Cycle (NEDC) represents the typical usage of a car in Europe. It shows the speed of vehicles in a drive cycle

The more representative test that is favoured by the current catalyst researchers and developers is the temperature ramp up and ramp down experiments. Typically, this test is carried out by keeping the velocity and the concentration of toxic compounds (e.g. CO, hydrocarbons) constant for the entering exhaust gas into the catalytic converter. The temperature of the entering exhaust gas is increased (ramp up) and decreased (ramp down) according to a set temperature program (see Figure 2.6). The conversion of the toxic compounds (e.g. CO) is then assessed and plotted on a conversion vs. temperature curve. An example of this graph for conversion of CO is shown in Figure 2.7.

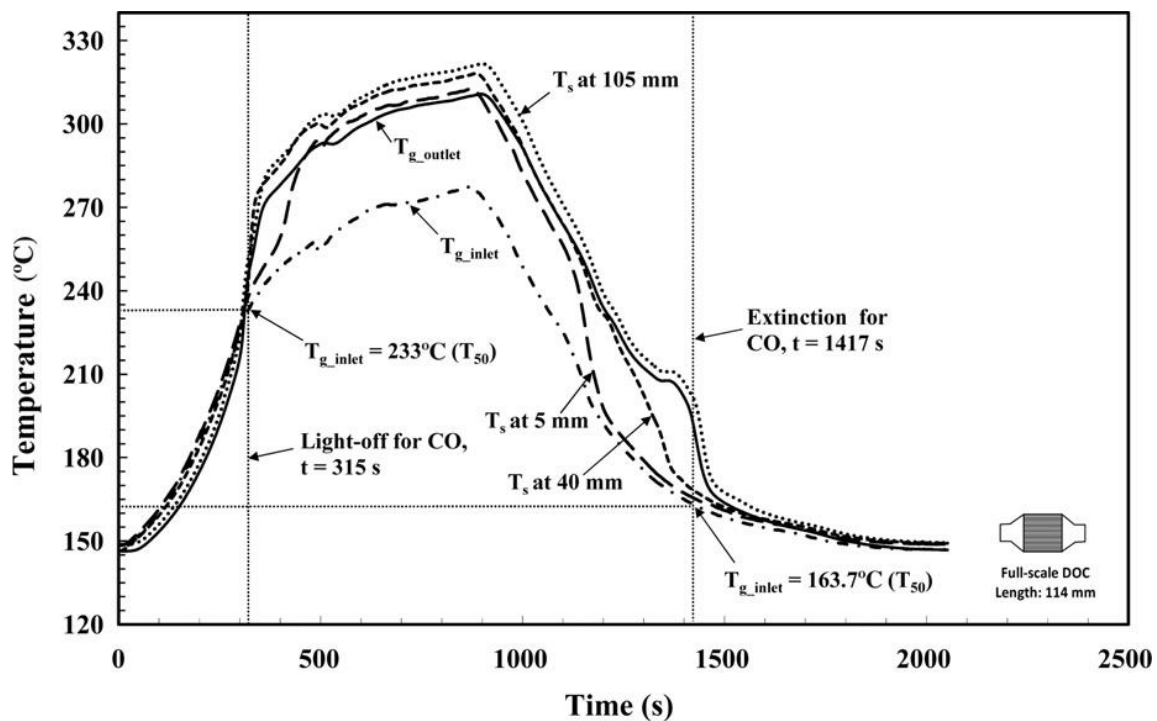


Figure 2.6: Typical temperature profile for the temperature ramp up and ramp down experiments (adapted from Ye, 2011)

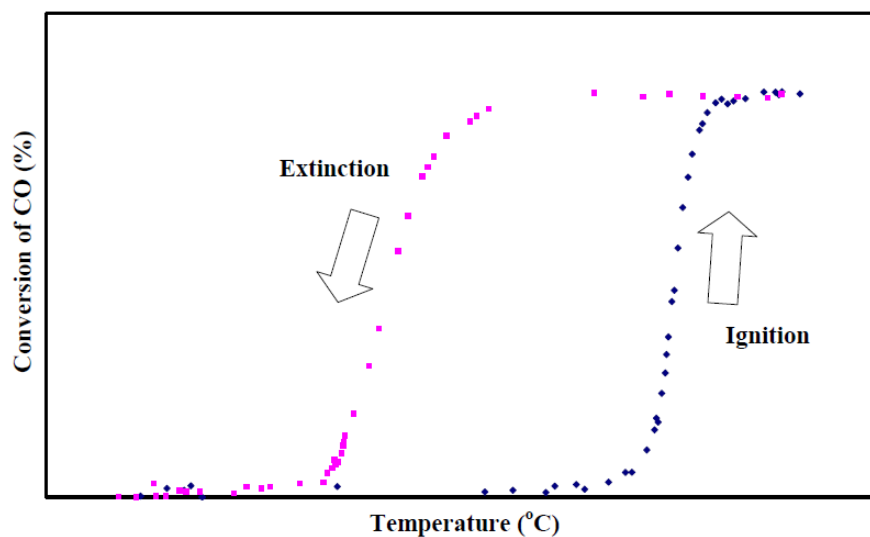


Figure 2.7: A typical ignition-extinction hysteresis curve (adapted from Yap, 2011)

There are two distinct curves in Figure 2.7: (i) ignition front at higher temperature and (ii) extinction front at lower temperature. Typically at low temperature (e.g. $< 170^{\circ}\text{C}$), there is zero conversion and reaction is inhibited. When the temperature of the entering

exhaust gas (to the catalytic converter) is increased from low temperature (i.e. $< 170^{\circ}\text{C}$) to high temperature ($> 170^{\circ}\text{C}$), there is a rapid surge in CO conversion. This is known as ignition, or more commonly known as “light-off” in the automotive industry. However, when the temperature of the entering exhaust gas is decreased (from high to low), the CO conversion remains high. It is only until a further drop in exhaust gas temperature (typically 130°C) that will result in the decrease in CO conversion. This is known as extinction.

The asymmetric behaviour between ignition and extinction curves is known as the ignition-extinction hysteresis. The ignition and extinction curves can be affected by several parameters such as the concentration of the pollutants (e.g. CO, hydrocarbons) for the inlet gas and the rate of temperature ramp up and ramp down. They are discussed in more detail in the following subsections.

2.4.1 Effects of change in inlet CO concentration to ignition-extinction hysteresis

Salomons *et al* (2006) have performed experiments to obtain the ignition-extinction curves for different inlet CO concentrations. The ignition-extinction curves are generated by steady increase in inlet gas temperature until 623K and maintained for about 30 min. After all temperatures in monolith were higher than 573K, inlet gas temperature is lowered at steady cooling rate. The result of the experiment is shown in Figure 2.8. The experiment shows that the inlet CO composition can affect the ignition and extinction points. Increasing CO concentration in inlet gas causes a higher light-off temperature or ignition point.

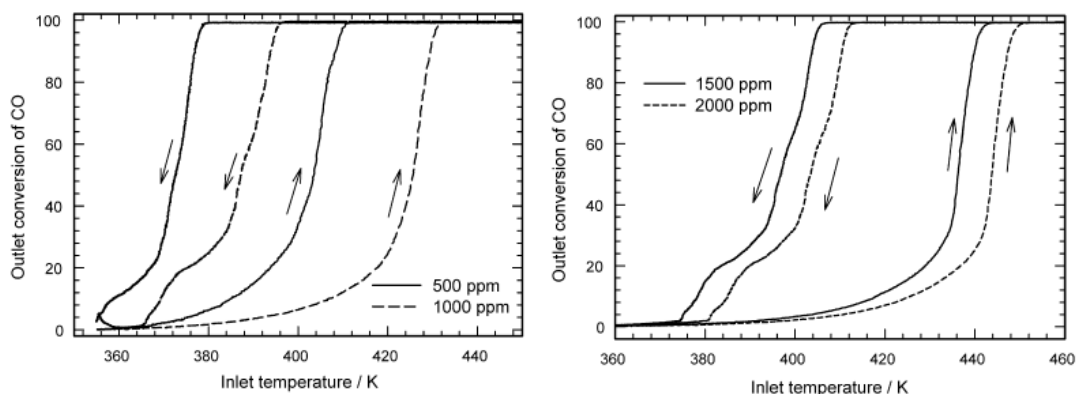


Figure 2.8: Experimental ignition-extinction curves generated from different inlet CO concentrations. (adapted from Salomons, 2006)

In another ignition-extinction experiment by Ye *et al* (2011) using a 5mm thin slice diesel oxidation catalyst, they also found that the increase in inlet CO concentration (3000 ppm to 5000 ppm) also shift the ignition and extinction curves to a higher temperature (see Figure 2.9). Unlike the experiment performed by Salomons (2006) where laboratory grade gases are used, Ye *et al* (2011) used the exhaust gas generated from on-line diesel engine as the inlet gas to the converter. Despite this difference, their observations confirmed the existence of both ignition and extinction.

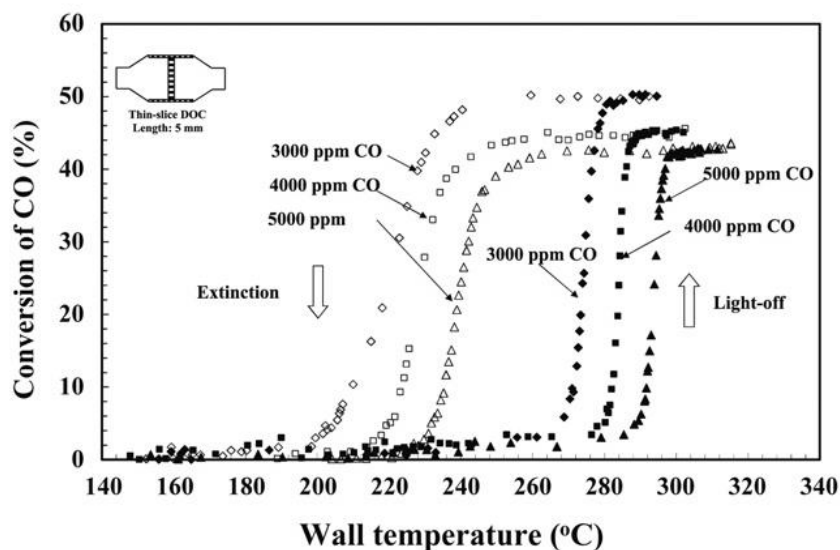


Figure 2.9: Ignition-extinction hysteresis curves for different inlet CO concentration on a 5mm thin slice diesel oxidation catalyst (adapted from Ye *et al*, 2011)

2.4.2 Effects of change in rate of temperature ramp up to ignition-extinction hysteresis

The effect of the rate of temperature ramp-up on the ignition was studied by Ye *et al* (2012). In their experiment, Ye *et al* maintained the inlet CO level at approximately 3000 ppm and increased the temperature of the inlet gas from 146K to 275K. The period of time (90s, 300s, 600s) at which the temperature ramped up was studied to see the change in the ignition curves. They found that when the rate of temperature ramp up is fast (from 146K to 275K in 90s), the ignition curve is at higher temperature than when the rate of temperature ramp up is slower (i.e. 300s and 600s) (see Figure 2.10).

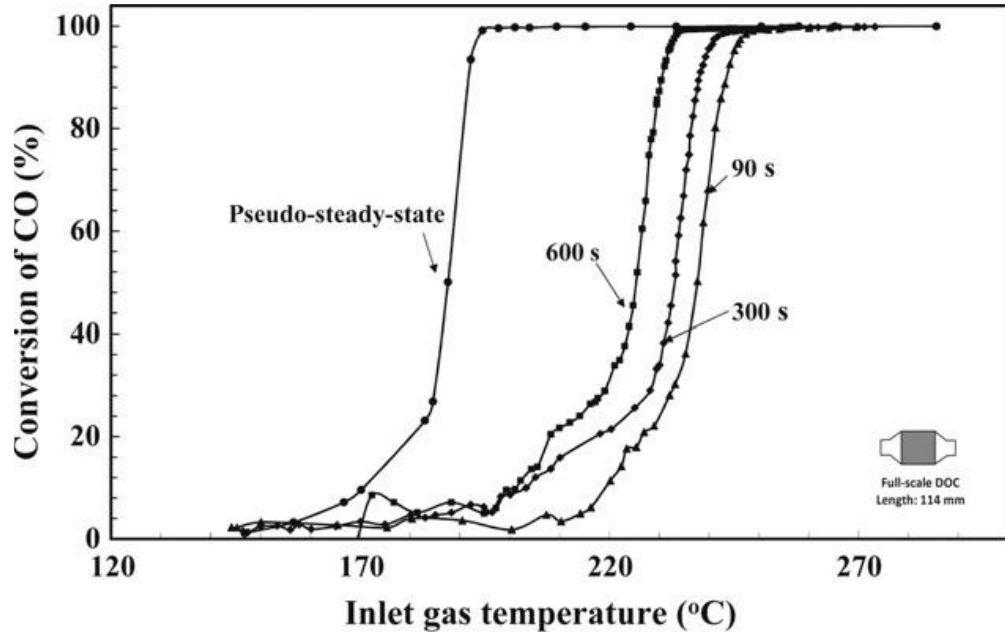


Figure 2.10: Transient ignition-extinction hysteresis curve for different ramp-up temperature (adapted from Ye *et al*, 2011)

Ye *et al* (2012) reasoned that this phenomenon can be explained by the fact that the catalyst requires time to allow the reaction take place and heat up the catalyst to achieve the ignition. A slower rate of temperature ramp up (e.g. 600s) will allow a longer period of time for the catalyst to heat up to higher temperature and produce higher rate, compared to that of a faster temperature ramp up (e.g. 90s) which only has a short period of time for the catalyst to heat up.

2.4.3 Other factors that affect the ignition-extinction hysteresis

Other factors can also affect the ignition and extinction curves such as the type of catalyst used, flow rate of the inlet gas and the presence of other gas species in the inlet gas to the catalytic converter (Yap, 2011). However, they are not discussed in this report.

2.4.4 Theoretical explanation for ignition-extinction hysteresis

Ignition-extinction hysteresis can be explained with the help from experimental observations under ultrahigh vacuum (UHV) condition. For example, Engel and Ertl (1979) explained that the asymmetric behaviour seen in ignition-extinction curve is due to high CO coverage on the catalyst surface that is unable to dissociatively adsorb oxygen and therefore inhibiting surface reaction. However, if oxygen is adsorbed on the surface first, CO molecules are still able to adsorb on the surface saturated with O atoms. This is due to the ability of CO to “compress” the adsorbed O layer.

As explained in more detail by Ertl (2000), the inhibition of CO oxidation at low temperature is due to the way the CO molecules and O₂ molecule adsorb on the catalyst surface. Take Pt(111) as example, CO molecules are bonded through the carbon atom in “on top” or in “bridge” positions as illustrated in Figure 2.11(i). On the other hand, O₂ molecule adsorb on to the catalyst surface by dissociating itself into two O atoms and both O atoms adsorb on threefold-coordinated sites which then form a more open mesh of a 2×2-structure as illustrated in Figure 2.11(ii).

Thus, in order to allow dissociation of O₂ molecules, an ensemble of neighbouring empty surface atoms is required. This explains why when the catalyst is covered with CO, oxygen is unable to adsorb on the catalyst due to lack of empty space and hence causing the inhibition of reaction. On the other hand, when the catalyst surface is covered with oxygen atoms, the open structure of the adsorbed O-layer still permits the adsorption of

CO with CO molecules occupying empty “on top” positions within the O-2×2 unit structure. CO molecules is said to “compress” their environment of adsorbed O into domains of a higher density oxygen phases (see Figure 2.11(iii)). As a result of the compression, the repulsive interaction between the adsorbed oxygen atoms lowers the effective bond strength with the surface and reactivity between adsorbed CO and O increases. The CO and O then combined and desorbed from the surface as CO₂.

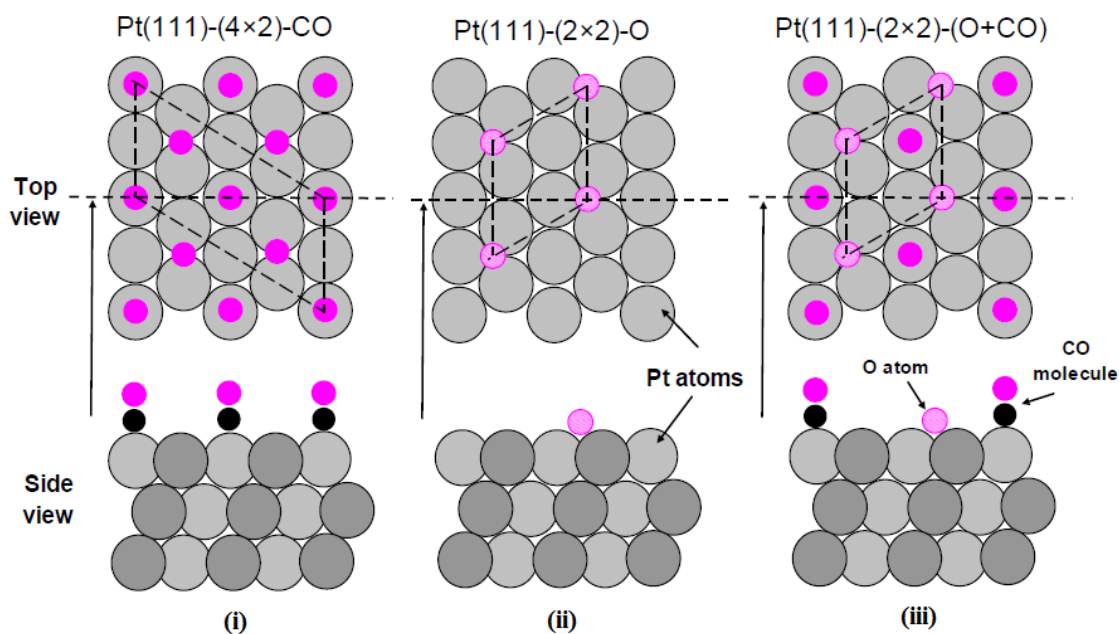


Figure 2.11: Chemisorbed species on a Pt (111) surface at low coverages: (i) adsorption of CO, (ii) adsorption of O and (iii) adsorption of CO within O-2×2 unit structure. (adapted from Engel, 2000)

In another review by Yap (2011), the ignition-extinction hysteresis (as seen in Figure 2.9) can be described by the following steps:

- 1) CO adsorption is favoured at low temperatures, when CO occupies most of the available active sites, this forbids the adsorption of oxygen. (see Figure 2.12a)
- 2) Ignition begins when CO starts to desorb from the catalyst surface at a sufficiently high temperature (e.g. 180°C), and thus allows molecular oxygen to dissociate and adsorb onto the active sites. (see Figure 2.12b)
- 3) When both CO and O are adsorbed on the active sites, surface reactions take place between adsorbed CO and O (see Figure 2.12c). As CO reacts with the adsorbed O, the depletion of adsorbed CO from the surface allows more O₂ to adsorb.
- 4) At some critical point, a catalytic ignition occurs, thus triggering an abrupt reaction rate and rapid transition from a CO covered surface to an O covered surface. At this point, the heat generated by the chemical reaction is not balanced by the heat losses and the catalyst temperature rises rapidly. The rise of temperature leads to an increased surface reaction rate, generating even more heat, further favouring the CO desorption and reaction, resulting in a self-accelerated reaction rate.
- 5) The catalytic system then stabilises in a new high reactive state where the heat generation is perfectly balanced by the heat losses.
- 6) At high temperatures, the oxygen covered surface allows the CO to compress the adsorbed oxygen into a high density phase (see Figure 2.12d). As a result of the compression, the repulsive interactions between the adsorbed oxygen atoms lower the effective bond strength with the surface, and gives rise to an enhanced reactivity (lower activation energy) with adsorbed CO.
- 7) The catalyst surface is still covered by a high density oxygen phase when the catalyst temperature drops, therefore the reaction rate remains high because of the enhanced reactivity between adsorbed CO and the high density oxygen phase. This gives rise to hysteresis (two values of reaction rates at one temperature point).

- 8) As catalyst temperature dropped, the surface environment no longer favours the production of the high density oxygen phase. Also when the catalyst temperature drops, the rate of CO adsorption will also increase. Eventually, the surface reaction rate drops because of a depletion in high density oxygen.
- 9) As the rate of CO adsorption increases, the catalyst surface returns back to a CO covered state. (see Figure 2.12a)

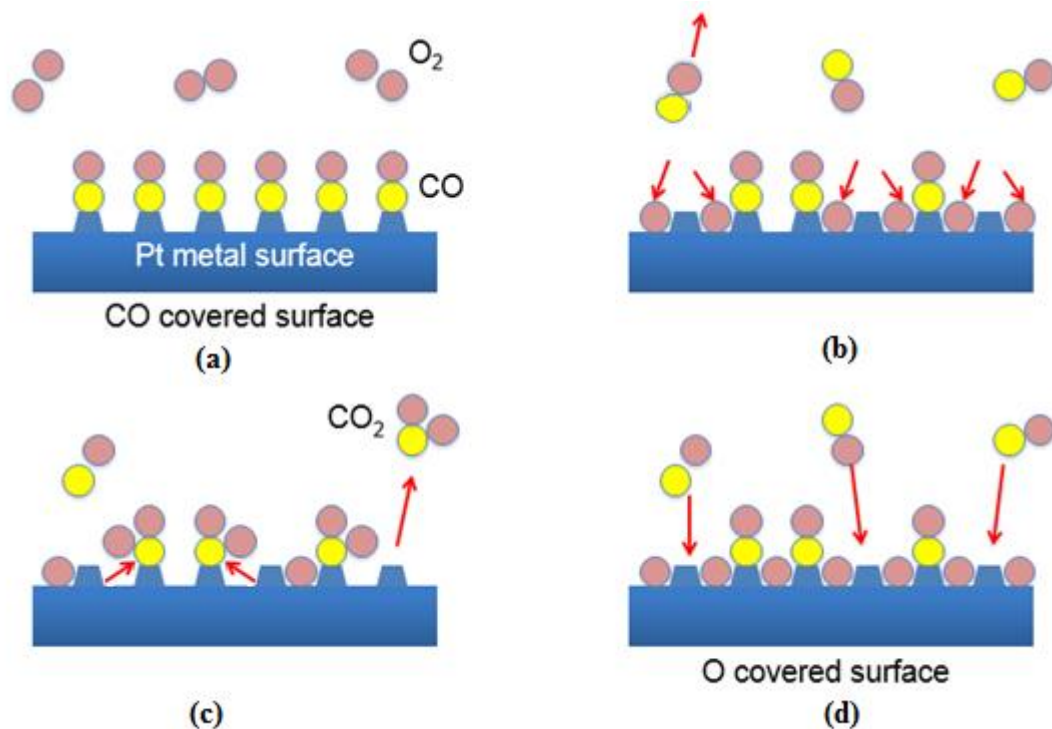


Figure 2.12: Illustration of CO and O adsorption on the surface during ignition and extinction (adapted from Yap, 2011)

2.5 Modelling ignition-extinction hysteresis

There is an increasing interest among automotive catalyst researchers in simulating the ignition-extinction hysteresis for catalytic converter as it captures a far richer detail than a steady-state ignition point (see Chapter 1.4).

From a chemical engineering perspective, a catalytic converter is basically a chemical reactor. Therefore, in addition to transport models (to account for mass and heat transfer), a kinetic model is necessary to calculate the reaction rate for the reactions taking place in the catalytic converter.

It is a well-known fact that every chemical reaction proceeds according to a reaction mechanism, which is a step-by-step description of what occurs during a reaction on the molecular level. Take the oxidation of CO on a catalyst as example, a possible reaction mechanism may involve:



CO is first adsorbed on an active site, θ_v on the catalyst surface and form adsorbed CO species as represented by equation (2.1). At the same time, oxygen molecules dissociate into two oxygen atoms forming two adsorbed oxygen species (equation 2.2). The adsorbed CO and adsorbed O then reacts and form CO_2 and leave behind two vacant active sites (equation 2.3).

There are three individual elementary steps in the CO oxidation above. At steady-state condition, the rates of these elementary steps are equal to one another and the overall rate is limited by the slowest step (rate limiting step). This enables the simplification of every elementary step into a single global rate expression in the form of power law where the rate is expressed in terms of bulk fluid concentration.

A classic example of power law rate expression that is used in many catalytic converter simulations is the Voltz *et al* (1973) type expression. For the oxidation of CO in oxygen with propylene and NO in the background on a Pt/Al₂O₃ catalyst the rate can be represented as:

$$r_{CO} = \frac{-k_1 c_{CO} c_{O_2}}{R(\theta)} \quad 2.4$$

where $R(\theta)$ is a resistance term which includes the inhibition effects of CO and hydrocarbons on the reaction rates. c_i is the concentration of component i , k_a is the rate constants and can be further derived as:

$$k_a = A_a \exp\left(-\frac{E_a}{RT}\right) \quad 2.5$$

where A_a is the pre-exponential factor, E_a is the activation energy, R is the universal gas constant and T is the temperature of the catalyst in K. The unit for rate of reaction is mol_{CO} m⁻² s⁻¹

For this type of equation, it is assumed that there is only a single rate determining step. Moreover, kinetic parameters are lumped together in a single equation and that means this type of expression is not well suited for transient reactions condition such as the ignition-extinction observed in the catalytic converter. Yap (2011, pg.4-28) has shown that the global reaction model is unable to simulate the ignition-extinction hysteresis in the diesel oxidation catalyst.

To simulate the ignition-extinction hysteresis, the rates of the individual elementary steps must be computed separately. Additionally, variation of surface coverage of adsorbed species with time should be taken into consideration. To account for this, mechanistic models have been developed by various researchers to simulate the ignition-extinction hysteresis.

In general, the mechanistic reaction models assume the following to simplify the computation:

- i) All active sites are identical (with no particular affinity to a specific adsorbate).
- ii) There is no interaction between adsorbed species other than reaction.
- iii) Adsorbed species are randomly distributed over the array of sites (mean-field).
- iv) Adsorbates compete for the same adsorption sites (competitive chemisorption).

The following subchapters discuss some of the examples of mechanistic models found in the literature specifically developed for catalytic converters.

2.5.1 Nibbelke *et al* (1998)

The transient kinetic model developed by Nibbelke *et al* (1998) is specifically developed for a Pt/Rh/CeO₂/γ-Al₂O₃ pellet catalyst. The reaction mechanism consists of the following steps:

Adsorption and desorption of CO:



where * denotes vacant active site and CO* denotes adsorbed CO species:

Adsorption of O₂:



Reaction (2.8): $* + O_2^* \rightarrow 2O^*$ is the instantaneous dissociation of adsorbed O_2 to O .

Surface reaction (Langmuir-Hinshelwood step):



Surface reaction (Eley-Rideal step):



Desorption of OCO^* :



It can be seen that the competitive adsorption of CO and O_2 , followed by a bimolecular surface reaction, will result in the inhibition of CO adsorption by pre-adsorbed oxygen. This means that without the Eley-Rideal step, exposure of the catalyst surface to both CO and oxygen will over time, result in a completely oxygen covered surface. With this, all sites will be covered by O and impossible for the CO to adsorb. To solve this problem, Nibbelke *et al* (1998) employed the Eley-Rideal step to account for the adsorption of CO onto active sites already covered by adsorbed oxygen. This resulted in the formation of OCO^* species as shown in equation (2.11).

2.5.2 Chatterjee *et al* (2001)

The mechanistic model was developed for three way catalysts $Pt/Rh/CeO_2/\gamma-Al_2O_3$. Chatterjee *et al* (2001) used a small variation of the Langmuir-Hinshelwood (LH) model. All steps in this reaction mechanisms are considered to be reversible. Reaction mechanisms proposed by Chatterjee *et al* (2001) consisted of the following steps:





This model accounts for the ability of CO adsorption on an oxygen-covered surface by allowing oxygen to desorb from the catalyst surface. Thus, Eley-Rideal step is no longer necessary to account for the ability of CO to adsorb on the oxygen-covered surface.

2.5.3 Salomons *et al* (2007)

As described by Engel *et al* (2000), CO can adsorb on the oxygen covered surface by compressing oxygen to a level not achievable by adsorption of oxygen alone. To account for this phenomenon, Salomons *et al* (2007) added an extra step to the CO oxidation mechanism developed from work by Chatterjee *et al* (2001). This extra step allows CO to adsorb on an oxygen covered surface, by “compressing” the already adsorbed oxygen onto fewer sites. From his modelling work, Salomons *et al* (2007) has shown that the simulation of kinetic model using this “compressed oxygen” reaction mechanism can produce ignition-extinction hysteresis.



2.6 Modelling

In recent years, the use of computer modelling and simulation in the research and development of catalytic converter has become more widespread as it helps save resources and shorten the product development time. Catalyst manufacturers have increasingly relied on it to design many complex emission control systems (discussed in Chapter 1.1) to meet the increasingly stringent environmental regulations. This trend will only continue in the future.

Despite the benefits offered by computer modelling, there are many considerations that have to be taken into account when modelling a catalytic converter and they are discussed in greater detail in the following subchapters.

2.6.1 Steady-state and Transient Modelling

In many industrial applications, reactors are almost always operated at steady state, with little change in temperature, feed rate and pressure throughout the operation. Therefore it makes sense to use a steady-state model to represent the reactor as a steady-state model can simplify the computation. In this type of model, the kinetic expressions are usually represented by a single power law equation (example see equation 2.4) as all reaction steps limited by the rate limiting step.

On the other hand, reactions taking place in catalytic converter is highly transient in nature with substantial change in temperature and flow rate as seen in a catalytic converter. At the same time, the coverage of adsorbed species on the catalyst surface also varies significantly. To accurately simulate and predict the behaviour in this type of reactor, unsteady-state model that describes the change of variables (e.g. temperature, concentration and coverage of surface species) with time is necessary. The simulation of ignition-extinction hysteresis in catalytic converter falls under this category.

2.6.2 Single channel and multi-channel models

A typical catalytic converter consists of thousands of channels arranged in parallel (Figure 2.2). As such, a detailed model of catalytic converter should reflect the design of multi-channel monolith structures. In this type of model, the entire monolith structure can be modelled, and the distribution of temperature and gas concentration in the radial direction can be readily investigated, which is not possible in a single channel model.

However, in most cases, catalytic converter is more often modelled as a single channel model. The main assumption with this model is that a single channel can represent all the channels in the monolith structure. The main advantage with single channel model is its simplicity as it greatly reduces the cost of computation (Mukadi and Hayes, 2000)

2.6.3 1D and 2D Modelling

The choice of 1D, 2D and 3D models can affect the accuracy of catalytic converter simulation. A higher level of details offered by 3D models can enhance the accuracy of the model at the expense of higher computation resource.

For 1D model, a simplifying assumption frequently made is that the fluid flows through the reactor in plug flow and therefore 1D models only consider axial variations while the radial and angular variations are ignored.

Flow pattern in monolithic channel are usually laminar flow, and this will result in velocity variation along the radial direction. Apart from that, reactions on washcoat can also create significant temperature gradient between the gas phase and the washcoat surface. Therefore, 2D models can be used to increase the accuracy of the converter models.

In 2D models, the axial and radial variations are considered while it assumes no angular variation. 2D models require that the parameters are symmetry about the axis of

the channel. Thus, 2D model limited its application on circular cross-section. The monolithic channel can be suitably modelled with 2D. Despite greater accuracy of the model on representing the actual system, simulation on 2D models require greater amount of computing power.

In a catalytic converter modelling, while 2D model is required to better represent the temperature variation in the radial direction in the solid phase, the fluid phase can be sufficiently modelled using 1D as the flow rate is usually quite high and plug flow can be assumed. However for simplicity, simulations conducted for this project uses 1D models for both gas-phase and solid-phase.

2.7 Python Programming

Python is a high level programming language. A “high-level” programming language is one that abstracts many of the details of how a computation will actually be implemented (Beal *et al*, 2011). With high level programming language, a simple description can be automatically expanded to produce a complete implementation that can be executed. High level programming language differentiate itself from low level programming language in accessibility, scalability and reliability. Minimal knowledge in programming is required to build a system with high level programming language. Thus, high level programming language can be handled easily by chemical engineers to simulate engineering problems involving mass transfer, energy transfer and momentum transfer in a system.

Python incorporates different modules or libraries of pre-defined functions which enable users to solve a wide range of problems more easily. These modules or libraries stored in python programming tool contain a set of pre-defined functions. These functions can be used directly by calling the specific function out from the library.

For example, the Numpy library used in the simulation for this project enable the interpretation of array function in Python. Array can be visualized as table with finite number of grid, whereby the size of the table can be determined by user or generated by specific function. Each of the grid in array can be called out individually. Thus, array is useful to store similar data especially during executing iterative process. Arrays can be one-dimensional, two-dimensional or even multi-dimensional. One-dimensional array is normally applied during solving the 1D model while two-dimensional array is used to save the parameters or variables along the catalytic converter channel for several time point.

To simulate the ignition-extinction in a catalytic converter, it is necessary to construct the mathematical equations describing the mass and energy (heat) transfer in catalytic converter. Mass and energy balance equation which are usually expressed in partial differential equations and ordinary differential equations can be solved the pre-built solver such as *odeint* available in the SciPy module. The results can be plotted in the form of graphs generated by using the Matplotlib module.

CHAPTER 3

METHODOLOGY

3.1 Introduction

The objective of this project is to simulate the ignition-extinction hysteresis as observed during the catalytic combustion in a diesel oxidation catalyst (see Figure 2.9). It is based on the experimental work carried out by Ye *et al* (2012) in which:

- The catalytic converter was a 5mm thin slice cut from a commercial diesel oxidation catalyst
- The exhaust gas entering the diesel oxidation catalyst was generated from a Ford 2.0L turbocharged diesel engine
- The concentration of CO were maintained at 3000 ppm, 4000 ppm and 5000 ppm while the concentration of propane (to represent hydrocarbon) was maintained at 500 ppm
- The temperature of the the gas and converter were measured using thermocouples
- The flow rate and concentration of CO, CO₂ and hydrocarbons in the exhaust gas were measured using Horiba MEXA-7000 series gas analyzer
- The ignition and extinction hysteresis were generated by temperature ramp up and ramp down of the entering exhaust gas, which was controlled by the engine throttle

The simulation of ignition-extinction hysteresis is based on a mathematical model that comprises the following components:

- A single channel monolith model that describes mass and heat transfer taking place in the open channel gas phase and the solid phase
- A kinetic model that describes the reaction mechanisms and rate expressions for the oxidation of CO and a one-step hydrocarbon oxidation on Pt active sites

The detail of the mathematical model is discussed in the following subchapters.

3.2 Single Channel Monolith Model

A diesel oxidation catalyst consists of thousands of channels in parallel, and a detailed model of diesel oxidation catalyst should reflect all the channels. However, the cost of computation with this type of model is very high. To simplify the computation, it is assumed that all the channels in the converter can be represented by a single channel. It is safe to make this assumption as the exhaust gas are well mixed and enters all the channels at the same time.

A graphical illustration of a single channel monolith model is shown in Figure 3.1. It is shown here that the 5mm long (to represent 5mm thin slice) single channel model consists of both gas phase that represents the open channel and solid phase that represents the washcoat and ceramic support. When the converter is operating, the exhaust gas containing components such as oxygen, CO, hydrocarbons, CO₂ and NO_x will enter the at the inlet of the open channel. As the exhaust gas flows along the open channel through diffusion and advection, some of it will be transported from the gas phase to the solid phase and diffuse throughout the porous network of the washcoat. Inside the solid phase, toxic compounds such as CO and hydrocarbons will adsorb onto the platinum nanoparticles and react with oxygen to form CO₂ and water.

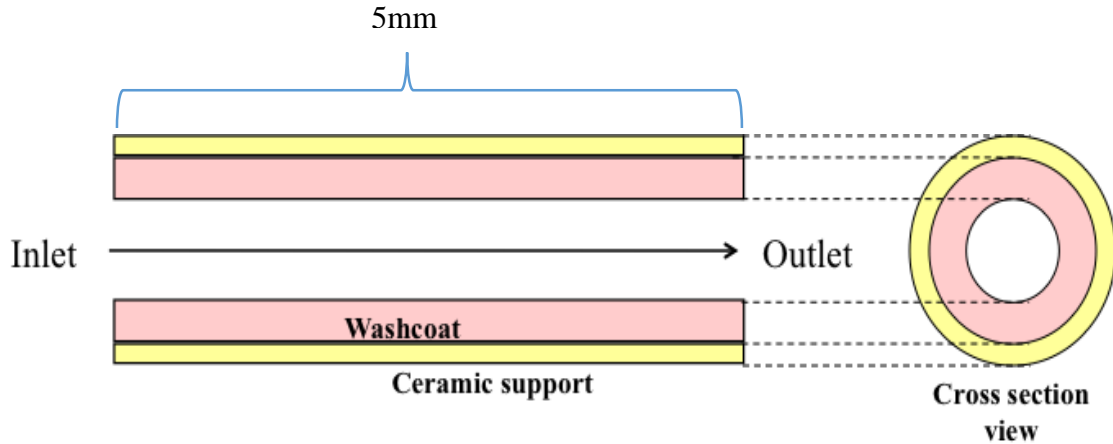


Figure 3.1: Graphical representation of a single channel monolith showing the side view and cross sectional view. A single channel model consists of an open channel gas phase and solid phase made of washcoat and ceramic substrate.

A mathematical model of the single channel monolith shown in Figure 3.1 can be separated into gas phase and solid phase. This will allow for easier computation as the mass and heat transfer in gas phase is very different than in the solid phase. For example, mass transport in gas phase includes diffusion and advection whereas there is only diffusion in the solid phase. If 1D model is chosen for the gas phase, the gas and solid phases can be coupled by a mass and heat transfer coefficient.

In this two phase model, the mass transfer and heat transfer will be modelled. As pressure drop along the channel is negligible, momentum transfer (fluid dynamics) will not be considered. This means that there will be mass transport model for the gas phase and for the solid phase and a heat transport model for both gas phase and solid phase respectively. The mass and heat transport models are represented by partial differential equations (PDE) and ordinary differential equations (ODE) in the following subchapters.

Three main compounds are considered and modeled in this model: (i) carbon monoxide; (ii) carbon dioxide; and (iii) propane. The choice is straightforward as CO and propane are both reacting species while CO_2 will be generated as a result of oxidation of

CO and hydrocarbons. Although there are other compounds such as nitrogen, they do not take part in reactions and therefore will not be considered. Although oxygen will be consumed during the oxidation process, the concentration of oxygen is assumed to be constant as the change in oxygen level is negligible. Thus, mass balance for oxygen will not be considered. For simplification of the codes, CO is denoted as species A, CO₂ as species B while propane is denoted as species C.

3.2.1 Mass Transport Model

For simplicity, 1D model was used for the mass transfer in the gas phase. The assumption with 1D model is that there is no variation in concentration in the radial and angular direction. For 1D gas phase, this assumption works well because the gas flow is well mixed and can be approximated as plug flow.

For the solid phase mass transport model, several researchers (e.g. Mukadi and Hayes, 2000) have simulated through their models that there exist significant concentration gradient within the washcoat layer, and it is necessary for the solid phase to be modelled in 2D. However, since the aim of the simulation is to obtain ignition-extinction hysteresis, the concentration gradient in the washcoat layer is of low importance and will have little impact on the outcome of ignition-extinction hysteresis. For simplicity, 1D model was also used for the solid phase.

The mass balance for the 1D gas phase is represented by three sets of partial differential equations as shown in Table 3.1. Similarly, the mass balance for the 1D solid phase are also represented by three sets of partial differential equations as shown in Table 3.2. The detailed derivation and assumptions made for the mass balance of solid phase are included in discussion in Appendix A. As the mathematical equations are complicated, a more detailed explanation is provided in the following paragraphs.

For the 1D gas phase mass transfer equations as shown in Table 3.1, the left hand side of the three equations represent the change in mol fraction of CO, CO₂ and propane with time. As for the right hand side of the three equations, the first term describes the bulk motion of the species (i.e. CO, CO₂ or propane), the second term describes the diffusion of species in the channel while the last term describes the mass transfer of the species between the gas phase and the solid phase.

For the 1D solid phase mass transfer equations as shown in Table 3.2, the left hand side of the three equations represent the change in mol fraction of CO, CO₂ and propane with time. On the right hand side of the three equations, the first term the mass transfer of the species between the gas phase and the solid phase, the second term represents the diffusion of species, while the last term describes the reactions. There is also a porosity term on the right hand side of the equations to show that the mass transport only takes place in the porous washcoat.

Table 3.1: Partial differential equations describing the mass transfer of CO, CO₂ and propane in the 1D gas phase

Mass Balance	Species	General Equation	
Gas Phase	CO (A)	$\frac{\partial Y_A}{\partial t} = -v \frac{dY_A}{dz} + D_{iA} \frac{d^2 Y_A}{dz^2} - k_{mA} (Y_A - Y_{As}) \frac{4}{D_H}$	(3.1)
	CO ₂ (B)	$\frac{\partial Y_B}{\partial t} = -v \frac{dY_B}{dz} + D_{iB} \frac{d^2 Y_B}{dz^2} - k_{mB} (Y_B - Y_{Bs}) \frac{4}{D_H}$	(3.2)
	C ₃ H ₈ (C)	$\frac{\partial Y_C}{\partial t} = -v \frac{dY_C}{dz} + D_{iC} \frac{d^2 Y_C}{dz^2} - k_{mC} (Y_C - Y_{Cs}) \frac{4}{D_H}$	(3.3)
where			
	Y_X	mol fraction of species X in gas phase	-
	Y_{Xs}	mol fraction of species X in solid phase	-
	D_{iX}	dispersion coefficient of species X	m ² /s
	k_{mX}	convective mass transfer coefficient of species X	m/s
	v	molar average velocity	m/s
	D_H	hydraulic diameter	m
	t	time	s
	z	position in monolith	m

Table 3.2: Partial differential equations describing the mass transfer of CO, CO₂ and propane in the 1D solid phase

Mass Balance	Species	General Equation			
Solid Phase	CO (A)	$\frac{\partial Y_{As}}{\partial t} = \frac{1}{por} \left[k_{mA}(Y_A - Y_{As})(WpAc) + D_{eA} \nabla^2 Y_{As} + \frac{P}{RT_s} RCO(H)(A_v) \right]$ (3.4)			
	CO ₂ (B)	$\frac{\partial Y_{Bs}}{\partial t} = \frac{1}{por} \left[k_{mB}(Y_B - Y_{Bs})(WpAc) + D_{eB} \nabla^2 Y_{Bs} + \frac{P}{RT_s} RCO_2(H)(A_v) \right]$ (3.5)			
	C ₃ H ₈ (C)	$\frac{\partial Y_{Cs}}{\partial t} = \frac{1}{por} \left[k_{mC}(Y_C - Y_{Cs})(WpAc) + D_{eC} \nabla^2 Y_{Cs} - \frac{P}{RT_s} RC_3H_8(H)(A_v) \right]$ (3.6)			
where					
	Y_X	mol fraction of species X - in gas phase	$WpAc$	wetted perimeter to cross-sectional area of washcoat	m/m ²
	Y_{Xs}	mol fraction of species X - in solid phase	H	mol of catalyst per internal surface area of washcoat	mol/m ²
	k_{mX}	convective mass transfer coefficient of species X	A_v	internal surface area to volume ratio of washcoat	m ² /m ³
	D_{eX}	effective diffusivity of species X	RX	desorption rate of species X per mol of catalyst	mol/mol m ³
	P	pressure	por	porosity	-
	R	universal gas constant	t	time	s
	T_s	solid phase temperature	z	position in monolith	m

3.2.2 Energy Transport Model

Similar to mass transfer, 1D model will be used for the energy transfer in the gas phase. The assumption with 1D model is that there is no variation in concentration in the radial and angular direction. For 1D gas phase, this assumption works well because as reported by Hayes, *et al.* (1992) and Lee and Aris (1997), the speed of the response of gas is several orders of magnitude faster than solid. This implied that the energy will distributed fast enough to minimize temperature gradient in gas phase.

For simplicity, 1D model will also be used for the heat transfer in the solid phase. The reason is that temperature gradient in the solid phase will have little impact on the outcome of ignition extinction hysteresis, which is the focus of this project. The detailed derivation and assumptions made for the energy balance of the solid phase are included in Appendix A. A more detailed explanation on mathematical equations is provided in the following paragraphs.

For the 1D gas phase energy transfer equation as shown in Table 3.3, the left hand side of the equation represent the change in gas phase temperature with time. As for the right hand side of the equation, the first term describes the heat transfer during bulk motion of fluid, the second term describes the dispersion of heat in the channel while the last term describes the heat transfer between the gas phase and the solid phase.

For the 1D solid phase energy transfer equation as shown in Table 3.4, the left hand side of the equation represent the change in solid phase temperature with time. On the right hand side of the equation, the first term describes the heat transfer between the gas phase and the solid phase, the second term represents the dispersion of heat along axial direction, while the last term describes the heat released from reactions.

Table 3.3: Partial differential equations describing the energy transfer of CO, CO₂ and propane in the 1D gas phase

Energy Balance	General Equation	
Gas Phase	$\frac{\partial T_g}{\partial t} = -v \frac{dT_g}{dz} + D_g \frac{d^2 T_g}{dz^2} + \frac{1}{\rho_{air} C_{p_{air}}} h (T_s - T_g) \frac{4}{D_H}$	(3.7)
where		
T_g	gas temperature	K
T_s	solid temperature	K
v	molar average velocity	m/s
D_g	thermal diffusivity in gas phase	m ² /s
ρ_{air}	density of gas phase (assume air density)	kg/m ³
$C_{p_{air}}$	specific heat capacity of gas phase (assume air heat capacity)	J/kg K
h	heat transfer coefficient	W/m ² ·K
D_H	hydraulic diameter	m
t	time	s
z	position in monolith	m

Table 3.4: Partial differential equations describing the energy transfer of CO, CO₂ and propane in the 1D solid phase

Energy Balance	General Equation		
Solid Phase	$\frac{\partial T_s}{\partial t} = -h(T_s - T_g)(WpAc)/(\rho_{wc}C_{p_{wc}}) + D_s \frac{d^2 T_s}{dz^2} + H(A_v)[RCO(Hr_{CO}) + RC_3H_8(Hr_{C_3H_8})]/(\rho_{wc}C_{p_{wc}}) \quad (3.8)$		
	where		
	T_g	gas temperature	K
	T_s	solid temperature	K
	ρ_{wc}	bulk density of washcoat	kg/m ³
	$C_{p_{wc}}$	specific heat capacity of washcoat	°C/J kg
	$WpAc$	wetted perimeter to cross-sectional area of washcoat	m/m ²
	H	mol of catalyst per internal surface area of washcoat	mol/m ²
	A_v	internal surface area to volume ratio of washcoat	m ² /m ³
	D_s	thermal diffusivity in solid phase	m ² /s
	h	heat transfer coefficient	W/m ² ·K
	RCO	desorption rate of CO per mol of catalyst	mol/mol m ³
	RC_3H_8	desorption rate of C ₃ H ₈ per mol of catalyst	mol/mol m ³
	Hr_{CO}	heat of reaction of CO	J/mol
	$Hr_{C_3H_8}$	heat of reaction of C ₃ H ₈	J/mol
	t	time	s
	z	position in monolith	m

3.2.3 Model Parameters, Operating Conditions and Chemical Properties

Table 3.5 and 3.6 shows the monolith channel physical properties and operating conditions defined in the simulation, which also represent the monolith channel used and operating conditions set by Ye *et al* (2011) for their experimental work.

Table 3.5: Monolith channel physical properties

Parameter	Symbol	Values	Unit
Reactor length	z_l	0.005	m
Channel radius	r	4.1×10^{-2}	m
Washcoat thickness	s	1.0×10^{-2}	m

Table 3.6: Operating conditions

Parameter	Symbol	Values	Unit
Pressure	P	101300	Pa
Inlet velocity	v	2.4	m/s
Inlet molar flow	M_{flow}	0.64	mol/s

Table 3.7 lists the physical properties for the reacting species that are involved during the catalytic oxidation in diesel oxidation catalyst. Molecular volume of an species are defined as volume of occupied by 1 kmol of molecules of the species at its boiling point.

Table 3.7: Physical properties for the reacting species

Parameter	Symbol	Values	Unit
Molar mass of air	M_{air}	28.96	kg/kmol
Molar mass of O ₂	M_{O_2}	32.00	kg/kmol
Molar mass of CO	M_{CO}	28.01	kg/kmol
Molar mass of CO ₂	M_{CO_2}	44.01	kg/kmol
Molar mass of C ₃ H ₈	$M_{C_3H_8}$	44.10	kg/kmol
Molecular volume of air(l)	V_{air}	20.10	m ³ /kmol
Molecular volume of CO(l)	V_{CO}	18.90	m ³ /kmol
Molecular volume of CO ₂ (l)	V_{CO_2}	22.262	m ³ /kmol
Molecular volume of C ₃ H ₈	$V_{C_3H_8}$	65.34	m ³ /kmol

Table 3.8 and Table 3.9 shows the physical properties of gas phase and solid phase defined for the simulation. Since CO, CO₂ and C₃H₈ is at low concentration, gas phase composition should be close to air composition. Properties of gas phase is assumed to be properties of air.

Table 3.10 and Table 3.11 lists the equations and correlations used to estimate heat transfer coefficient and mass transfer coefficient respectively.

Table 3.8: Properties of Gas Phase

Parameter	Relating equation	Unit
Density of air	$\rho_{air} = \frac{P(M_{air})}{1000(R)(T_g)}$	kg/m ³
Heat capacity of air	$Cp_{air} = \frac{1}{0.02896} [28.09 + 0.1965 \times 10^{-2}(T_g) + 0.4799 \times 10^{-5}(T_g)^2 - 1.965 \times 10^{-9}(T_g)^3]$	J/kg·K
Thermal conductivity of air	$k_{air} = 1.679 \times 10^{-2} + 5.073 \times 10^{-5}(T_g)$	W/m·K
Thermal diffusivity of air	$D_{air} = \frac{k_{air}}{\rho_{air}(Cp_{air})}$	m ² /s
Thermal dispersion coefficient	$D_g = D_{air} + \frac{(v \cdot r)^2}{48D_{air}}$	m ² /s

Table 3.9: Properties of Solid Phase

Parameter	Relating equation	Unit
Bulk density of washcoat	$\rho_{wc} = 1.3 \times 10^6$	g/m^3
Heat capacity of washcoat	$Cp_{wc} = 948 + 0.2268(T_s)$	$\text{J/kg}\cdot\text{K}$
Thermal conductivity of solid phase	$k_s = 0.9558 - 2.09 \times 10^{-4}(T_s)$	$\text{W/m}\cdot\text{K}$
Thermal diffusivity of solid phase	$D_s = \frac{k_s}{\rho_{wc}(Cp_{wc})}$	m^2/s
Equivalent pore radius	$r_e = 1.2 \times 10^{-8}$	m
Porosity	$por = 0.55$	-
Tortuosity	$\tau = 1$	-
Internal surface area to washcoat ratio	$A_V = 130$	m^2/g
Active sites to washcoat ratio	$LPt = 6.6667 \times 10^{-6}$	mol/g

Table 3.10: Heat Transfer Coefficient Related Equations

Parameter	Relating equation	Unit
Distance from inlet	L	m
Viscosity of air	$\mu = 7.701 \times 10^{-6} + 4.166 \times 10^{-8}(T_g) - 7.531 \times 10^{-12}(T_g)^2$	Pa·s
Reynolds number	$Re = \frac{\rho_{air} v D_H}{\mu}$	-
Prandtl number	$Pr = \frac{Cp_{air} \mu}{k_{air}}$	-
Graetz number	$Gz = \frac{Re Pr D_H}{L}$	-
Nu for wall temperature	$Nu_T = 3.657 + 8.827 \left(\frac{1000}{Gz}\right)^{-0.545} \exp\left(\frac{-48.2}{Gz}\right)$	-
Nu for wall flux	$Nu_H = 4.364 + 13.18 \left(\frac{1000}{Gz}\right)^{-0.524} \exp\left(\frac{-60.2}{Gz}\right)$	-
Nusselt number	$Nu = \frac{Nu_T + Nu_H}{2} + 1$	-
Heat transfer coefficient	$h = \frac{Nu \cdot k_{air}}{D_H}$	W/m ² K

Table 3.11: Mass Transfer Coefficient Related Equations

Parameter	Relating equation	Unit
Sherwood number	$Sh = Nu$	
Bulk diffusion coefficient of species X in gas phase	$D_{bX} = 1.013 \times 10^{-2} T_g^{\frac{7}{4}} \left(\frac{1}{M_X} + \frac{1}{M_{air}} \right)^{\frac{1}{2}} \left(\frac{1}{V_X + V_{air}} \right)^2$	m ² /s
Dispersion coefficient of species X	$D_{iX} = D_{bX} + \frac{(v \cdot r)^2}{48D_{bX}}$	m ² /s
Convective mass transfer coefficient of species X	$k_{mX} = Sh \frac{D_{bX}}{D_H}$	m/s
Knudsen diffusion coefficient of species X	$D_{kX} = 97r_e \left(\frac{T_s}{M_X} \right)^{0.5}$	m ² /s
Bulk diffusion coefficient of species X in solid phase	$D_{bXs} = 1.013 \times 10^{-2} T_s^{\frac{7}{4}} \left(\frac{1}{M_X} + \frac{1}{M_{air}} \right)^{\frac{1}{2}} \left(\frac{1}{V_X + V_{air}} \right)^2$	m ² /s
Diffusion coefficient of species X in the pores	$D_{vX} = \frac{1}{\frac{1}{D_{bXs}} + \frac{1}{D_{bX}}}$	m ² /s
Effective diffusivity of species X	$D_{eX} = \frac{ff}{\tau} (por)(D_{vX})$	m ² /s

3.3 Kinetic Model

In the solid phase, the kinetic model will account for the generation rate of CO₂ and the consumption rate of CO and hydrocarbons in washcoat. The kinetic model consists of:

- Reaction mechanisms for CO oxidation and the detailed rate equations for the individual elementary reaction
- Global reaction model for propane oxidation

To simulate the light-off hysteresis phenomenon, CO oxidation will be expressed in more detailed mechanistic model which every reaction steps is considered during computation. For propane oxidation, simpler global kinetic model is employed to account for the mass balance of propane and energy balance from heat released by oxidation of propane.

3.3.1 Mechanistic Model of CO Oxidation

Compressed oxygen model were used to simulate the CO oxidation reaction in monolith channel. According to Salomons (2006), compressed oxygen model is the better model to simulate light-off hysteresis in catalytic converter. This model is able to account for CO adsorption on oxygen covered surface. At the same time, reaction mechanism proposed in this model is consistent with observation from surface science.

Compressed oxygen model consists of 6 reaction steps:

1. Reversible adsorption of CO onto the catalyst surface
2. Dissociative adsorption of oxygen, O₂ onto the catalyst surface
3. Surface reaction between adsorbed CO and adsorbed oxygen, O
4. Compression of adsorbed oxygen on the surface by adsorption of CO
5. Surface reaction between adsorbed CO and compressed oxygen, OO
6. Dissociation of compressed oxygen on the surface

These 6 reaction steps are be denoted as reaction a to f. Reaction equation for individual reaction steps and their respective reaction rate equation are listed in Table 3.12 on the next following pages. Parameters for every reaction rate equation are listed in Table 3.13:

Table 3.12: Reaction rate equations

Reaction	Rate Equation
Reaction a: $CO_{(g)} + \theta_V \leftrightarrow \theta_{CO}$	$R_a = \frac{S_{CO}}{GRT_s} P Y_{As} f_{cv} \left[\frac{R(1000)T_s}{2\pi M_{CO}} \right]^{0.5} - A_{aB} f_{cCO} \exp \left[\frac{E_{aB}(1000)}{RT_s} \right]$
	where
S_{CO}	stick coefficient of CO
G	constant
R	universal gas constant Pa m ³ /mol K
T_s	solid temperature K
P	pressure Pa
M_{CO}	molar mass of CO g/mol
	Y_{As} mol fraction of solid phase CO -
	f_{cv} fractional coverage of vacant site -
	f_{cCO} fractional coverage of CO -
	A_{aB} pre-exponential value of backward reaction a mol/mol·s
	E_{aB} activation energy of backward reaction a kJ/mol
	Y_{As} mol fraction of solid phase CO -

Table 3.12: Reaction rate equations (cont.)

Reaction	Rate Equation			
Reaction b:				
$O_{2(g)} + 2\theta_v \leftrightarrow 2\theta_O$	$R_b = \frac{S_{O_2}}{GRT_s} PY_{O_2} f_{cV}^2 \left[\frac{R(1000)T_s}{2\pi M_{O_2}} \right]^{0.5}$			
	where			
S_{O_2}	stick coefficient of O ₂	P	pressure	Pa
G		M_{O_2}	molar mass of O ₂	g/mol
R	universal gas constant	Pa m ³ /mol K	Y_{O_2}	mol fraction of gas phase O ₂ -
T_s	solid temperature	K	f_{cV}	fractional coverage of vacant site -
Reaction c:				
$\theta_O + \theta_{CO} \rightarrow CO_{2(g)} + 2\theta_v$	$R_c = A_{cF} f_{cCO} f_{cO} \exp \left[\frac{E_{cF}(1000)}{RT_s} \right]$			
	where			
R	universal gas constant	Pa m ³ /mol K	f_{cO}	fractional coverage of O atom -
T_s	solid temperature	K	A_{cF}	pre-exponential value of forward reaction c mol/mol·s
f_{cCO}	fractional coverage of CO	-	E_{cF}	activation energy of forward reaction c kJ/mol

Table 3.12: Reaction rate equations (cont.)

Reaction	Rate Equation																				
Reaction d: $CO_{(g)} + 2\theta_O \rightarrow \theta_{CO} + \theta_{OO}$	$R_d = \frac{A_{dF}}{RT_s} P Y_{As} f_{CO}^2 \exp \left[\frac{E_{dF}(1000)}{RT_s} \right]$																				
	where																				
	<table border="0"> <tr> <td>R</td> <td>universal gas constant</td> <td>Pa m³/mol K</td> <td>f_{CO}</td> <td>fractional coverage of O atom</td> </tr> <tr> <td>T_s</td> <td>solid temperature</td> <td>K</td> <td>A_{dF}</td> <td>pre-exponential value of forward reaction d</td> </tr> <tr> <td>P</td> <td>pressure</td> <td>Pa</td> <td>E_{dF}</td> <td>activation energy of forward reaction d</td> </tr> <tr> <td>Y_{As}</td> <td>mol fraction of solid phase CO</td> <td></td> <td></td> <td></td> </tr> </table>	R	universal gas constant	Pa m ³ /mol K	f_{CO}	fractional coverage of O atom	T_s	solid temperature	K	A_{dF}	pre-exponential value of forward reaction d	P	pressure	Pa	E_{dF}	activation energy of forward reaction d	Y_{As}	mol fraction of solid phase CO			
R	universal gas constant	Pa m ³ /mol K	f_{CO}	fractional coverage of O atom																	
T_s	solid temperature	K	A_{dF}	pre-exponential value of forward reaction d																	
P	pressure	Pa	E_{dF}	activation energy of forward reaction d																	
Y_{As}	mol fraction of solid phase CO																				

Table 3.12: Reaction rate equations (cont.)

Reaction	Rate Equation
Reaction e:	
$\theta_{CO} + \theta_{OO} \rightarrow CO_{2(g)} + \theta_O + \theta_V$	$R_e = A_{eF} f_{cCO} f_{cOO} \exp \left[\frac{E_{eF}(1000)}{RT_s} \right]$
	where
R	universal gas constant Pa m ³ /mol K
T_s	solid temperature K
f_{cCO}	fractional coverage of CO
	f_{cOO} fractional coverage of compressed O
	A_{eF} pre-exponential value of forward reaction e mol/mol·s
	E_{eF} activation energy of forward reaction e kJ/mol
Reaction f:	
$\theta_{OO} + \theta_V \rightarrow 2\theta_O$	$R_f = A_{fF} f_{cOO} f_{cV} \exp \left[\frac{E_{fF}(1000)}{RT_s} \right]$
	where
R	universal gas constant Pa m ³ /mol K
T_s	solid temperature K
f_{cOO}	fractional coverage of compressed O
	f_{cV} fractional coverage of vacant site
	A_{fF} pre-exponential value of forward reaction f mol/mol·s
	E_{fF} activation energy of forward reaction f kJ/mol

Table 3.13: Reaction Rate Equation Parameters

Parameter	Equations/Values	Unit
S_{CO}	$0.85 \frac{1 - f_{CCO}}{1 - 0.85 f_{CCO}}$	
S_{O_2}	0.15	
G	2.0573×10^{-5}	
R	8.3144621	Pa m ³ /mol K
M_{CO}	28.01	g/mol
M_{O_2}	32.00	g/mol
A_{aB}	1.0×10^8	mol/mol·s
A_{cF}	8.2×10^8	mol/mol·s
A_{dF}	1.0×10^8	mol/mol·s
A_{eF}	1.0×10^{15}	mol/mol·s
A_{fF}	1.0×10^{15}	mol/mol·s
E_{aB}	$-126.4 + 33f_{CCO}$	kJ/mol
E_{cF}	$-104.6 + 46.024f_{CCO}$	kJ/mol
E_{dF}	-50	kJ/mol
E_{eF}	-50	kJ/mol
E_{fF}	-105	kJ/mol

Rate of change of fractional coverage can be computed by employing mol balance which sums up every formation and disappearance of specific adsorbed species by reaction. Equations for rate of change of fraction coverage of adsorbed species and vacant site are listed in table 3.17:

Table 3.14: Equations for Rate of Change of Fractional Coverage of Adsorbed Species and Vacant Site

adsorbed species/vacant site	Rate of appearance of adsorbed species/vacant site
vacant site	$\frac{\partial f_{cv}}{\partial t} = -R_a - 2R_b + 2R_c + R_e - R_f$
CO	$\frac{\partial f_{cCO}}{\partial t} = R_a - R_c + R_d - R_e$
O	$\frac{\partial f_{cO}}{\partial t} = 2R_b - R_c - 2R_d + R_e + 2R_f$
Compressed O	$\frac{\partial f_{cOO}}{\partial t} = R_d - R_e - R_f$

Equations for overall rate of production of CO, O₂ and CO₂ are determined and listed in Table 3.18. CO₂ is assumed to be immediately desorbed from surface into solid phase after CO oxidation.

Table 3.15: Equations for Rate of Release of Chemical Species into Solid Phase

species	Rate of release of species into solid phase
CO	$R_{CO} = -R_a - R_d$
O ₂	$R_{O_2} = -R_b$
CO ₂	$R_{CO_2} = R_c + R_e$

3.3.2 Global Kinetic Model of Propane Oxidation

A global kinetic model were used to simulate the propane oxidation reaction in monolith channel. Rate of propane oxidation is represented in Table 3.16. An inhibition factor is added into the model to better relate the response of rate of oxidation of propane to the condition in the channel. Inhibition factor is calculated by using equation in Table 3.16.

Table 3.16: Reaction Rate Equation

Reaction	Equations
Oxidation of Propane	$R_{C_3H_8i} = \left[1 + A_{C_3H_8i} Y_{C_S} \exp\left(\frac{E_{C_3H_8i}}{T_S}\right) \right]^2$
Inhibition Factor	$R_{C_3H_8} = \frac{A_{C_3H_8}}{R_{C_3H_8i}} Y_{O_2} Y_{C_S} \exp\left(\frac{E_{C_3H_8}}{T_S}\right)$

Table 3.17: Reaction Rate Equation Parameters

Parameter	Equations/Values	Unit
$A_{C_3H_8i}$	0.208	-
$A_{C_3H_8}$	3.0×10^{12}	mol/mol·s
$E_{C_3H_8i}$	380	K
$E_{C_3H_8}$	-1.08×10^4	K

3.4 Numerical Methods

Monolith channel model consists of partial differential equation (PDEs) and ordinary differential equation (ODEs). Equations such as mass balance and energy balance equations presented in Table 3.1, 3.2, 3.3 and 3.4 are PDEs. PDE relate the change of a dependent variable to more than one independent variables. For example, in the case of gas phase energy balance in Table 3.3, temperature (independent variable) is related to two independent variables which are time and position in the monolith. For rate of change of fractional coverage of a species, those equations are ODEs such as in Table 3.14. ODEs relates the change of a dependent variable to only one variable.

PDEs are more complex to solve compared to ODEs as PDEs is related to more variables. According to Hayes and Kolaczowski (1997), discretization can be done to representing PDEs in ODEs form through application of finite difference method. The solution domain of PDE will be divided into finite number of nodes or mesh point. Every ODEs can be solved as initial value problem. Taking gas phase energy as example:

$$\frac{\partial T_g}{\partial t} = -v \frac{dT_g}{dz} + D_l \frac{d^2 T_g}{dz^2} + \frac{1}{\rho_{air} C_{p_{air}}} h(T_s - T_g) \frac{4}{D_H}$$

Through discretization first order differential term by applying backward difference method:

$$\frac{dT_g}{dz} = \frac{T_{g_{i+1}} - T_{g_i}}{\Delta z}$$

where $T_{g_{i+1}}$ and T_{g_i} are two consecutive nodes which separated by distance of Δz .

For discretization of second order differential term by applying central difference method:

$$\frac{d^2 T_g}{dz^2} = \frac{T_{g_{i+1}} - T_{g_i} + T_{g_{i-1}}}{\Delta z^2}$$

where $T_{g_{i+1}}$, T_{g_i} and $T_{g_{i-1}}$ are three consecutive nodes which each node is separated by distance of Δz

Due to the complexity of the mechanistic model, it is impossible to solve analytically. Method of lines which is a type of numerical method is employ to solve the model. Through this method, initial values is used to solve the ODEs and estimate the values of next time point. Method of lines is done by ODEINT, an ODE solver pre-load in the Sci-Py python programming module.

3.5 Algorithms for Programming

The mathematical model of diesel oxidation catalyst consists of partial differential equations which are:

1. Mass balance for gas phase
2. Mass balance for solid washcoat phase
3. Energy balance for gas phase
4. Energy balance for solid washcoat phase

The following are the steps used to develop the Python coding to simulate diesel oxidation catalyst.

Step 1: Discretization of monolith channel

Length of monolith channel is defined. Gas phase and solid washcoat phase are discretized. Discretization divides the channel into finite number of equally divided portion. Each portion is known as a grid.

Each grid is representing small portion of the monolith. Condition in spatial space of each grid is assumed to be the same. Thus, accuracy will increase when grid size is greatly reduced.

Number of grid is calculated and stored. Number of grid will be used during initialization of parameters in each of every grids.

```
z1 = 0.005
dz = 0.001
z = np.arange(0, z1+dz, dz)
N = len(z)
```

Figure 3.1: Example of grids set up in Python

Step 2: Input monolith parameter

Monolith channel parameters such as channel radius and solid washcoat thickness are declared. Details of solid washcoat such as porosity and tortuosity are also declared. Other operating conditions such as pressure, gas flow velocity. These parameters represents the monolith channel used and operating conditions set by Ye *et al* (2011) in the experiment. Constants such as universal gas constant are declared as well.

```

## Monolith parameter
s0 = 100E-6 #m #washcoat thickness
r0 = 510E-6 - s0 #m #channel radius
dm = 0.106 #m #diameter of monolith block
WpAc = 2*r0/((r0+s0)**2 - r0**2) #m2/m3 #perimeter per volume of washcoat

## Details of porous media (Assume parallel pore)
re = 12.00E-9 #m #equivalent pore radius
por = 0.55 # #Porosity
tau = 1 # #Tortuosity
LPT = 2.0E-6/0.3 #mol(Pt)/g(wc) #Active sites per catalyst/washcoat

```

Figure 3.2: Example of monolith parameter declaration in Python

Step 3: Initialization of variable to be investigated

CO, CO₂, C₃H₈ and O₂ are four types of compounds that are involved in reaction occurred in automobile catalytic converter. Initial mol fraction of these molecules in gas phase and solid phase is declared.

Fractional coverage of catalyst surface is important as it determines the individual reaction rate.

In light-off hysteresis, temperature plays an important role in determining the reaction rate. Initial gas phase temperature and solid washcoat phase temperature for each grid is also declared.

These initial value will be used for prediction through numerical iteration.

```

Y02 = 0.0933

YA = np.ones(N)*3000E-6
YAs = np.ones(N)*3000E-6

YB = np.zeros(N)
YBs = np.zeros(N)

YC = np.ones(N)*500E-6
YCs = np.ones(N)*500E-6

fcV = np.ones(N)*0.00272
fcCO = np.ones(N)*0.99228
fcO = np.ones(N)*0.005
fcOO = np.ones(N)*0.000

Tg = np.ones(N)*417
Ts = np.ones(N)*417

```

Figure 3.3: Example of initialization of variable in Python

Step 4: Setting up stages and inlet gas temperature profile

Ignition and extinction point are commonly defined as the inlet gas temperature corresponding to specific conversion. Thus, in this simulation, inlet gas temperature is varied and overall conversion across monolith catalyst is studied.

Throughout the investigating period, it is divided into several stages. Different stages will have different rate of changes of temperature. Rate of changes of temperature is calculated by using value declared in initial inlet gas temperature and duration of each stages.

Inlet gas temperature should increase until oxygen dominate the catalyst surface. Then, inlet gas temperature is made to decrease until initial inlet gas temperature.

```

start = 0

dr_st = np.zeros(6)
dr_st[0]= 200.0
dr_st[1]= 500.0
dr_st[2]= 300.0
dr_st[3]= 100.0
dr_st[4]= 200.0
dr_st[5]= 500.0

stage = np.zeros(len(dr_st)+1)
stage[0]= start
for a in range(0,len(stage)-1):
    stage[a+1] = stage[a] + dr_st[a]

T_st = np.zeros(len(stage))
T_st[0] = Tg[0]
T_st[1] = 505.0
T_st[2] = 545.0
T_st[3] = 545.0
T_st[4] = 485.0
T_st[5] = 445.0
T_st[6] = 417.0

mp = (T_st[i+1]-T_st[i])/(dr_st[i]/dt) #rate of change of inLet gas temperature

```

Figure 3.4: Example of stages and inlet gas temperature profile setup in Python

Step 5: Setting up the “parameter” function

The equation that predict actual velocity, molecular diffusion, dispersion coefficient, thermal conductivity and other parameters at each grid is defined in this function. The main purpose of this function is to predict all parameters by using value generated from mechanistic model at each time step.

Parameter function is also included in model function to keep the ODE solver ‘odeint’ updated with the latest parameter values as it computing values for next time point through iteration.

Value of major parameters will be displayed as it is computed during each iteration. These value will be stored in respective storing variable for graph plotting and data storing purposes.

```
def parameter(y0):
    for i in range(0,N):
        YA[i] = y0[i]
        •
        •
        •
    return np.concatenate([0],Tst,[Tst_end])
```

Figure 3.5: Example of “parameter” function setup in Python

Step 6: Setting up the “model” function

“Model” function included physical properties estimation and mass and energy balance equation. Partial differential equations of mass and energy balance for gas and solid phase are converted into ordinary differential equations by using finite difference method before declared in “model” function.

```
def model(y0,t):
    •
    •
    •
    ## Differential equation
    # Gas phase
    YAt = -v[1:-1]*np.diff(YA[: -1])/dz + DiA[1:-1]*((YA[2:] -2*YA[1:-1]+YA[: -2])/dz**2) - 4/Dh*kmA[1:-1]*(YA[1:-1]-YAS[1:-1])
    YBt = -v[1:-1]*np.diff(YB[: -1])/dz + DiB[1:-1]*((YB[2:] -2*YB[1:-1]+YB[: -2])/dz**2) - 4/Dh*kmB[1:-1]*(YB[1:-1]-YBS[1:-1])
    YCt = -v[1:-1]*np.diff(YC[: -1])/dz + DiC[1:-1]*((YC[2:] -2*YC[1:-1]+YC[: -2])/dz**2) - 4/Dh*kmC[1:-1]*(YC[1:-1]-YCS[1:-1])

    YAt_end = -v[-1]*(YA[-1]-YA[-2])/dz + DiA[-1]*((2*YA[-2]-2*YA[-1])/dz**2) - 4/Dh*kmA[-1]*(YA[-1]-YAS[-1])
    YBt_end = -v[-1]*(YB[-1]-YB[-2])/dz + DiB[-1]*((2*YB[-2]-2*YB[-1])/dz**2) - 4/Dh*kmB[-1]*(YB[-1]-YBS[-1])
    YCt_end = -v[-1]*(YC[-1]-YC[-2])/dz + DiC[-1]*((2*YC[-2]-2*YC[-1])/dz**2) - 4/Dh*kmC[-1]*(YC[-1]-YCS[-1])

    •
    •
    •
    # Solid washcoat
    YAst = 1/por*(kmA[1:-1]*(YA[1:-1]-YAS[1:-1])*WpAc + DeA[1:-1]*(YAS[2:] -2*YAS[1:-1]+YAS[: -2])/dz**2+RCO[1:-1]*H*Av*Rg*Ts[1:-1]/P)
    YBst = 1/por*(kmB[1:-1]*(YB[1:-1]-YBS[1:-1])*WpAc + DeB[1:-1]*(YBS[2:] -2*YBS[1:-1]+YBS[: -2])/dz**2+RCO2[1:-1]*H*Av*Rg*Ts[1:-1]/P)
    YCst = 1/por*(kmC[1:-1]*(YC[1:-1]-YCS[1:-1])*WpAc + Dec[1:-1]*(YCS[2:] -2*YCS[1:-1]+YCS[: -2])/dz**2-RC3H8[1:-1]*H*Av*Rg*Ts[1:-1]/P)

    YAst_end = 1/por*(kmA[-1]*(YA[-1]-YAS[-1])*WpAc + DeA[-1]*(2*YAS[-2]-2*YAS[-1])/dz**2+RCO[-1]*H*Av*Rg*Ts[-1]/P)
    YBst_end = 1/por*(kmB[-1]*(YB[-1]-YBS[-1])*WpAc + DeB[-1]*(2*YBS[-2]-2*YBS[-1])/dz**2+RCO2[-1]*H*Av*Rg*Ts[-1]/P)
    YCst_end = 1/por*(kmC[-1]*(YC[-1]-YCS[-1])*WpAc + Dec[-1]*(2*YCS[-2]-2*YCS[-1])/dz**2-RC3H8[-1]*H*Av*Rg*Ts[-1]/P)

    fcvt = - Ra[1:] -2*Rb[1:] +2*Rc[1:] +Re[1:] -Rf[1:]
    fccOT = Ra[1:] - Rc[1:] + Rd[1:] -Re[1:]

    •
    •
    •
    return D
```

Figure 3.6: Example of mechanistic model setup in Python

Step 7: Declaration of step size of time for each iteration

This step size will determine the time interval before the next value generated from ODE solver ‘odeint’ to be stored for display and graph plotting purposes. This step size does not necessarily represent the actual time step used by ODE (ordinary

differential equation) solver to predict the value on the next time step as the solver will determine the optimum step size where the error is kept under a tolerance value.

Sequence of time points is generated by taking in two consecutive time points declared in step 6. ODE solver ‘odeint’ will store the result at every time points specified in the time sequence.

```
dt      = 1
time    = np.linspace(stage[i],stage[i+1],2)
time    = np.linspace(stage[i],stage[i+1],round((dr_st[i]/dt)+1))
```

Figure 3.7: Example of step size of time declaration in Python

Step 8: Setting up the loop for stages

Every time a new stage is initiated. Rate of change of inlet gas temperature is recalculated as explained in step 4.

```
for i in range(0,len(stage)-1):
    mp      = (T_st[i+1]-T_st[i])/(dr_st[i]/dt) #rate of change of inlet gas temperature
            ⋮
            ⋮
            ⋮
```

Figure 3.8: Example of loop for stages setup in Python

Step 9: Setting up the loop for numerical iteration

ODE solver ‘odeint’ can only be initiated with the input of initial values and sequence of time points.

Next, every investigating variable is concatenated into one long array.

ODE solver ‘odeint’ is set up to solve the mass and energy balance which declared in a self-defined function. The solver will start iterate and calculate the next value by using the initial values sent into the solver.

As the solver finished computing the result, values generated for every time points will be stored in separate storing variable for graph plotting and data storing purposes. Then, the investigating variable will be updated with value of the last time points. Updated value will acting as initial value for next loop.

Every function in the loop will repeat itself until all values for every time points in sequence declared in step 6 is computed.

```

for j in range(0,len(time)-1):
    time_minor = np.linspace(time[j],time[j+1],round((time[j+1]-time[j])/dt + 1)) #for each temperature step

    y0 = np.concatenate([YA,YB,YC,YAs,YBs,YCs,fcV,fcCO,fcO,fcOO,Tg,Ts])

    value = parameter(y0)

    sol = odeint(model,y0,time_minor)

    •
    •
    •

    ## Update value for next iteration
    YA = np.copy(sol[-1, 0: N])
    YB = np.copy(sol[-1, N: 2*N])
    YC = np.copy(sol[-1, 2*N: 3*N])
    YAs = np.copy(sol[-1, 3*N: 4*N])
    YBs = np.copy(sol[-1, 4*N: 5*N])
    YCs = np.copy(sol[-1, 5*N: 6*N])
    fcV = np.copy(sol[-1, 6*N: 7*N])
    fcCO = np.copy(sol[-1, 7*N: 8*N])
    fcO = np.copy(sol[-1, 8*N: 9*N])
    fcOO = np.copy(sol[-1, 9*N:10*N])
    Tg = np.copy(sol[-1,10*N:11*N])
    Ts = np.copy(sol[-1,11*N:12*N])

    YAs[0]= np.copy(sol[-1,3*N+1])      # Boundary Condition (inlet)
    YBs[0]= np.copy(sol[-1,4*N+1])      # Boundary Condition (inlet)
    YCs[0]= np.copy(sol[-1,5*N+1])      # Boundary Condition (inlet)
    Ts[0] = np.copy(sol[-1,11*N+1])      # Boundary Condition (inlet)

    ## Save values for graph plotting
    YA_save = np.append(YA_save, sol[-1, 0: N])
    YB_save = np.append(YB_save, sol[-1, N: 2*N])
    YC_save = np.append(YC_save, sol[-1, 2*N: 3*N])
    YAs_save = np.append(YAs_save, sol[-1, 3*N: 4*N])
    YBs_save = np.append(YBs_save, sol[-1, 4*N: 5*N])
    YCs_save = np.append(YCs_save, sol[-1, 5*N: 6*N])
    fcV_save = np.append(fcV_save, sol[-1, 6*N: 7*N])
    fcCO_save = np.append(fcCO_save, sol[-1, 7*N: 8*N])
    fcO_save = np.append(fcO_save, sol[-1, 8*N: 9*N])
    fcOO_save = np.append(fcOO_save, sol[-1, 9*N:10*N])
    Tg_save = np.append(Tg_save, sol[-1,10*N:11*N])
    Ts_save = np.append(Ts_save, sol[-1,11*N:12*N])

```

Figure 3.9: Example of loop for numerical iteration setup in Python

Step 10: Extracting and displaying value

To allow the user to follow up the progress of the simulation, the code is designed in such a way that it will display latest value of parameters and investigating variables from numerical iteration. Display function is inserted at the end of loop for stages set up in step 8 so that the user will be kept updated with the latest value right after each iteration.

```

for i in range(0,len(stage)-1):
    ●
    ●
    ●
    ## Display parameter
    print '/n'
    print 'time'      , time[j+1]
    print 'YA'       , YA[0]      ,YA[-1]
    print 'YB'       , YB[0]      ,YB[-1]
    print 'YC'       , YC[0]      ,YC[-1]
    print 'YAs'      , YAs[0]     ,YAs[-1]
    print 'YBs'      , YBs[0]     ,YBs[-1]
    print 'YCs'      , YCs[0]     ,YCs[-1]
    print 'Tg'       , Tg[0]      ,Tg[-1]
    print 'Ts'       , Ts[0]      ,Ts[-1]
    print 'fcV'      , fcV[0]     ,fcV[-1]
    print 'fccO'     , fccO[0]    ,fccO[-1]
    print 'fcO'      , fcO[0]     ,fcO[-1]
    print 'fcoO'     , fcoO[0]    ,fcoO[-1]
    print 'mp'       , mp

```

Figure 3.10: Example of value display setup in Python

Step 11: Data storing

Every values in storing variable will be stored in a single file which can be read in separate code for further analysis. With data storing, user can skip all the waiting for computation and using those stored value for other analysis.

```

np.savez('C:\Users\kim_y_000\Desktop\FYP\mechanistc.npz',
YA      =YA_save,
YB      =YB_save,
YC      =YC_save,
YAs     =YAs_save,
YBs     =YBs_save,
YCs     =YCs_save,
fcV     =fcV_save,
fccO    =fccO_save,
fcO     =fcO_save,
fcoO    =fcoO_save,
Tg      =Tg_save,
Ts      =Ts_save,
Ra      =Ra_save,
Rb      =Rb_save,
Rc      =Rc_save,
Rd      =Rd_save,
Re      =Re_save,
Rf      =Rf_save,
run     =run,
dr_st   =dr_st,
T_st    =T_st,
start   =start)

```

Figure 3.11: Example of data storing in Python

Step 12: Graph plotting

Overall reaction rate across monolith channel are computed. The temperature profile, concentration profile, individual reaction rate and hysteresis graph are plotted.

```
plt.figure('hysteresis 0.000m')

plt.plot(Tg_graph[      :phase1 ,2],(r2CO[      :phase1 ]),label='ignition')
plt.plot(Tg_graph[phase1:      ,2],(r2CO[phase1:      ]),label='extinction')
plt.legend(loc=4)
plt.xlabel('Inlet Gas Temperature, K',fontsize='x-large')
plt.ylabel('CO reaction rate, mol/m3s',fontsize='x-large')
plt.title('Light-Off Hysteresis')
plt.grid()
plt.grid(which='minor',linestyle='-')
plt.subplots_adjust(left=0.085, bottom=0.1, right=0.65, top=0.95, wspace=None, hspace=None)
```

Figure 3.12: Example of graph plotting in Python

3.5.1 Flow Chart

A flow chart representing the flow of the computer program is shown in Figure 3.13 in the following pages.

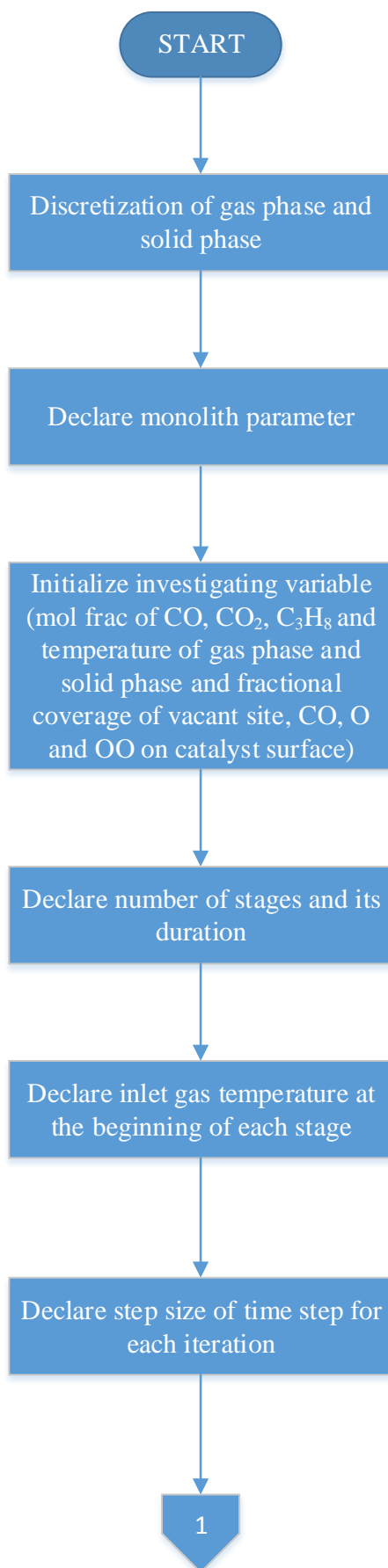


Figure 3.13: Flow chart

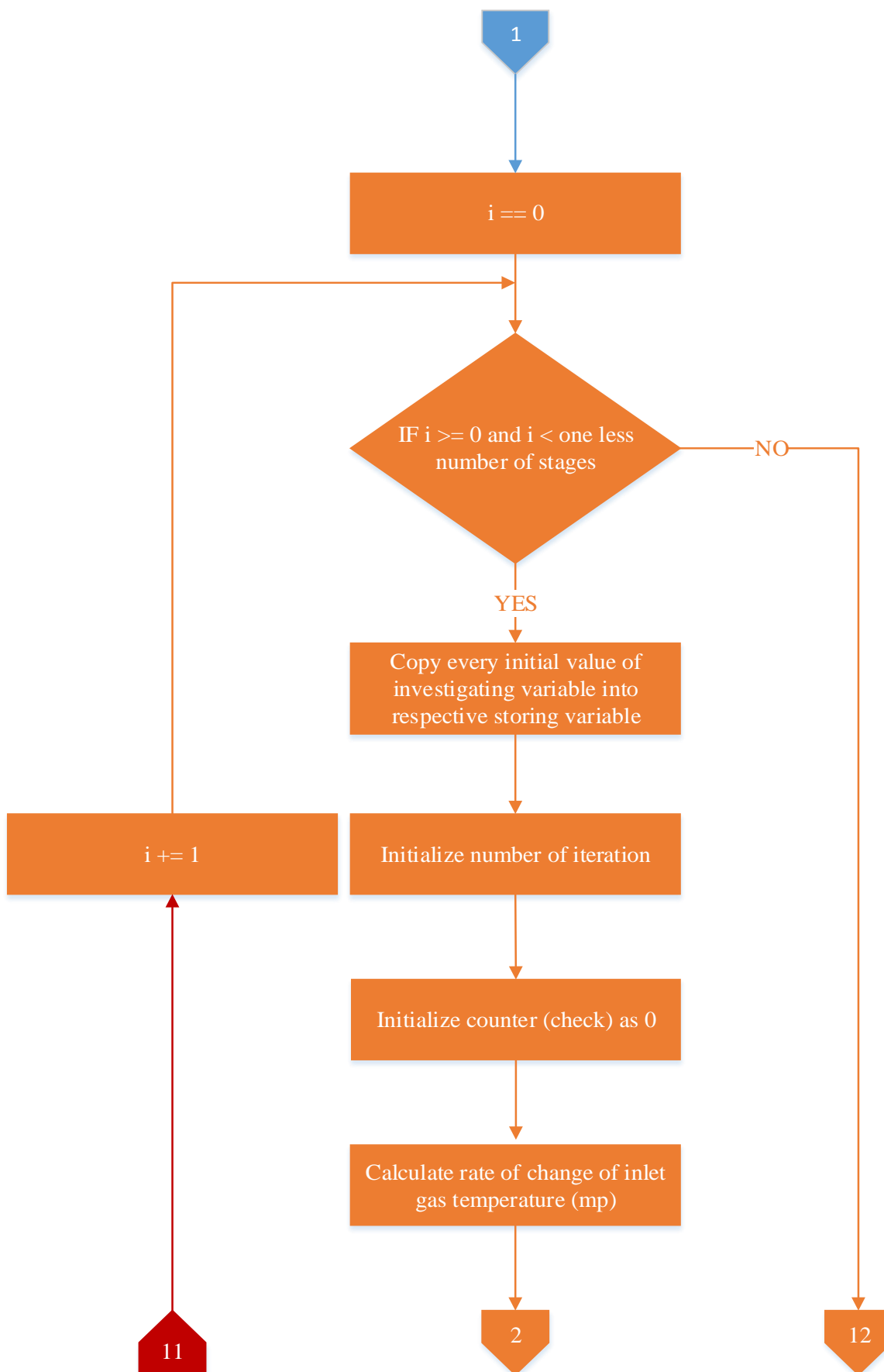


Figure 3.13: Flow chart (cont.)

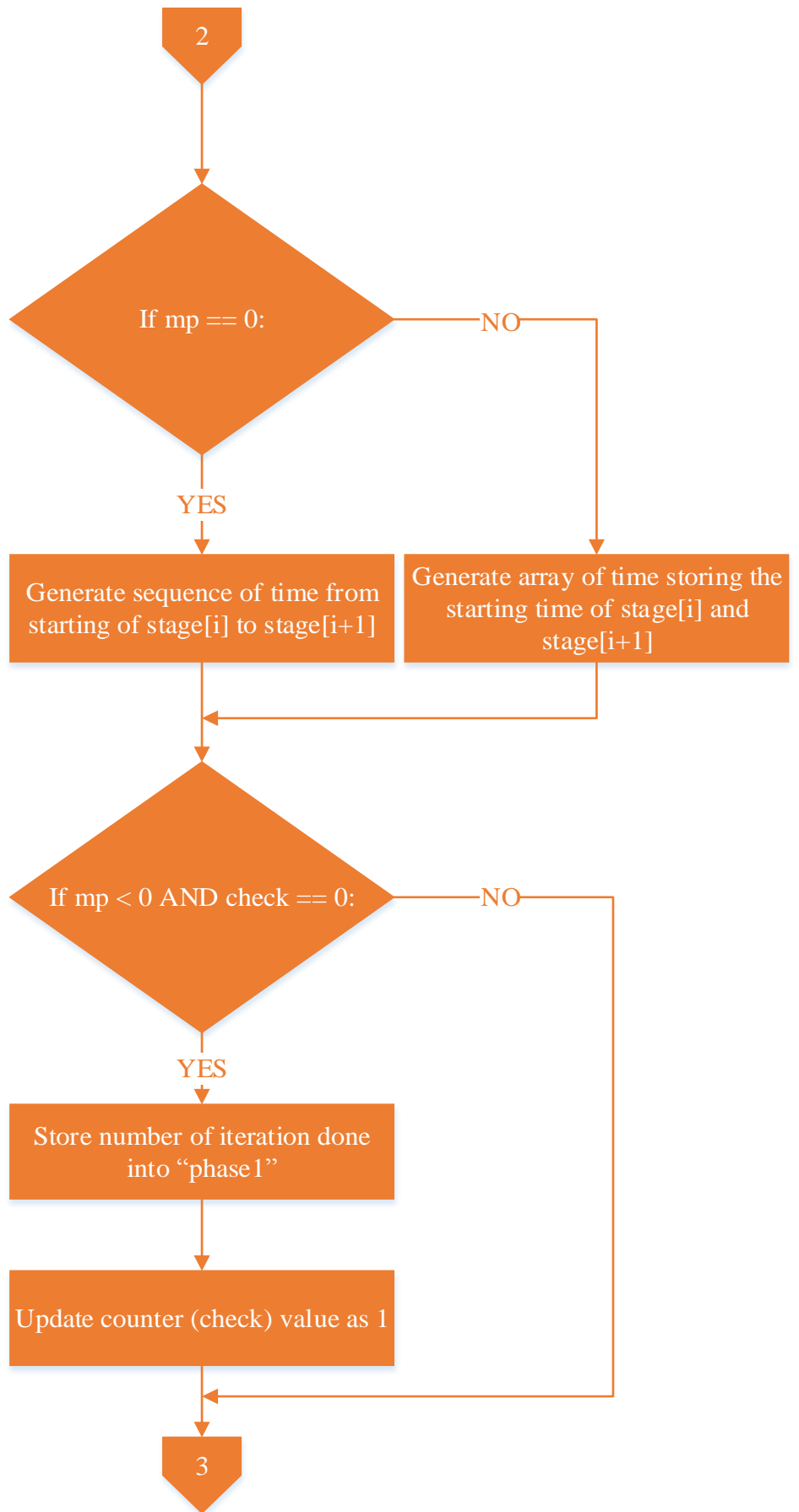


Figure 3.13: Flow chart (cont.)

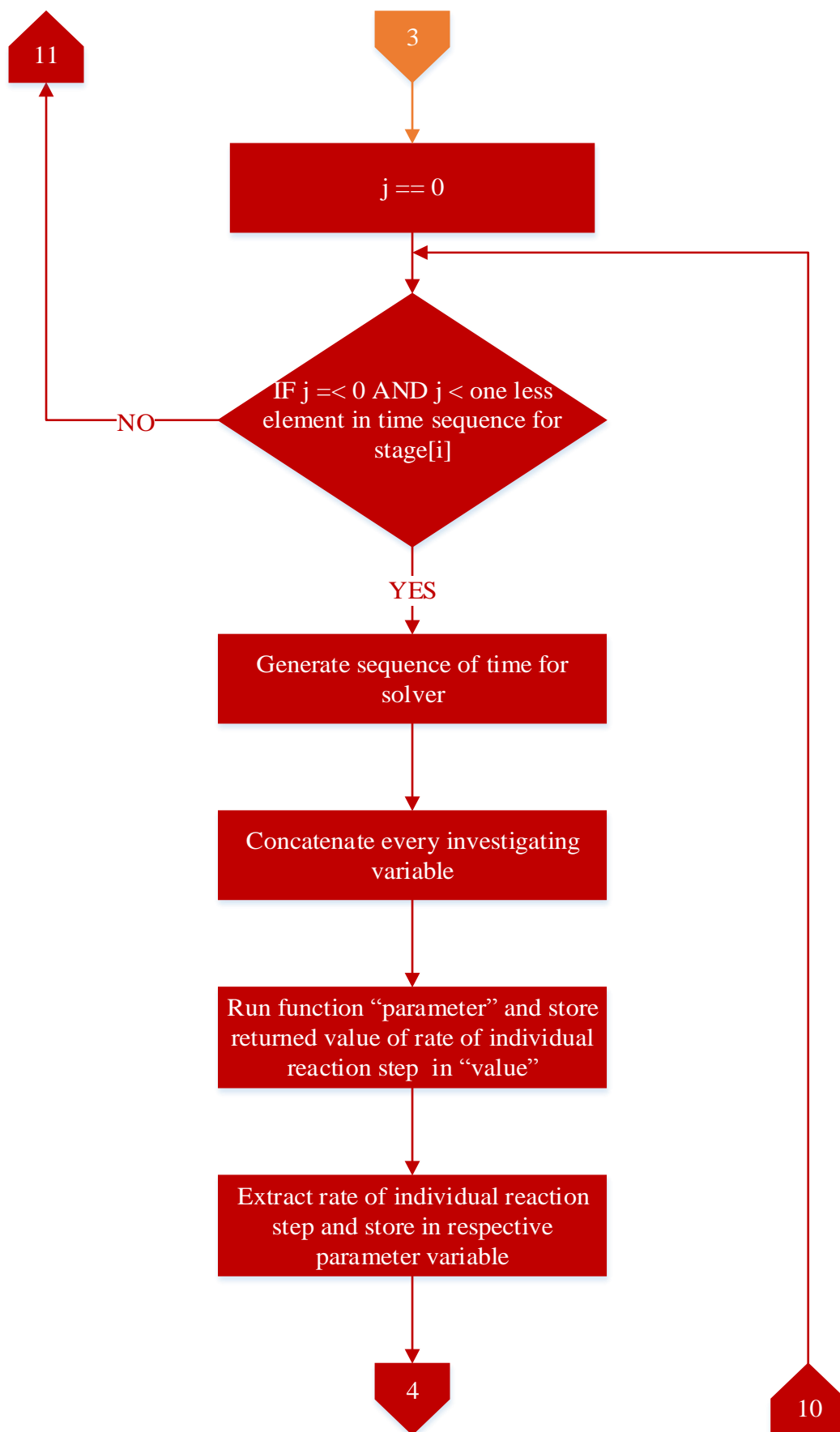


Figure 3.13: Flow chart (cont.)

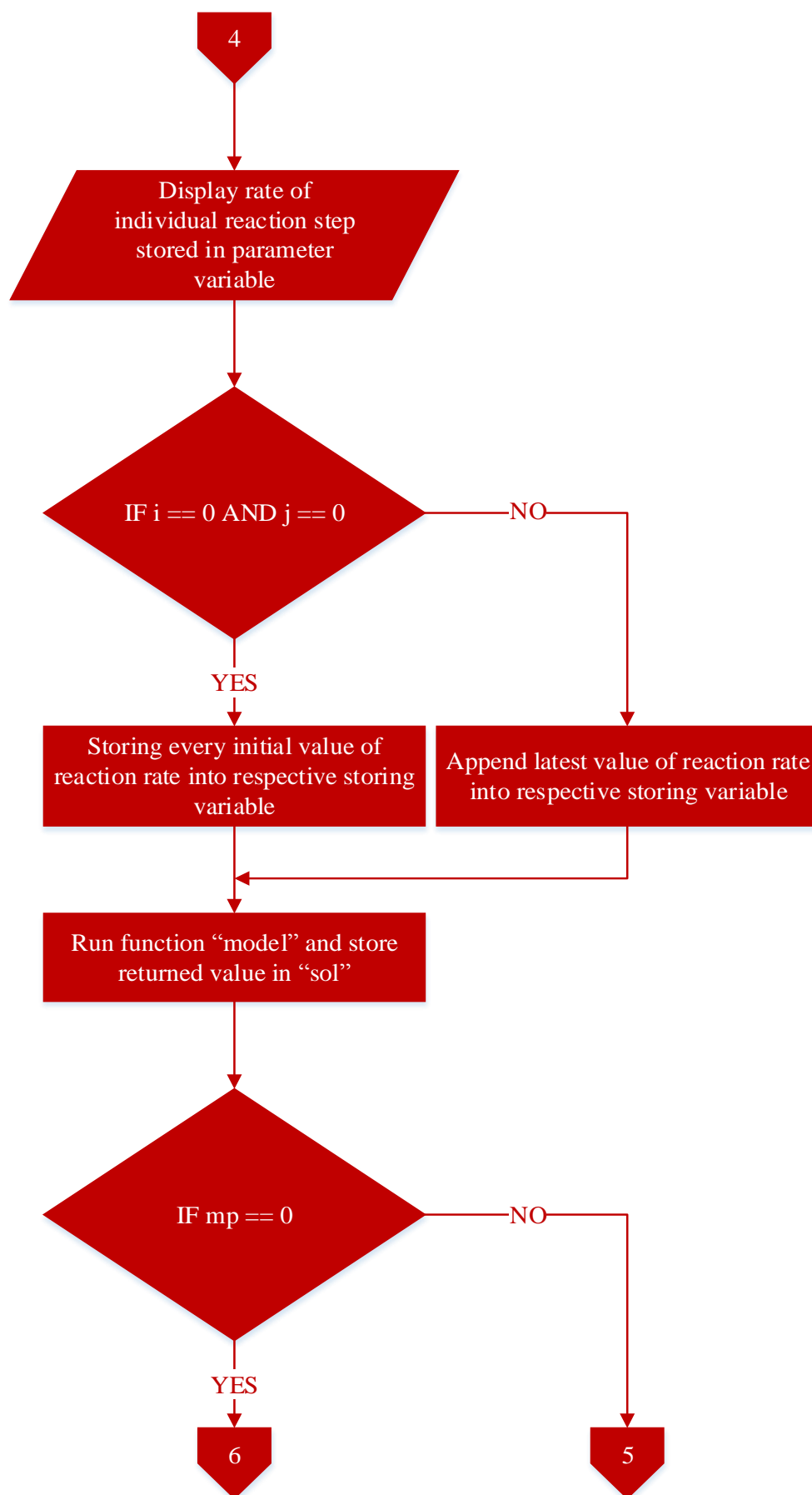


Figure 3.13: Flow chart (cont.)

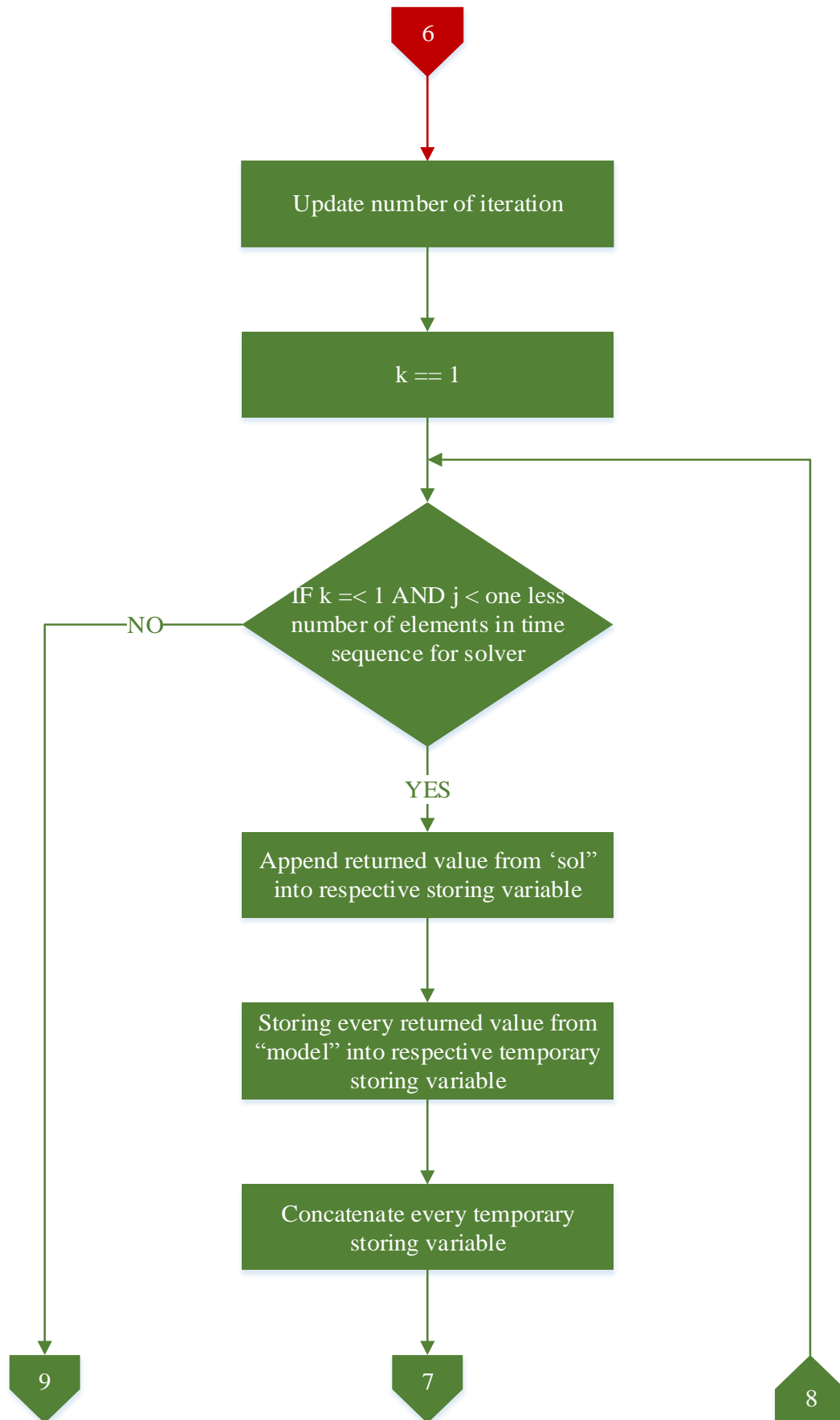


Figure 3.13: Flow chart (cont.)

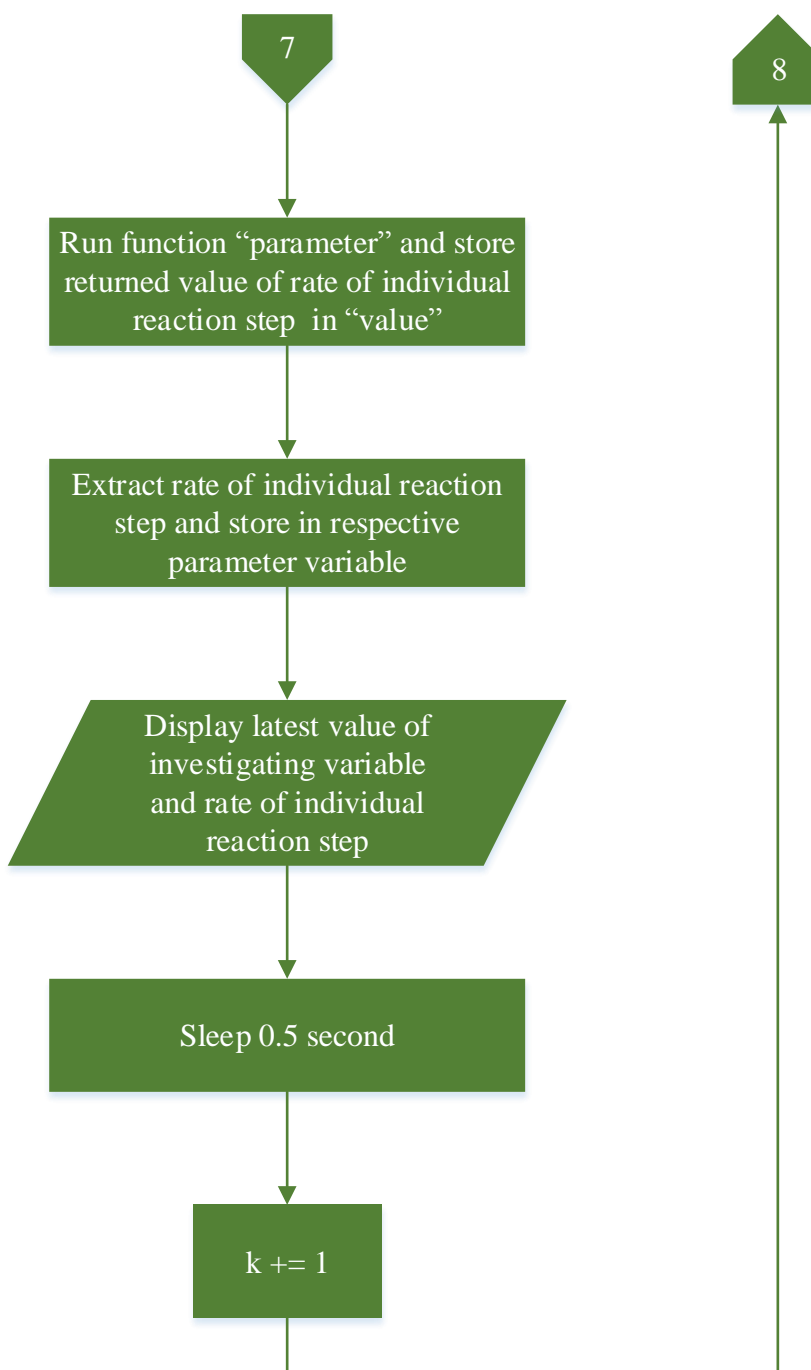


Figure 3.13: Flow chart (cont.)

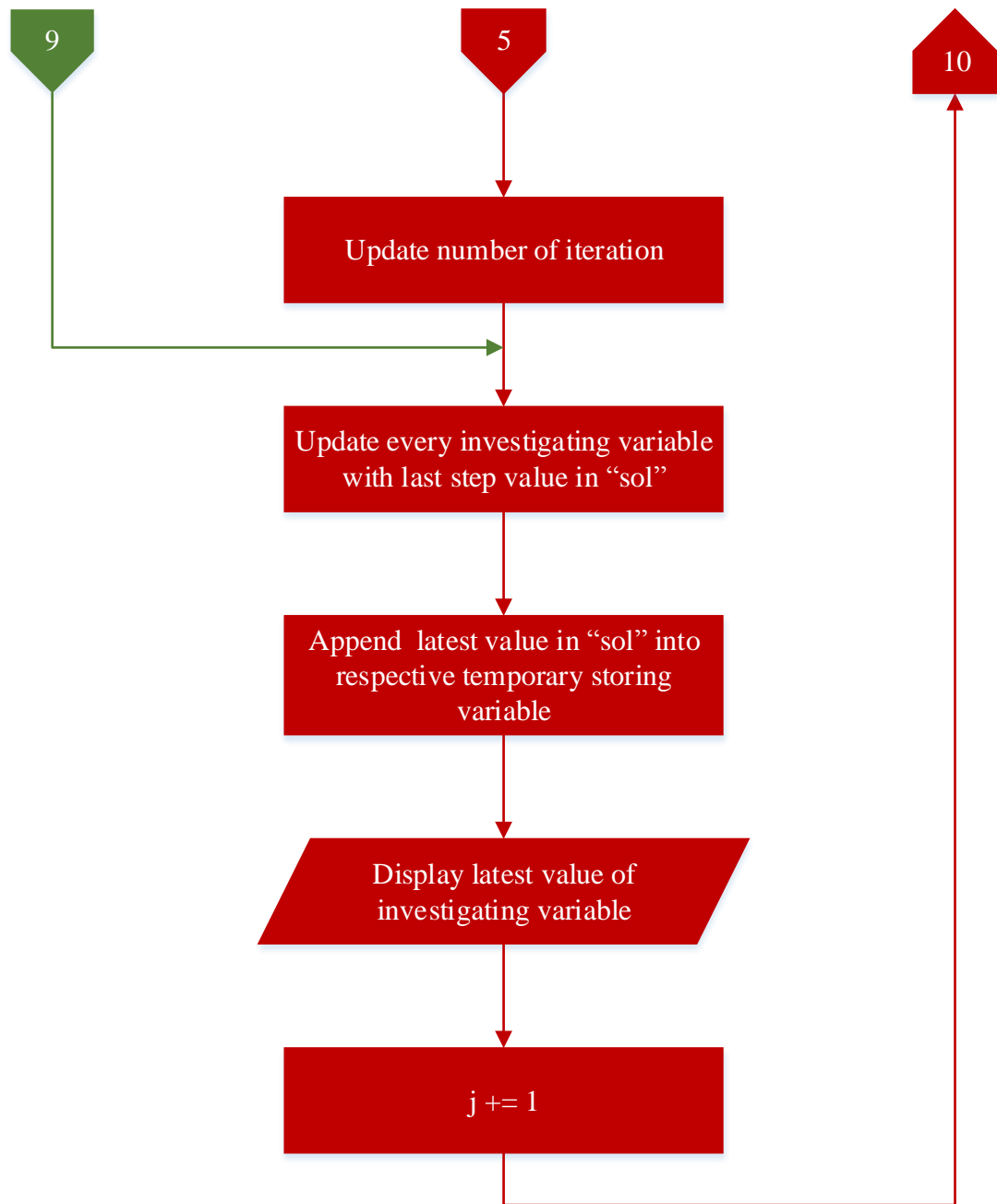


Figure 3.13: Flow chart (cont.)

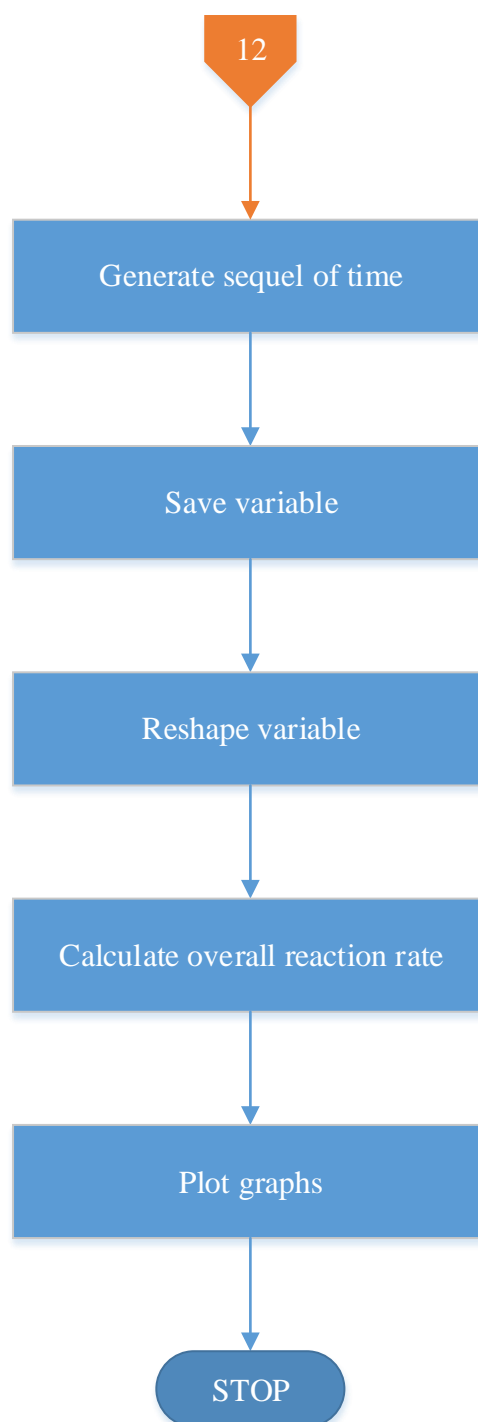


Figure 3.13: Flow chart (cont.)

CHAPTER 4

RESULT AND DISCUSSION

4.1 Ignition-Extinction Curve

The ignition-extinction curve was generated through simulation of a 0.005m or 5mm single monolith channel. Experimentally (Ye *et al*, 2011), this is done by changing the inlet gas temperature to the diesel oxidation catalyst. In the simulation, both solid phase and gas phase inside the monolith and inlet gas had an initial temperature of 417K. The temperature of inlet gas is then increased to 505K at 0.44Ks^{-1} . Heating rate is reduced to 0.08Ks^{-1} until inlet gas temperature is increased to 545K, where it was held constant for 5 mins. The inlet gas temperature is then lowered to 485K by 0.6Ks^{-1} followed by cooling to 445K with the cooling rate of 0.2Ks^{-1} . The inlet gas is further cooled to 417K by 0.056Ks^{-1} . The inlet gas temperature is set up in such a way to simulate the temperature variation of diesel exhaust stream into catalytic converter where engine is cold when started and maintained at specific torque before the engine is gradually cool down. Variation of inlet gas temperature with time is shown in Figure 4.1.

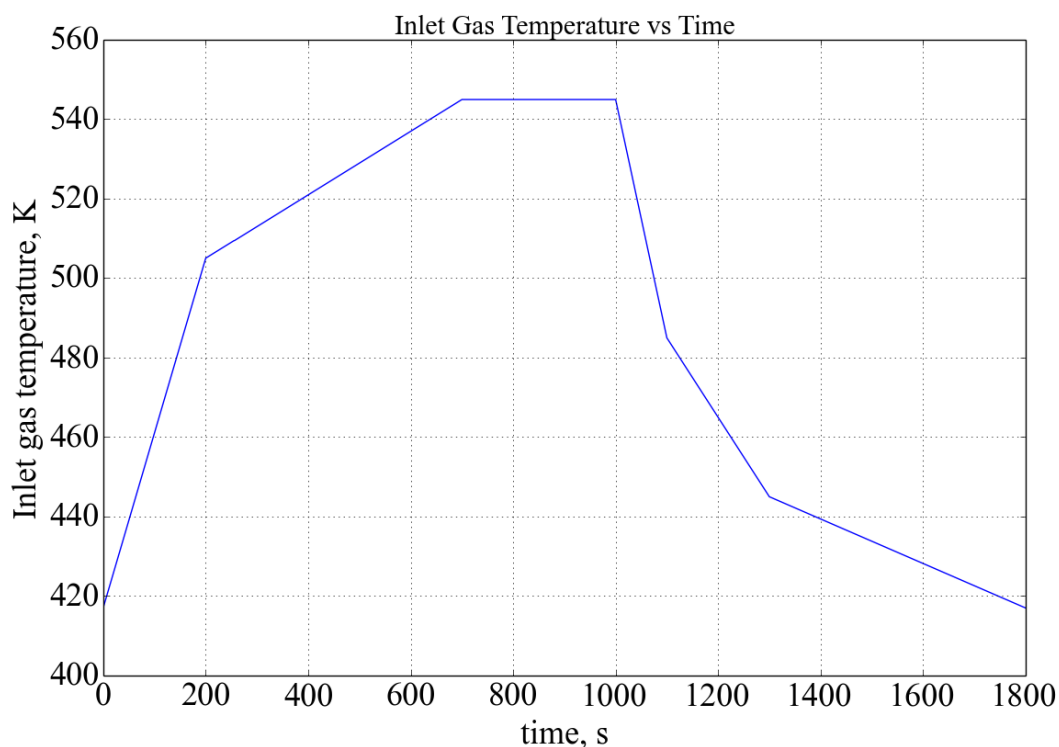


Figure 4.1: Inlet gas temperature versus time

Figure 4.2 shows the ignition-extinction curve generated from constant 3000ppm of CO in the inlet stream. The ignition-extinction curve is plotted as conversion of CO versus inlet gas temperature graph. Figure 4.3 shows the ignition-extinction curve obtained from experiment (Ye *et al*, 2011) is included for comparison. The theoretical explanation for the ignition-extinction hysteresis has been covered in Chapter 2.4.4.

As seen in Figure 4.2, there is clear ignition-extinction hysteresis generated from the computer simulation, where ignition takes place at 510K and extinction at around 445K. Compared to experiment performed by Ye *et al* (2011), the ignition-extinction curves generated from experiment consists of no significant step-increase or decrease during ignition and extinction. Steps observed in ignition-extinction curves generated from simulation is probably due to incomplete representation of actual reaction mechanism in compressed oxygen model.

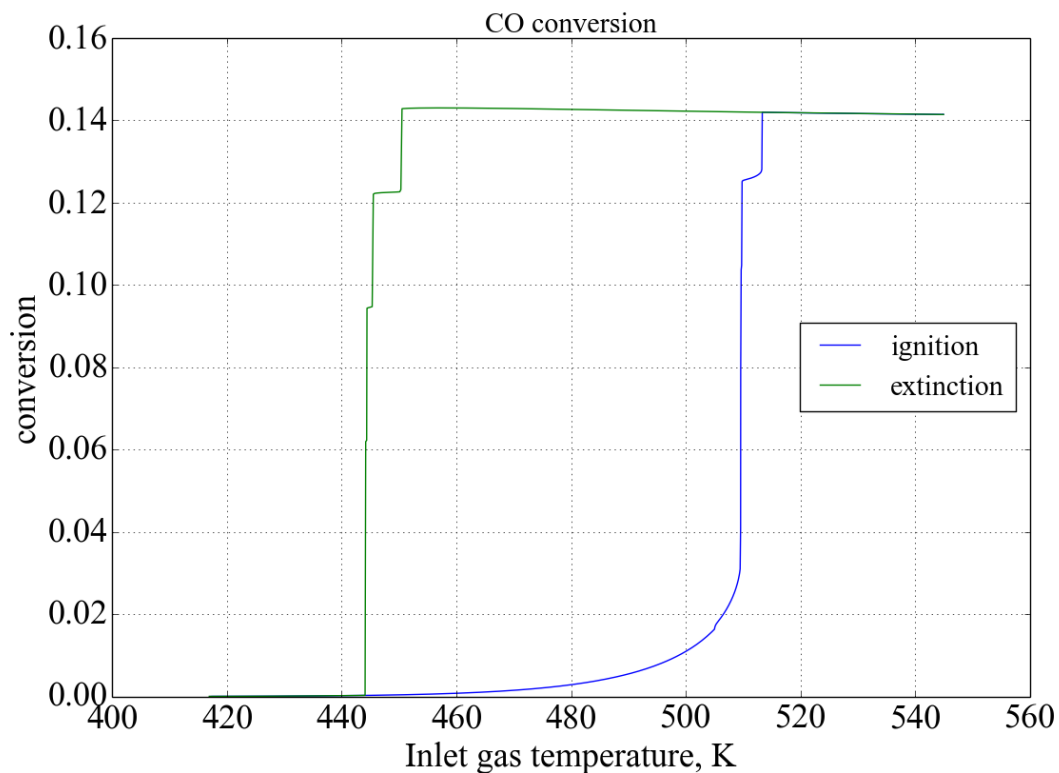


Figure 4.2: Ignition and extinction hysteresis of CO oxidation in a single channel 0.005m monolith

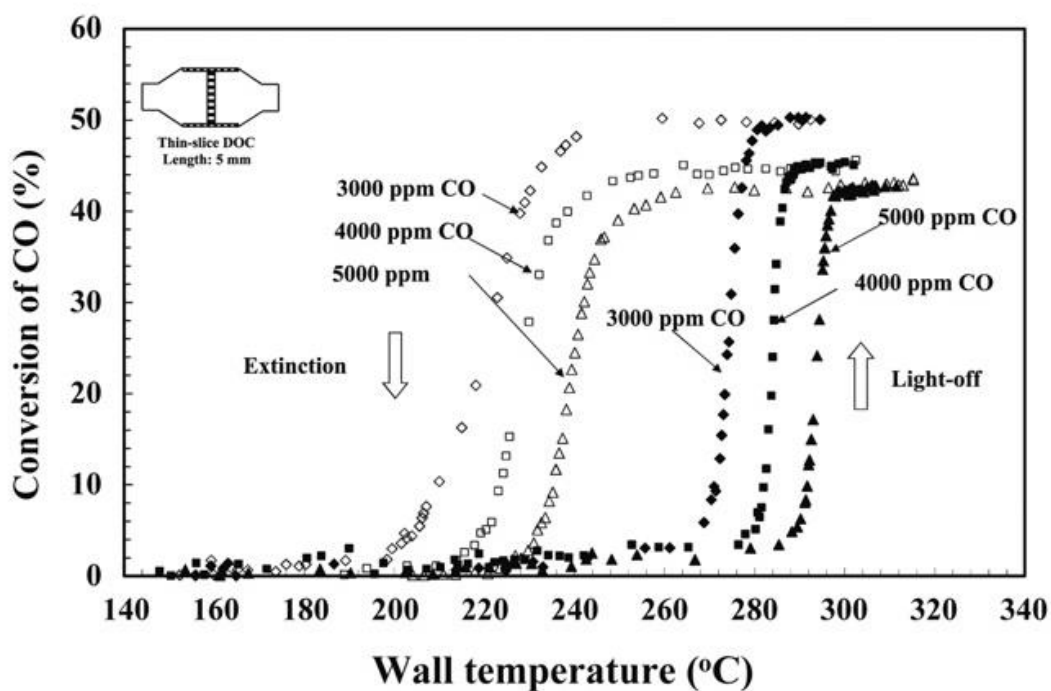


Figure 4.3: Thin slice diesel oxidation catalyst ignition-extinction hysteresis curve for different inlet CO concentration (adapted from Ye et al, 2011)

To explain the step observed in the hysteresis curve from viewpoint of mathematical model, the step is created as pseudo-steady state in catalytic converter is reached and maintained for a period. As highlighted in Figure 4.4, gas phase CO concentration gradient between ignited volume and its upstream becomes significantly large during ignition. Higher rate of convective mass transfer induced by increased concentration gradient tend to carry more CO into the ignited volume. At the same time, diffusion rate of CO into solid phase decreased as the concentration gradient between gas phase and solid phase reduced. Transportation of CO into and out from gas phase balanced up. Gas phase CO concentration becomes pseudo-steady. The gas phase CO concentration plateau.

According to Hayes and Kolaczkowski (1994), the pseudo-steady state exists when temperature and concentration profiles satisfied the mole and energy balance equations. From a catalytic converter operation standpoint, each pseudo-steady state represent an operating point. During the pseudo-steady state, reaction changes from kinetic control to mass transfer control.

As inlet gas temperature further increases, upstream solid phase is getting ignited as highlighted in Figure 4.5. Ignition reduces the gas phase CO concentration on upstream. Insufficient concentration gradient between upstream and downstream causes the pseudo-steady state in gas phase to collapse.

Similar phenomenon can be observed during extinction. However, extinction curve consists of more steps as there is more delay between extinctions.

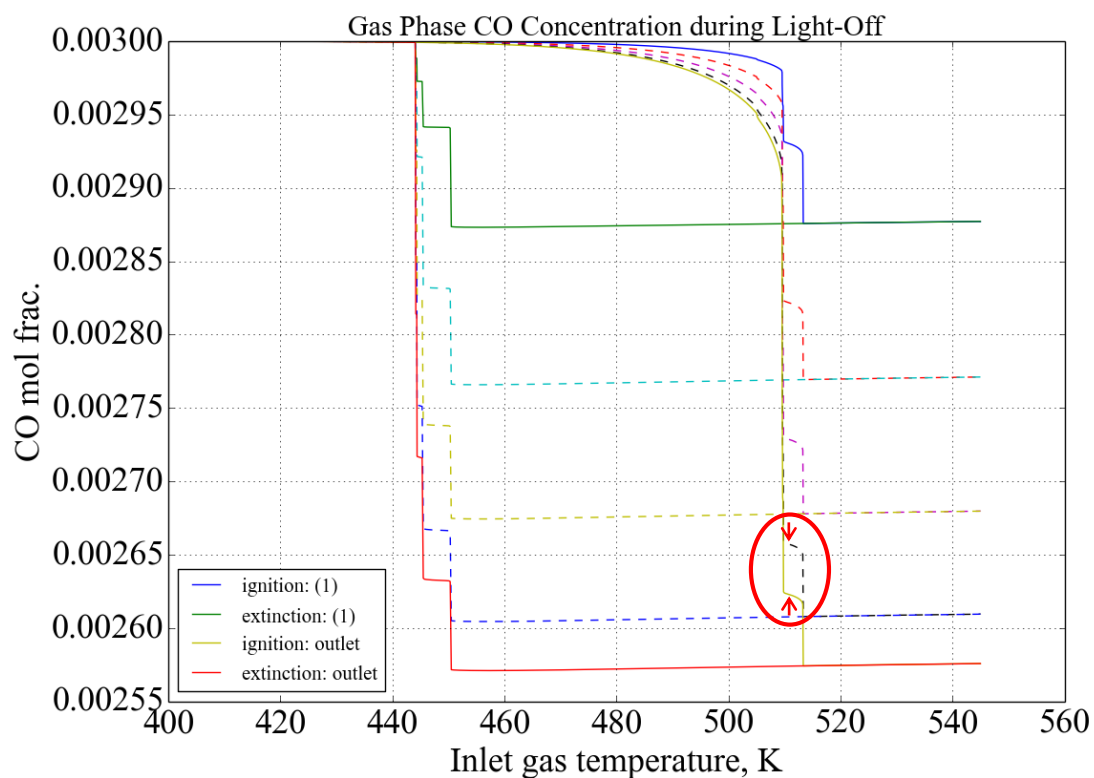


Figure 4.4: Gas phase CO concentration at various position along 0.005m channel

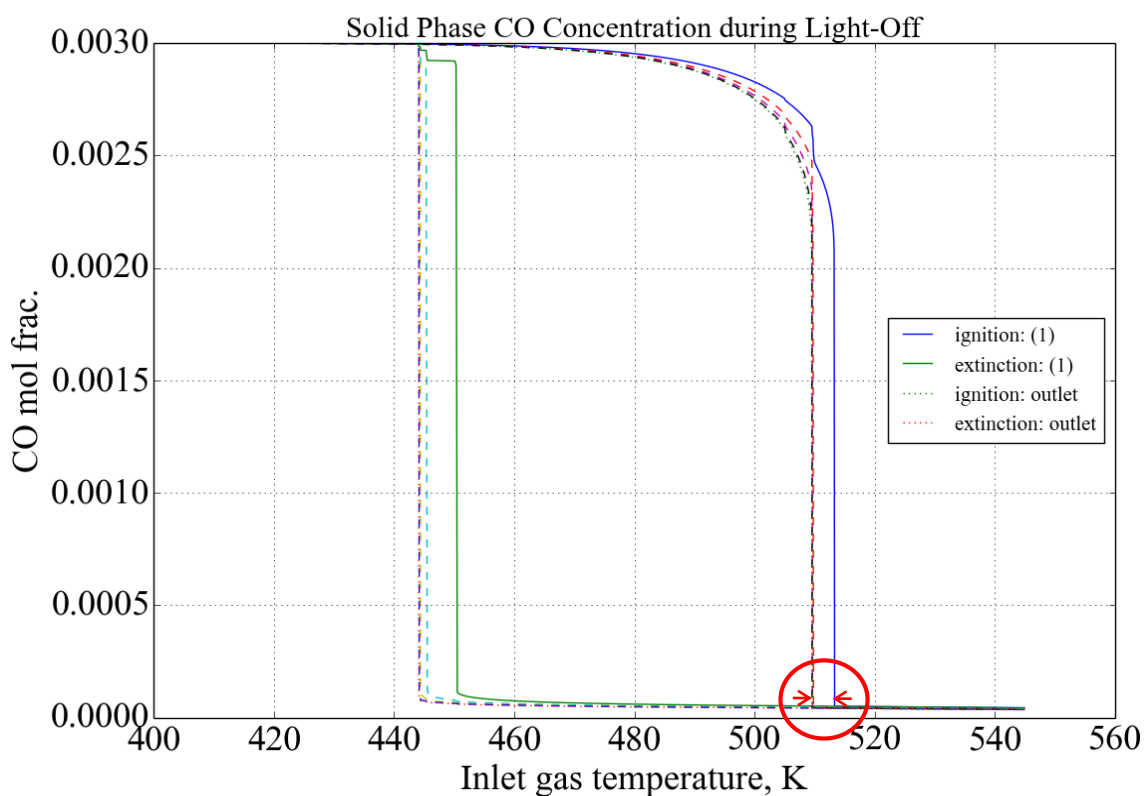


Figure 4.5: Solid phase CO concentration at various position along 0.005m channel

As it can be seen in mechanistic model in section 3.3.1, coverage of each species plays an important role during ignition-extinction. Variation of fractional coverage of CO, O, OO and vacant site with time is plotted in Figure 4.6, Figure 4.7, Figure 4.8 and Figure 4.9 respectively.

Initially, catalyst surface coverage is pre-dominated by CO. Figure 4.6 shows that the fractional coverage of CO started to drop during ignition. This opens up opportunity for oxygen to adsorb on the surface. Fractional coverage of oxygen increases as shown in Figure 4.7. High oxygen coverage also encourages compression of oxygen by carbon monoxide. However, the coverage of compressed oxygen is not significant as shown in Figure 4.8.

After constant temperature period, the catalyst surface has more than 50% coverage of oxygen. When the inlet gas temperature drops below the temperature which there is no oxidation occurred previously, catalyst surface is still covered with significant amount of oxygen. Thus, CO oxidation continue despite lower temperature than ignition temperature. As inlet gas temperature drops further, coverage of oxygen gradually dropped to zero. Extinction occurred and oxidation reaction ceased.

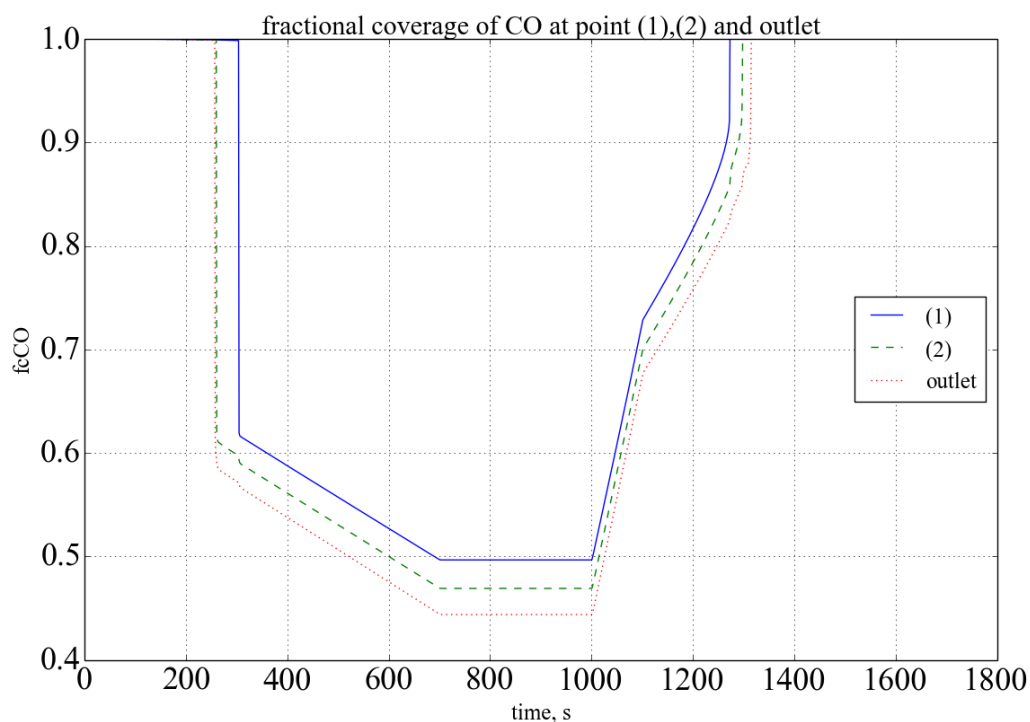


Figure 4.6: Fractional coverage of CO on washcoat in 0.005m channel

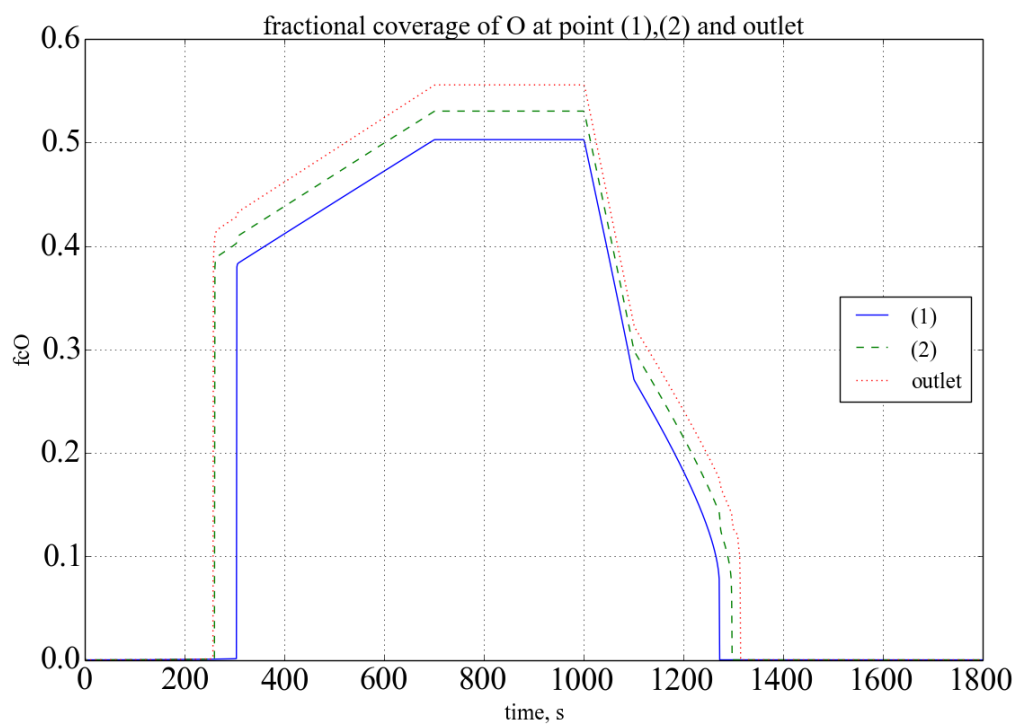


Figure 4.7: Fractional coverage of O on washcoat in 0.005m channel

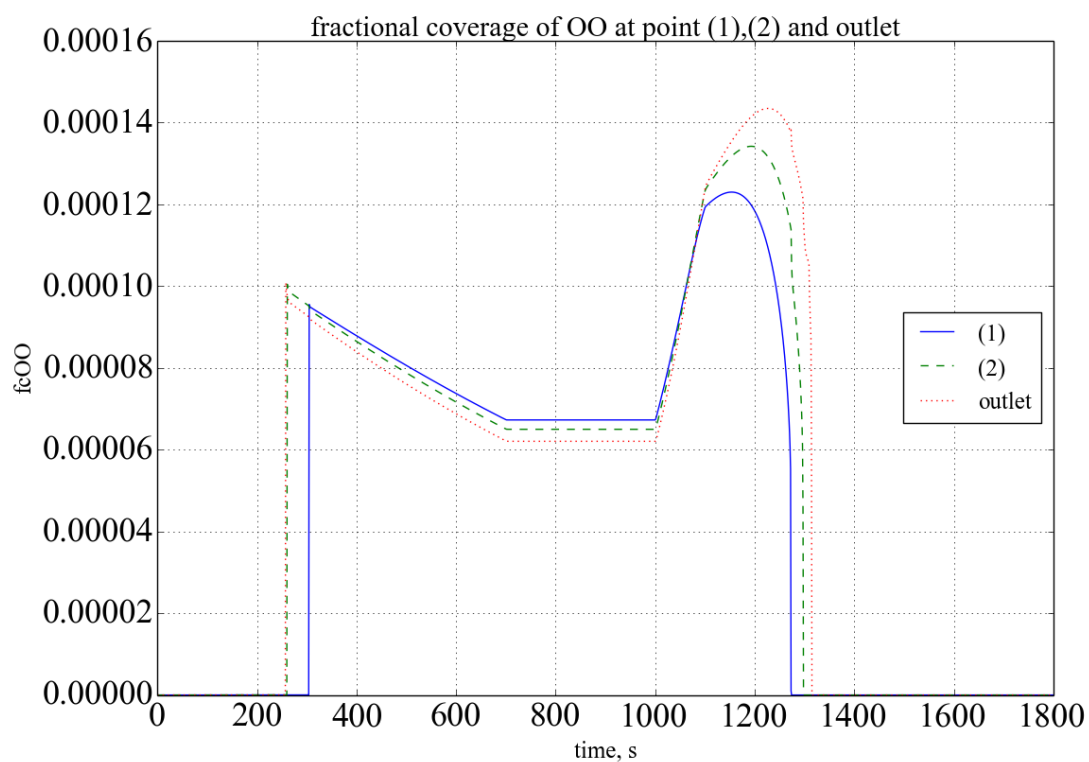


Figure 4.8: Fractional coverage of compressed oxygen OO on washcoat in 0.005m channel

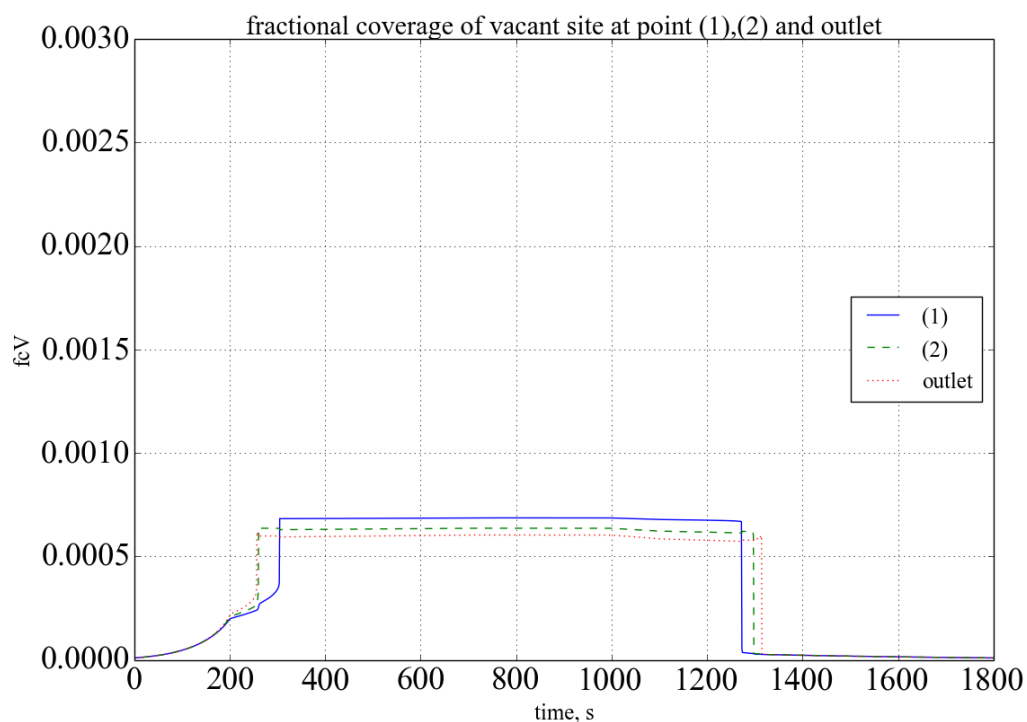


Figure 4.9: Fractional coverage of vacant site on washcoat in 0.005m channel

4.2 Study on the Effect of Change of the Length of Channel

In reality, full scale catalytic converter is much longer than 5 mm. Thus, simulations are conducted with 0.010m, 0.015m, 0.020m and 0.025m long channel respectively. Ignition extinction curve for each case is superimposed on Figure 4.10.

Figure 4.10 shows the ignition-extinction curve is smoothen when the length of the channel increased. Longer channel also achieves higher overall conversion of CO.

Beside better conversion, both ignition and extinction occurred at lower inlet gas temperature for a longer channel. Lower ignition point indicates conversion of CO in diesel exhaust gas starts at lower temperature. As a result, efficiency of diesel oxidation catalyst increases as its length increases.

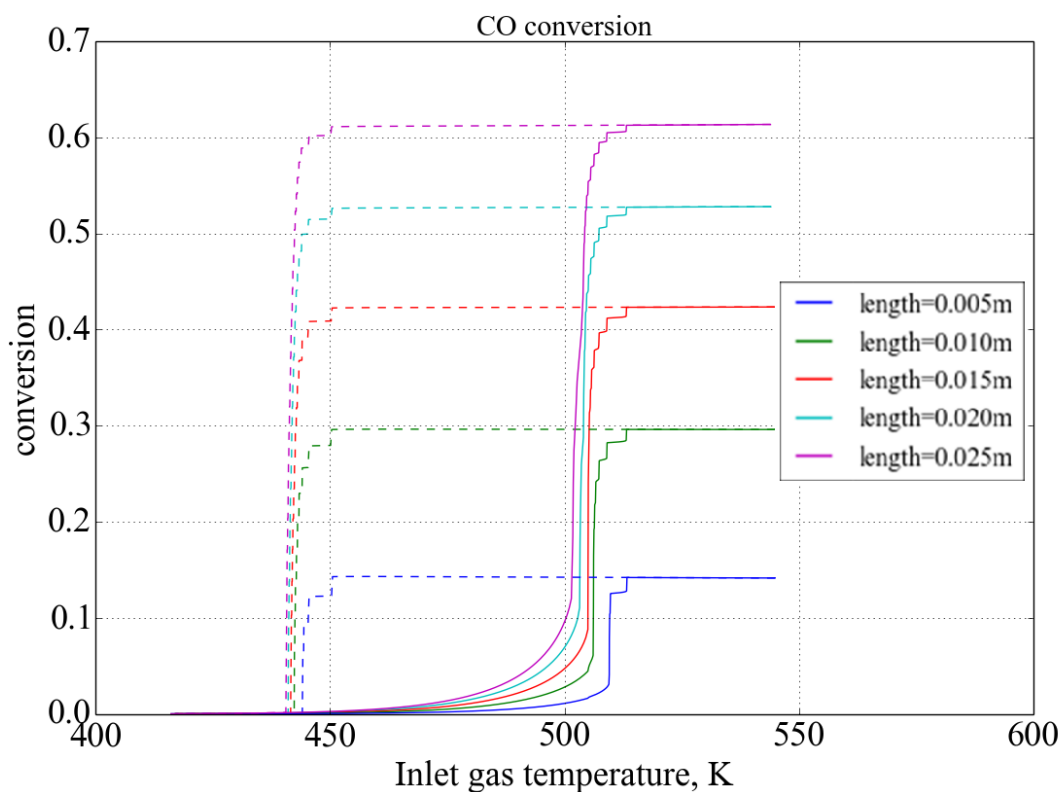


Figure 4.10: Hysteresis Curves for Various Channel Length

4.3 Study on the Effect of Change of the CO Concentration in Inlet Gas of Channel

Carbon monoxide concentration in diesel exhaust varies depend on several conditions such as fuel quality and operation factors (Takizad, 2012). In this section, CO concentration in diesel exhaust stream into catalytic converter is raised to 4000ppm and 5000ppm. Ignition extinction curve for each case is superimposed on Figure 4.11.

Figure 4.11 shows conversion drops as inlet CO concentration increases to 5000ppm. This could be due to incomplete ignition throughout the catalytic converter. This indicates that the catalytic converter operate at lower efficiency when CO concentration of engine effluent increases.

Figure 4.11 also shows the ignition and extinction takes place at higher temperature when the CO concentration of inlet gas increased. At higher CO concentration, adsorption rate of CO is higher. Oxygen can only start to adsorb on the

surface at elevated temperature as desorption rate of CO becomes higher. Ignition point and extinction point observed in simulation and experiment (Ye *et al*, 2011) for 3000ppm, 4000ppm and 5000ppm is listed in Table 4.1:

Table 4.1: Ignition Point and Extinction Point for Different CO Concentration

CO concentration	Simulation		Experiment	
	Ignition Point, (K)	Extinction Point, (K)	Ignition Point, (K)	Extinction Point, (K)
3000ppm	510	445	533	503
4000ppm	525	450	553	508
5000ppm	540	455	563	513

Comparing to experiment performed by Ye *et al* (2011) as illustration in Figure 4.3, the ignition point and the extinction point is lower in simulation. The hysteresis observed in simulation is also greater. Tuning of parameters in the mechanistic model of CO oxidation is necessary to fit the hysteresis curve obtained experimentally. Result from tuning parameters in the mechanistic model is included in the section 4.6.

Conversion is also relatively higher in the experiment. However, it should be understood that multi-channel diesel oxidation catalyst is used in the experiment while simulation only computes the conversion across a single channel. More channels provide greater residence time of engine effluent in the catalytic converter as the gas flow is distributed into the multiple channels. High residence time will lead to greater conversion as shown in section 4.3.

4.4 Study on the Effect of Ramping Up and Ramping Down of the CO Concentration in Inlet Gas of Channel

In the previous section, effect of carbon monoxide concentration in diesel exhaust on hysteresis is determined. However, previous simulation assumed constant CO concentration in diesel exhaust which is only applicable for the case when engine operates under same speed (Ye, 2011). As engine speed increases, carbon monoxide concentration in diesel exhaust ramp up (Grenier, 2005). In this section, effect of ramping up and ramping down of the CO concentration on catalytic converter inlet based on compressed oxygen model were studied. The simulation starts with the catalyst surface mostly covered with adsorbed oxygen. CO concentration in catalytic converter inlet is ramped up from zero till 2500ppm followed by ramping down to zero. Simulated result is shown in Figure 4.12.

Initially, CO is oxidized as the exhaust stream through the catalyst converter. For feed temperature at 394.0K, 407.0K and 417.0K, CO oxidation ceased when inlet CO concentration increased to extinction point. Oxidation reaction resumed when CO concentration dropped low enough to ignition point. Figure 4.6 shows extinction point takes place at higher CO concentration compared to ignition point.

At higher temperature such as 450.0K, extinction point is at higher CO concentration. Thus, no extinction occurred during simulation at feed temperature of 450.0K.

By comparing to result from experiment with same ramping up and ramping down rate done by Salomons (2006) as shown in Figure 4.13, reaction sustained for longer period of time before extinction point is reached. This is probably due to greater platinum loading or longer channel used in the experiment.

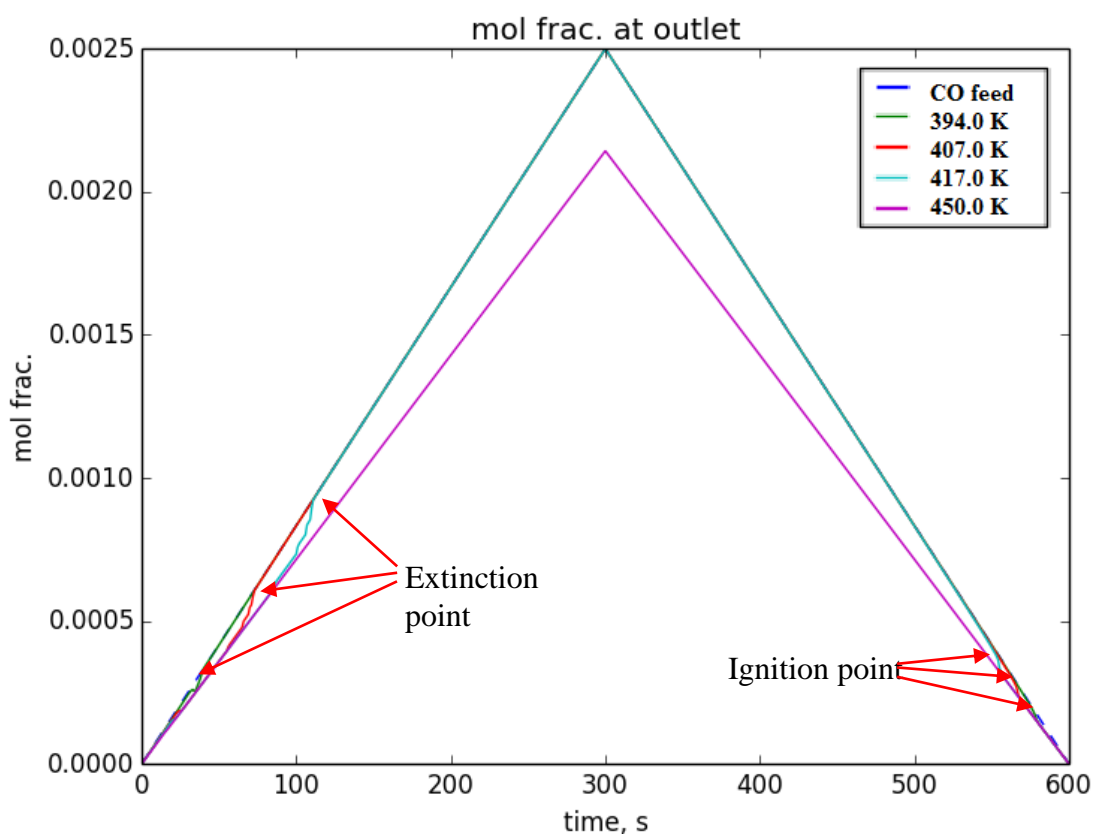


Figure 4.12: Simulation output from a continuous linear ramp of CO concentration at constant feed temperature of 394.0K, 407.0K, 417.0K and 450K in a single channel 0.005m monolith

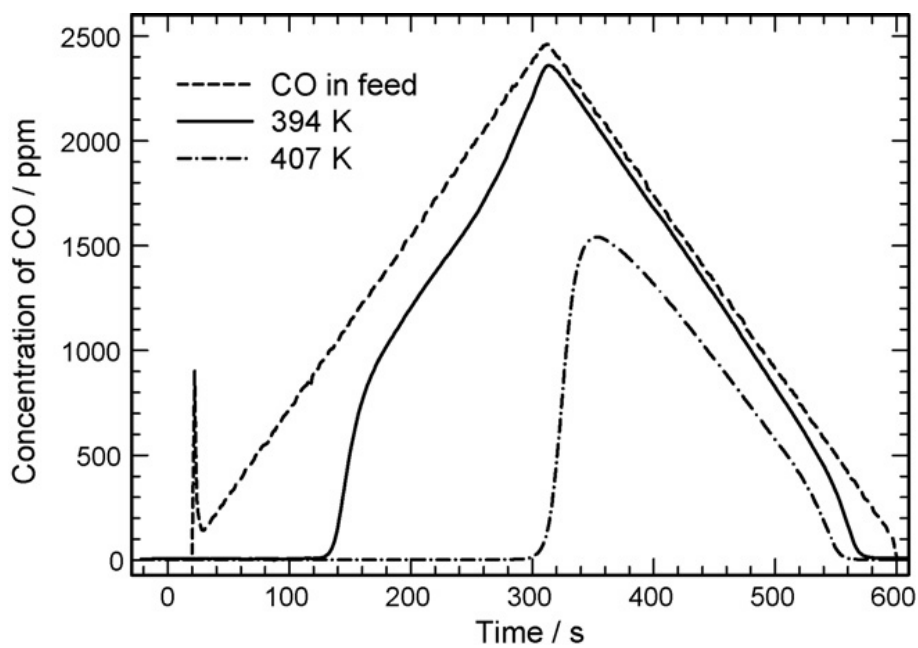


Figure 4.13: Experimental CO output from a continuous linear ramp of CO concentration in feed at constant feed temperature of 394K and 407K. (adapted from Salomons, 2006)

4.5 Study on the Effect of Square Pulse of the CO Concentration in Inlet Gas of Channel

In this section, simulation is conducted by injecting a square pulse of CO with concentration 2500 ppm into the catalytic converter which its surface is oxygen pre-dominated. Figure 4.14 shows the variation of mol fraction of CO at the catalytic converter outlet with time.

From Figure 4.14, CO oxidation reaction is initiated as 2500ppm of CO is injected into the catalytic converter. However, the reaction failed to sustain as CO is continuously feeding into the catalytic converter when the inlet gas temperature is 417K or lower. This is because 2500ppm of CO is high enough to cause extinction at temperature lower than 417K as shown in section 4.4. After the initial adsorbed oxygen is used up by CO oxidation, reaction ceased. As for higher exhaust temperature which is 450K, CO oxidation reaction start to stabilize after 0.5s of the pulse is injected. Reaction continued until the CO feed is cut off.

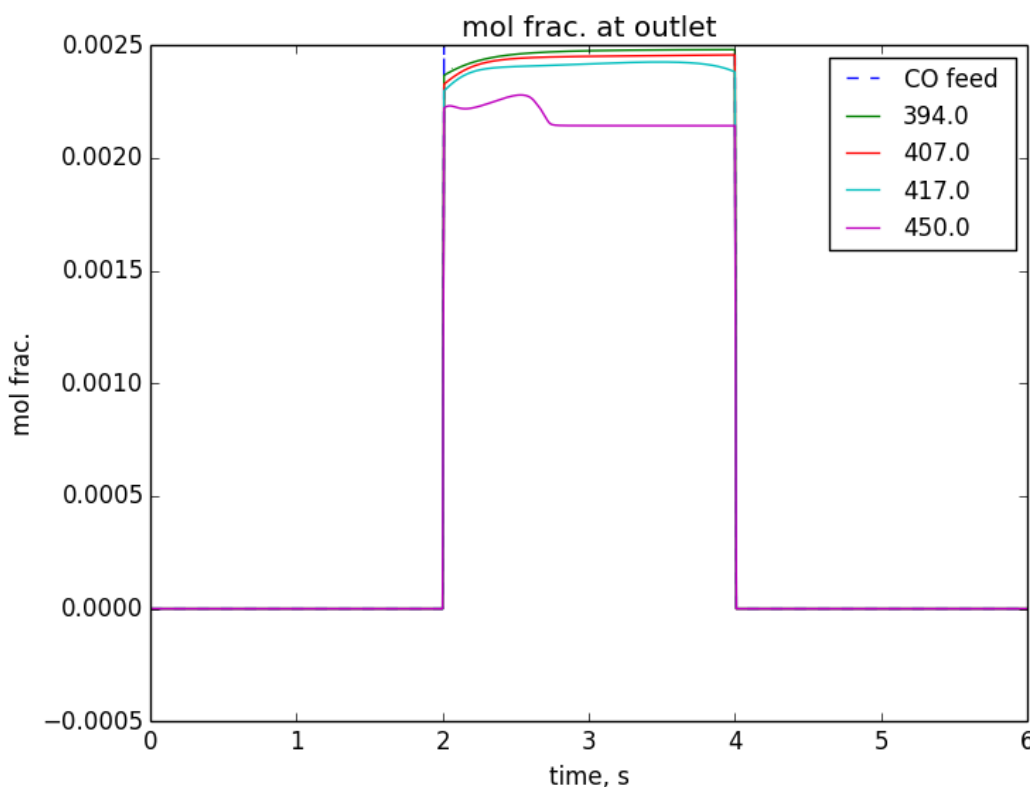


Figure 4.14: Simulation output from a square pulse of CO concentration at constant feed temperature of 394.0K, 407.0K, 417.0 K and 450K in a single channel 0.005m monolith

4.6 Mechanistic Model Tuning

In this section, six parameters in mechanistic model is tuned to study its effect on hysteresis curve and thus, improve the fitting of the simulated curve with experimentally obtained curve (Ye *et al*, 2011). The six parameters are:

1. Pre-exponential Value for Carbon Monoxide Desorption
2. Pre-exponential Value for Oxygen Adsorption
3. Pre-exponential Value for Reaction between CO and O
4. Pre-exponential Value for Oxygen Compression
5. Pre-exponential Value for Reaction between CO and OO
6. Pre-exponential Value for Reverse Oxygen Compression

As illustrated in Figure 4.15, when pre-exponential value for carbon monoxide desorption is tuned to greater magnitude, hysteresis becomes smaller as ignition temperature reduces. However, fourfold increase of pre-exponential values does not affect much on extinction temperature. This indicates that carbon monoxide desorption have no or less effect on extinction.

Figure 4.16 shows hysteresis becomes smaller as ignition temperature reduces greatly when pre-exponential value for oxygen adsorption is tuned to greater magnitude. At fourfold increase of pre-exponential value for oxygen adsorption, extinction temperature reduced slightly. However, compared to carbon monoxide desorption, oxygen adsorption have greater effect on reducing the broadness of hysteresis.

On the other hand, increase in pre-exponential value for reaction between CO and O shifted hysteresis curve to the left without affecting the broadness of the hysteresis as shown in Figure 4.17. When pre-exponential of the reaction increased by fourfold, CO oxidation does not ceases and no extinction occurred when temperature dropped to 417K.

Figure 4.18, Figure 4.19 and Figure 4.20 show that no significant changes in hysteresis curve despite increase in pre-exponential value for oxygen compression, reaction between CO and OO and reverse compression of oxygen respectively. Low

coverage of compressed oxygen as shown in Figure 4.8 limits the reaction rate for CO and OO and rate of reverse compression.

To improve fitting of simulated ignition-extinction hysteresis, pre-exponential value for oxygen adsorption rate can be tuned to higher magnitude to reduce the broadness of the hysteresis. At the same time, magnitude of pre-exponential value for reaction between CO and O should be lowered to shift the hysteresis curve to the right. As a result of tuning of two parameters simultaneously, the curve is expected to have smaller hysteresis but with higher ignition temperature and extinction temperature which is similar to the curve obtained experimentally (Ye *et al*, 2011).

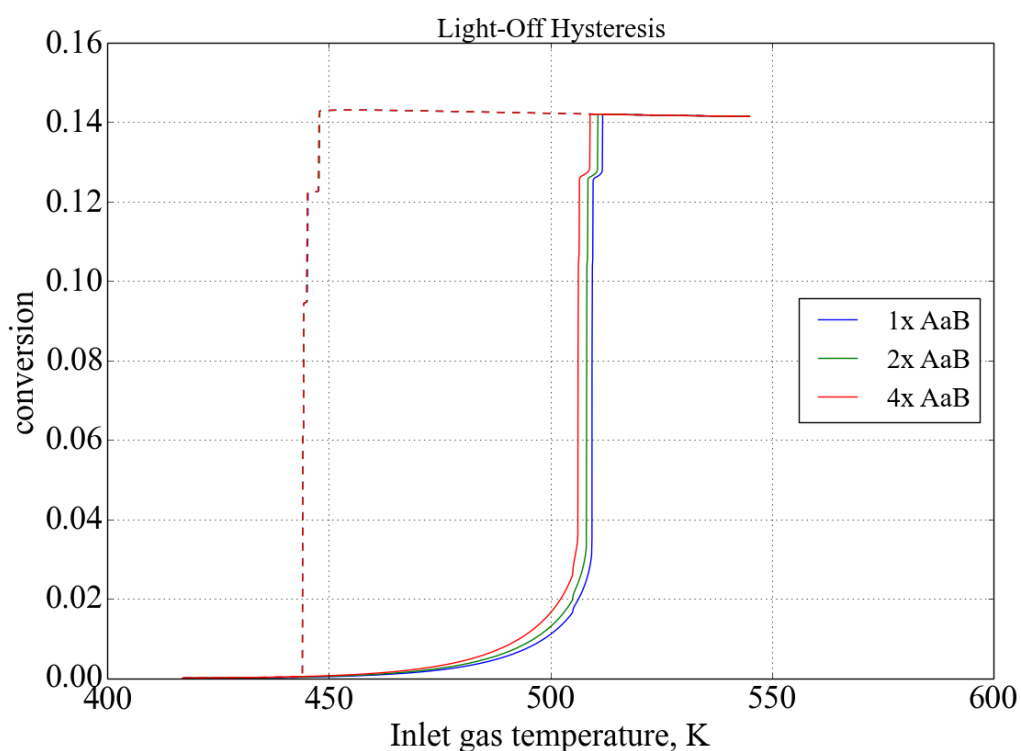


Figure 4.15: Hysteresis diagram of CO oxidation in a single channel 0.005m monolith with Tuned Pre-exponential for Carbon Monoxide Desorption

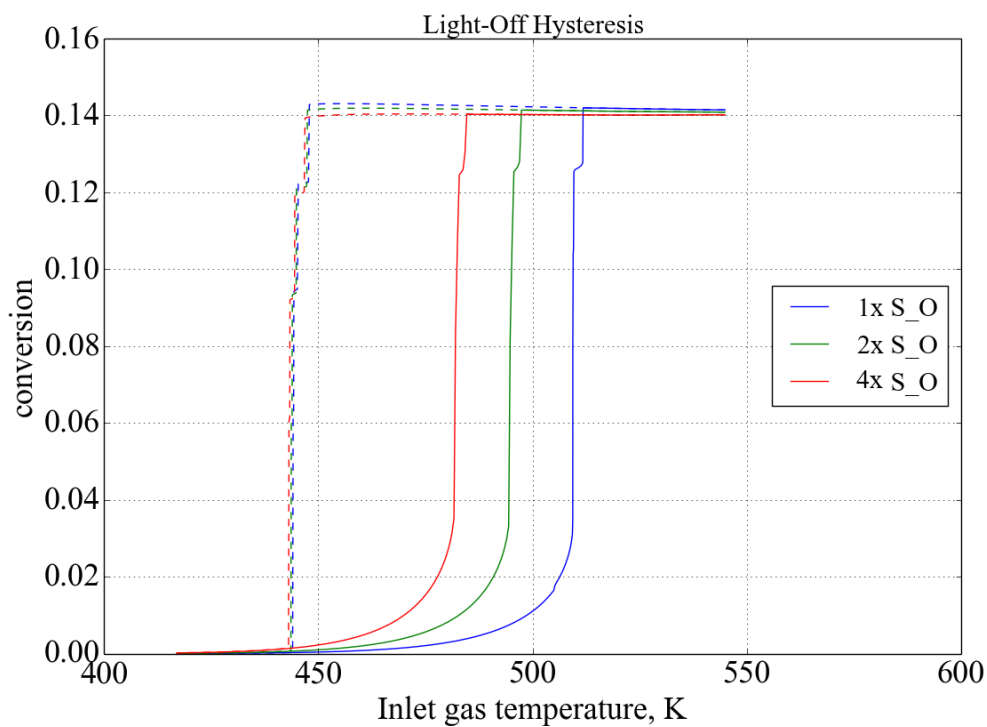


Figure 4.16: Hysteresis diagram of CO oxidation in a single channel 0.005m monolith with Tuned Pre-exponential value for Oxygen Adsorption

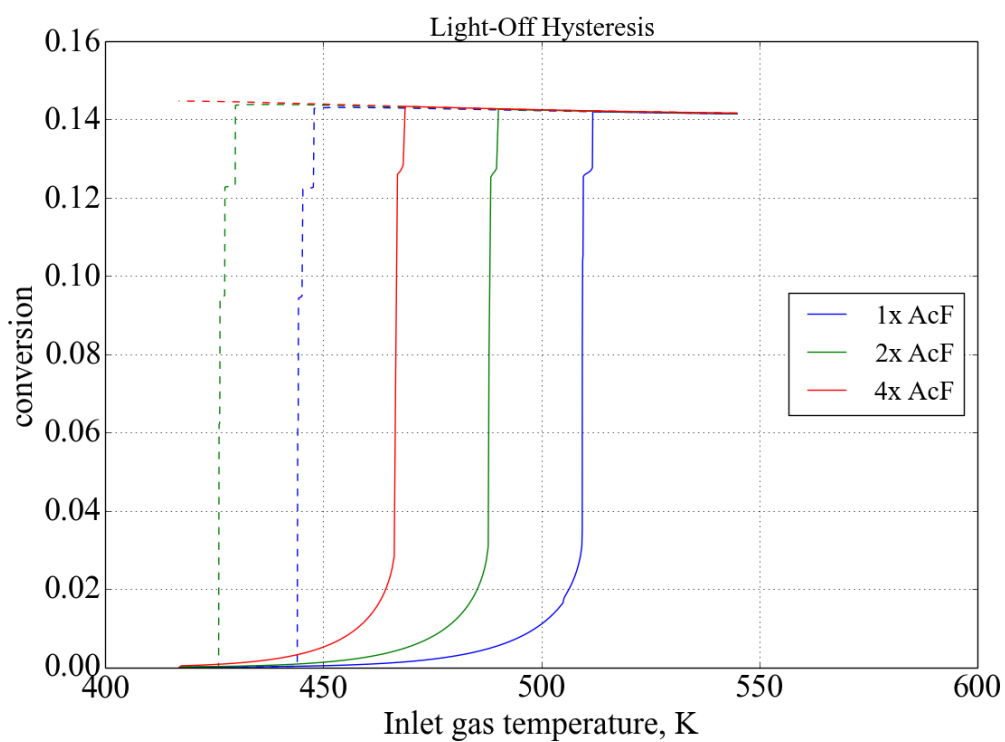


Figure 4.17: Hysteresis diagram of CO oxidation in a single channel 0.005m monolith with Tuned Pre-exponential for Reaction between CO and O

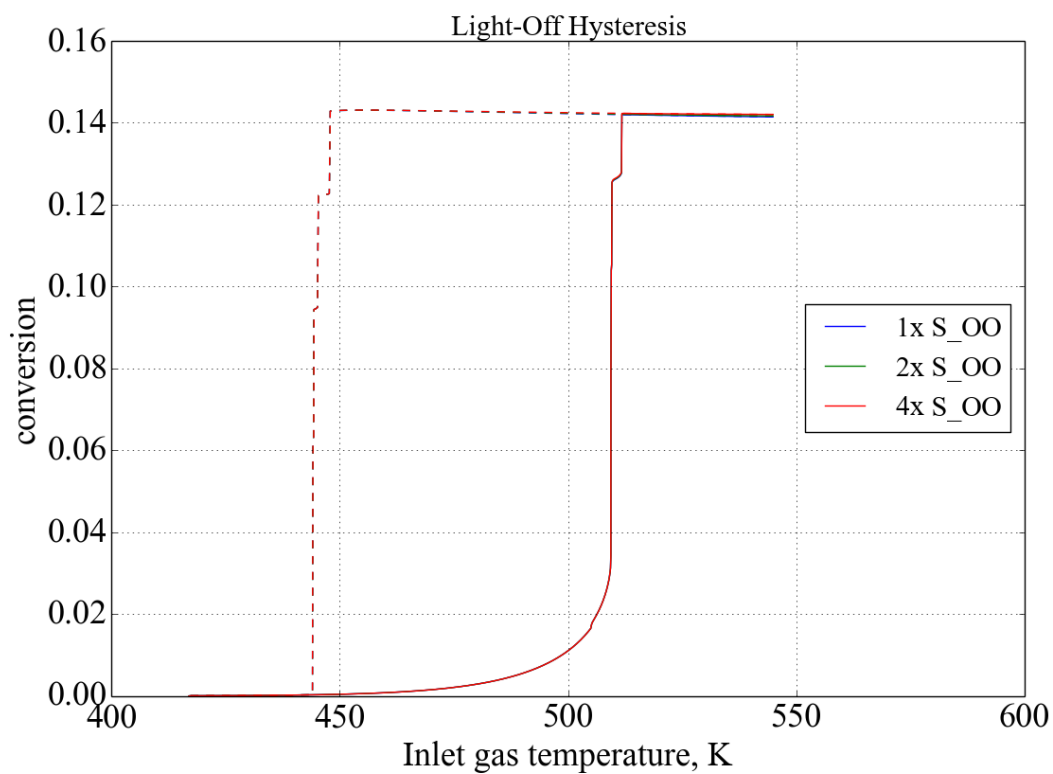


Figure 4.18: Hysteresis diagram of CO oxidation in a single channel 0.005m monolith with Tuned Pre-exponential for Oxygen Compression

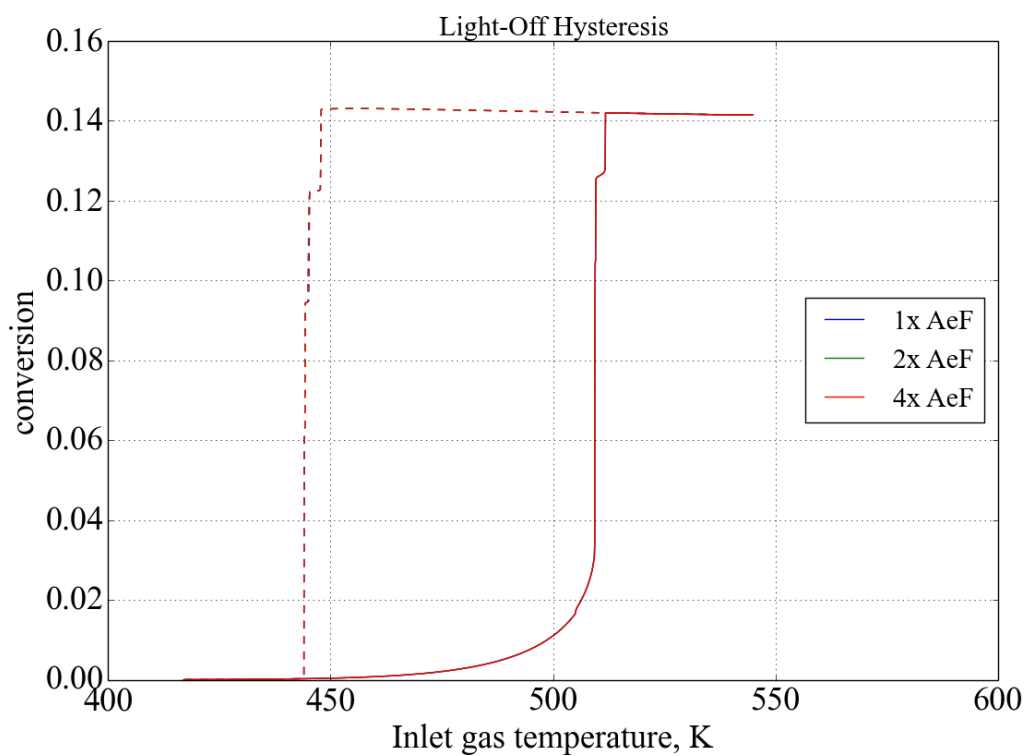


Figure 4.19: Hysteresis diagram of CO oxidation in a single channel 0.005m monolith with Tuned Pre-exponential for Reaction between CO and OO

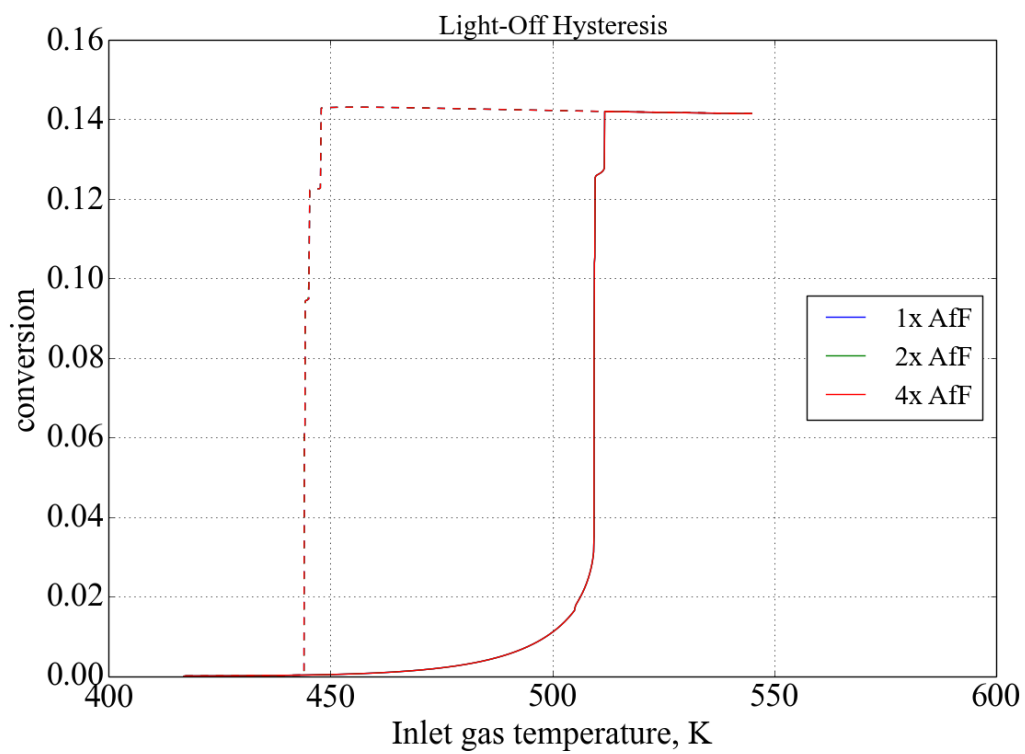


Figure 4.20: Hysteresis diagram of CO oxidation in a single channel 0.005m monolith with Tuned Pre-exponential for Reverse Oxygen Compression

CHAPTER 5

CONCLUSION AND RECOMMENDATION

5.1 Conclusion

In this project, the simulation of transient CO oxidation in single channel monolith by using oxygen compression model was carried out. In summary, the following has been achieved:

- Ignition-extinction hysteresis was simulated by ramping up and down the inlet gas temperature. It is shown that CO only starts to oxidize when inlet gas temperature increased to ignition temperature (at 510K). At ignition temperature, oxygen was able to competitively adsorb on surface. As inlet gas temperature decreases, high coverage of oxygen allows the CO oxidation to sustain even at lower than ignition temperature. However, further reduce in inlet gas temperature to 445K causes the surface to completely covered by CO. and result in extinction.
- Changes in gas phase CO concentration, solid phase CO concentration and fractional coverage of vacant site and three adsorbed species which are CO, O and OO throughout the hysteresis are studied.
- The effect of change of channel length and CO concentration in inlet gas on overall CO conversion was studied. It was found that increase in channel length improves CO conversion as higher residence time of exhaust gas in the monolith channel. Ignition temperature and extinction temperature reduces as well which result in higher efficiency in longer channel.

- The effect of change of CO concentration in inlet gas on overall CO conversion was studied. It was found that increase in inlet CO concentration reduces the overall CO conversion.
- Response from two different inlet concentration profile which are linear ramp and impulse input were also studied. It was found that CO oxidation cannot sustain when the CO concentration is greater than extinction point.
- The pre-exponential values for each reaction steps have been tuned to study the effect of each reaction steps to the overall CO conversion across the channel. Tuning of pre-exponential value of each reaction steps shows that the steps of adsorption of CO and oxygen and the step of reaction between CO and adsorbed oxygen are having greater effect on the ignition-extinction hysteresis. Increase of pre-exponential value for oxygen compression, reaction between CO and O₂ and reverse compression does not result in much changes in hysteresis. Pre-exponential value of oxygen adsorption and reaction between CO and O can be tuned simultaneously to generate the curve which is similar to the curve obtained experimentally (Ye *et al*, 2011).

5.2 Recommendations

Below are several recommendations proposed for future research:

- In this project, 1D model was used to model the gas phase and solid phase of the single channel monolith. However, the accuracy of 1D model is limited. Higher dimensional catalytic converter model especially 3D model where variation in radial and angular can be captured is probably the best way to represent the catalytic converter.
- Despite the ability to simulate the ignition-extinction hysteresis, it can be seen that the compressed oxygen model could not capture the smooth curves (as opposed to steps) as obtained experimentally by Ye *et al* (2011). Furthermore, a global kinetic model was used to represent the oxidation of hydrocarbons. A better reaction mechanism that could capture the reaction of other species such as hydrocarbons should be used.

REFERENCES

- Barshad Y., Zhou, X. and Gulari, E., 1985. Carbon monoxide oxidation under transient conditions: A fourier-transform infrared transmission spectroscopy study. *Journal of Catalysis*, 94(1), pp. 128-144.
- Berger, A., Hatling, O. and Rodriguez, D.O., 2009. Background Catcon. *College of Chemistry – University of California*, [online] available at http://www.cchem.berkeley.edu/molsim/teaching/fall2009/catalytic_converter/bkgcatcon.html[Accessed: 9 April 2015]
- Boodram, S., 2012. Car chemistry: What is a catalytic converter and how does it work? *Curiosity*, [online] available at: <http://www.explorecuriosity.org/Content.aspx?contentid=1779>[Accessed: 19 August 2014]
- Burch, R., 2004. Knowledge and know-how in emission control for mobile applications. *Catalysis Review*, 46 (2004), pp. 271-334.
- Charterjee, D., Deutschmann, O. and Warnatz, J., 2001. Detailed surface reaction mechanism in a three-way catalyst. *Faraday Discuss*, 119, pp. 371-384
- Chen, R., Pan, G., Zhang, Y., Xu, Q., Zheng, G., Xu, X., Chen, B. and Kan, H., 2011. Ambient carbon monoxide and daily mortality in three Chinese cities: The China air pollution and health effects study. *Science of the Total Environment*, 40 (2011), pp. 4923-4928.
- eMercedesBenz, [online] available at: http://www.emercedesbenz.com/Oct06/09_E_320_BLUETEC_Begins_Mercedes_Diesel_Campaign_In_The_USA.html[Accessed: : 20 July 2014]
- Engel, T. and Ertl, G., 1979. Elementary steps in the catalytic oxidation of carbon monoxide on platinum metals. *Advances in Catalysis*, 28, pp. 1-78
- Ertl, G., 2000. Heterogeneous catalysis on atomic scale. *The Chemical Record*, 1(1), pp. 33-45.
- Froment, G. F. and Bischoff, K. B., 1990. *Chemical reactor analysis and design*, 2nd edition, John Wiley & Sons.
- Hayes, R. E. and Kolaczkowski S. T., 1997. *Introduction to Catalytic Combustion*. The Netherlands:Gordon and Breach Science Publishers
- James E. Parks II, H. Douglas Ferguson III, John M. E. Storey, 2012, NOx reduction with natural gas for lean large-bore engine applications using lean NOx trap aftertreatment, Oak Ridge National Laboratory
- Johnson Matthey, 2002. *Platinum 2002*, [online] available at: http://www.platinum.matthey.com/uploaded_files/Pt%202002/chapter3.pdf. [Accessed: 23 August 2014]

- Lynch, D. T. 1984. Use of elementary step mechanisms to explain resonant behavior for co oxidation on platinum. *The Canadian Journal of Chemical Engineering*, 62(5), pp. 691-698.
- Masters, G.M. and Ela, W.P., 2008. *Introduction to environmental engineering and science*, Pearson Education, London.
- Neeft, J. P. A., Makkee, M. and Mouljin, J. A., 1996. Diesel particulate emission control. *Fuel Processing Technology*, 47, pp 1-69.
- Nievergeld, A., 1998. Automotive exhaust gas conversion: Reaction kinetics. *Reactor Modeling and Control. Ph. D. Thesis, Technische Universiteit Eindhoven*.
- Psyllos, A. and Philippopoulos, C., 1993. Modelling of monolithic converters with axial catalyst distribution. *Applied Mathematical Modelling*, 17, pp. 459-467.
- Salomons, S., Hayes, R. E., Votsmeier, M., Dronchner, A., Vogel, H., Malmberg. and Gieshoff, J., 2006. On the use of mechanistic CO oxidation models with a platinum monolith catalyst. *Applied Catalysis*, 70 (2007), pp. 305-315.
- Takizad, F., 2012. Investigation of exhaust emission factors based on vehicle models. *Current World Environment*, 7(1), pp.79-85.
- Thomas, J. M. and Thomas, W. J., 1997. *Principles and practice of heterogeneous catalysis*, VCH Verlagsgesellschaft mbH, Weinheim, Germany.
- United States Environmental Protection Agency, [online] available at: <http://www.epa.gov/otaq/consumer/milestones.htm>[Accessed: 20 July 2014]
- United States Environmental Protection Agency, [online] available at: <http://www.epa.gov/otaq/consumer/glossary.htm#naaqs>[Accessed: 20 July 2014]
- Volkswagen UK, [online] available at: <http://www.volkswagen.co.uk/technology/glossary/three-way-catalytic-converter>[Accessed: 9 April 2015]
- RTI International, 2003. Determination of Emissions Reductions from Selective Catalytic Reduction Control Technologies for Highway, Nonroad, and Stationary Use Diesel Engines, *Environmental Technology Verification Protocol, North Carolina, United States*.
- Ye, S., Yap, Y. H., Kolaczowski, S. T., Robinson, K. and Lukyanov, D., 2011. Catalyst 'light-off' experiments on a diesel oxidation catalyst connected to a diesel engine-Methodology and techniques. *Chemical Engineering Research and Design*, 90 (2012), pp. 834-845.